

**Molecular dynamics of the neuronal Ca<sup>2+</sup> -binding proteins  
Caldendrin and Calneurons**

**Dissertation**

**zur Erlangung des akademischen Grades**

**doctor rerum naturalium**

**(Dr. rer. nat.)**

**genehmigt durch**

**die Fakultät für Naturwissenschaften**

**der Otto-von-Guericke-Universität Magdeburg**

**von Diplom-Biologin Marina Gennadievna Mikhaylova  
geb. am 1 März 1981 in Ufa, Russland**

**Gutachter:**

**Prof. Dr. E.D. Gundelfinger**

**am: 30.07.2009**

**vorgelegt von: Diplom-Biologin Marina Gennadievna Mikhaylova**

## **Acknowledgements**

This thesis is the account of almost four years of devoted work at the Leibniz Institute for Neurobiology Magdeburg in the group of Michael R. Kreutz (Project Group Neuroplasticity) which would not have been possible without the help of many friends and colleagues.

First of all, I would like to thank Michael for being a great advisor. His ideas and tremendous support had a major influence on this thesis.

I want to thank Anna Karpova for being my friend and colleague for many years. I enjoyed to do research together with her as well as the nice discussions we daily had.

Many thanks also to Prof. Eckart D Gundelfinger for his encouraging discussions and help with corrections of the papers.

My thanks to Thomas Munsch, Peter Landgraf, Karl-Heinz Smalla, Ulrich Thomas, Oliver Kobler, Yogendra Sharma and Thomas Behnisch for the great collaboration over the years. It was a pleasure to work with all these people and to benefit from their knowledge.

My thanks to Paramesh Pasham Reddy, Anne-Christin Lehman, Johannes Hradsky and Philipp Bethge for their collaboration, support and friendship while doing their Ph.D studies, diploma theses or internships in our group.

My thanks to my Nplast colleagues Christina Spilker, Sujoy Bera, Jale Sahin, Rahul Kashuk, and Vivian Dambeck for the great time I had with them in our group.

I am particularly grateful to our technicians Corinna Borutzki, Stefanie Hochmuth and Monika Marunde for preparing primary neuronal culture and also taking care of our everyday lab work.

I would like to thank P. Aravind for reviewing my thesis and giving valuable suggestions on my future projects.

Thanks a lot to people from the Department of Neurochemistry and Molecular Biology at the IfN for providing a “training ground” and for the discussions we had on the seminars.

And at the end I would like to thank my family and my friends in Russia for the emotional support they gave me over these years.

## **Erklärung**

Hiermit erkläre ich, dass ich die von mir eingereichte Dissertation zum dem Thema **”Molecular dynamics of the neuronal Ca<sup>2+</sup>-binding proteins Caldendrin and Calneurons”** selbständig verfasst, nicht schon als Dissertation verwendet habe und die benutzten Hilfsmittel und Quellen vollständig angegeben wurden.

Weiterhin erkläre ich, dass ich weder diese noch eine andere Arbeit zur Erlangung des akademischen Grades doctor rerum naturalium (Dr. rer. nat.) an anderen Einrichtungen eingereicht habe.

---

(Ort, Datum)

---

(Marina Mikhaylova)

## **Index**

<b>Summary</b>	7
<b>1 Introduction</b>	9
1.1 Neuronal calcium signaling	9
1.1.1 The role of calcium as a second messenger	9
1.1.2 Sources and processes regulated by Ca <sup>2+</sup>	9
1.1.2.1 Endoplasmic reticulum	10
1.1.2.2 The Golgi apparatus	11
1.1.2.3 Ca <sup>2+</sup> is a regulator of secretory processes	12
1.1.2.4 Synaptic plasticity	13
1.1.2.5 Gene transcription	14
1.2 Calcium binding proteins	15
1.2.1 Types of calcium binding proteins	15
1.2.2 Neuronal calcium sensor proteins	17
1.2.2.1 NCS-1/Frequenin: Its role for regulation of PI-4K $\beta$ activity and Golgi trafficking	18
1.2.2.3 The Caldendrin/CaBP1-5 gene family	20
1.2.2.4 Jacob is a Caldendrin interaction partner in the synapse	22
1.2.2.5 The identification of Calneurons	23
1.2.3 Aims of the study	24
<b>2 Materials and methods</b>	25
2.1 Materials and production of materials	25
2.1.1 Chemicals	25
2.1.2 Enzymes and kits	25
2.1.3 cDNA constructs	25
2.1.4 Cloning of Jacob constructs into a Semliki Forest Virus vector and production of viral particles	26
2.1.5 <i>In situ</i> hybridization (oligonucleotides)	27
2.1.6 Generation of Calneuron-specific antibodies	27
2.1.7 Antibodies used for IB, IF and IPs	28
2.1.8 Common buffers and cell culture media	29
2.1.9 Prokaryotic and eukaryotic cell lines	29
2.1.10 Animals	30
2.2 Methods	30
2.2.1 Cell culture, transfections and immunocytochemistry	30
2.2.2 Stimulation of primary hippocampal neurons	31
2.2.3 Confocal laserscan microscopy	31
2.2.4 Immunoblotting	31
2.2.5 Subcellular fractionation and microsomal preparation	32
2.2.6 Gel filtration	32
2.2.7 Co-immunoprecipitation	33
2.2.8 Bacterial expression and purification of recombinant proteins	33
2.2.9 Isothermal titration calorimetry (ITC)	35
2.2.10 Steady-state fluorescence studies	36
2.2.11 8-Anilino-1-naphthalene sulfonic acid binding	36
2.2.12 Pull-down assays	36
2.2.13 Competition pull-down assays	37

2.2.14	Surface plasmon resonance analysis	37
2.2.15	PI-4K $\beta$ activity assays	38
2.2.16	PI(4)P assay	39
2.2.17	hGH release assay	39
2.2.18	VSV-G trafficking assay	40
2.2.19	Ca <sup>2+</sup> imaging	40
2.2.20	FRAP experiments	41
2.2.21	Life imaging experiments	42
2.2.22	Analysis of Golgi complexes and PTVs in primary neurons	42
2.2.23	Structural modeling	43
2.2.24	Statistical analysis	43
<b>3</b>	<b>Results</b>	44
3.1	Jacob is a Caldendrin binding partner in brain and competes with Importin- $\alpha$ for an overlapping binding site	44
3.2	Importin-bound Jacob translocates to the nucleus after stimulation of NR2B- containing NMDARs	46
3.3	Caldendrin binding targets Jacob outside the nucleus only after synaptic NMDAR stimulation	49
3.4	Jacob is part of the CREB shut-off pathway	53
3.5	The primary structure of Caldendrin and Calneurons	54
3.6	Comparative modeling of Caldendrin and Calneurons EF-hand structures	56
3.7	Caldendrin and Calneurons are abundant in brain	59
3.8	Calneurons are localized at the Golgi apparatus and associate with PI-4K $\beta$ <i>in vivo</i>	60
3.9	Calneurons physically interact with PI-4K $\beta$ and compete with NCS-1 binding in a Ca <sup>2+</sup> -dependent manner	65
3.10	The Ca <sup>2+</sup> binding affinity of NCS-1 but not of Calneurons is regulated by Mg <sup>2+</sup>	69
3.11	Calneuron-1 regulates PI-4K $\beta$ activity in a Ca <sup>2+</sup> -dependent manner and opposing to NCS-1	72
3.12	Calneurons regulate vesicular trafficking of the VSV-G protein	74
3.13	Calneuron over-expression inhibits hGH release in PC12 cells	76
3.14	Overexpression of Calneurons in cortical neurons induces a prominent enlargement of TGN	77
3.15	Calneurons regulate vesicle trafficking at neuronal Golgi	80
3.16	Calneurons regulate the number of PTVs in axon at early developmental stages	83
<b>4</b>	<b>Discussion</b>	86
4.1	Caldendrin and Calneurons are close but still rather different ‘relatives’ in the brain	87
4.2	Caldendrin and Jacob are key molecules on a novel pathway from the synapse to the nucleus	88
4.2.1	Jacob is a synaptic binding partner of Caldendrin	88
4.2.2	Caldendrin is a first example when interaction of a Ca <sup>2+</sup> -sensor with a NLS can mask the site and prevents nuclear translocation by competing with Importin- $\alpha$ –binding	90
4.2.3	The Caldendrin - Jacob interaction in the frame of neuronal function	91

4.2.4	Nuclear Jacob induces pleiotropic negative effects on synapto-dendritic cytoarchitecture and induces CREB shut-off	91
4.2.5	What is the physiological role of Jacob in the nucleus?	92
4.3	Calneurons provide a $\text{Ca}^{2+}$ threshold for trans-Golgi network to plasma membrane trafficking	94
4.3.1	PI-4K $\beta$ is an interaction partner of Calneurons in the Golgi	94
4.3.2	Calneurons are setting a ' $\text{Ca}^{2+}$ threshold' for PI-4K $\beta$ activation	95
4.3.3	The competitive binding of Calneurons and NCS-1 to PI-4K $\beta$ is regulated by $\text{Mg}^{2+}$	97
<b>5</b>	<b>References</b>	100
<b>6</b>	<b>Supplementary information</b>	110
6.1	Supplementary Table 1. List of the constructs produced in the lab	110
6.2	Supplementary Table 2. List of the constructs obtained from the collaborators	111
6.3	Supplementary Table 3. Plasmids used for the cloning and protein expression	111
6.4	Supplementary Table 4. Common buffers	112
6.5	Supplementary Table 5. Common media	112
6.6	Supplementary Table 6. Solutions for PSD preparation	113
6.7	Supplementary Scheme 1. PSD preparation	114
<b>7</b>	<b>Abbreviations</b>	116

## Curriculum Vitae

### Scientific publications

## **Summary**

The calcium sensor protein Caldendrin is an EF-hand protein with a high homology of Calmodulin (CaM). Calneurons are two novel calcium binding proteins that apart from CaM represent the closest homologues of Caldendrin in brain. Caldendrin and Calneuron-1 and -2 are abundantly expressed in neurons and retinal cells. Caldendrin is highly abundant in the postsynaptic density (PSD) of a subset of excitatory synapses in brain whereas the cellular localization of Calneurons is more restricted to the Golgi complex.

Previously it was shown that Caldendrin is a binding partner of Jacob. Strictly depending upon activation of N-methyl-D-aspartate-type glutamate receptors (NMDARs) Jacob is recruited to neuronal nuclei, resulting in a rapid stripping of synaptic contacts and in a drastically altered morphology of the dendritic tree. The nuclear trafficking of Jacob from distal dendrites crucially requires the classical Importin pathway. In this thesis it was shown that Caldendrin controls the extra-nuclear localization of Jacob by calcium ( $\text{Ca}^{2+}$ )-dependently competing with the binding of Importin- $\alpha$  to the nuclear localization signal (NLS) of Jacob. The NLS of Jacob partially overlaps with an incomplete IQ-motif – an interaction domain for Caldendrin. Interaction of Caldendrin with Jacob is specific and cannot be substituted by CaM. The Caldendrin-Jacob interaction requires sustained synaptodendritic  $\text{Ca}^{2+}$ -levels, which presumably cannot be achieved by activation of extrasynaptic NMDARs, but are confined to  $\text{Ca}^{2+}$ -microdomains such as postsynaptic spines. Extrasynaptic NMDARs as opposed to their synaptic counterparts trigger the CREB shut-off pathway and cell death. We found that nuclear knock down of Jacob prevents CREB shut-off after extrasynaptic NMDARs activation while its nuclear overexpression induces CREB shut-off without NMDAR stimulation. This defines a novel mechanism of synapse-to-nucleus communication via a synaptic  $\text{Ca}^{2+}$ -sensor protein, which links the activity of NMDARs to nuclear signaling events involved in modelling synaptodendritic input and NMDAR induced cellular degeneration.

In the second part of the thesis the characterization of a new subfamily of neuronal calcium sensor (NCS) proteins – the Calneurons was provided. By virtue of their biophysical properties Calneurons are high affinity  $\text{Ca}^{2+}$  sensors that exhibit a relatively narrow dynamic range of  $\text{Ca}^{2+}$ -binding with respect to the resting  $\text{Ca}^{2+}$ -levels in neurons. In this study we show that Calneuron-1 and -2 physically associate with Phosphatidylinositol 4-OH kinase III $\beta$  (PI-4K $\beta$ ), an enzyme involved in the regulated local synthesis of phospholipids that are crucial for trans-Golgi network to plasma membrane trafficking. This interaction causes the inhibition of the enzyme at resting and low  $\text{Ca}^{2+}$  levels, and negatively interfere with Golgi-to-plasma membrane trafficking. At high  $\text{Ca}^{2+}$  levels this inhibition is released via a preferential association of PI-4K $\beta$  with NCS-1 that competes for the binding site with Calneurons. The opposing roles of Calneurons and NCS-1 provide a molecular switch to decode local  $\text{Ca}^{2+}$  transients at the Golgi and impose a  $\text{Ca}^{2+}$  threshold for PI-4K $\beta$  activity and vesicle trafficking.

## Zusammenfassung

Caldendrin ist ein Calcium-Bindungsprotein der EF-hand Familie mit großer Ähnlichkeit zu Calmodulin. Neben Calmodulin sind die Calneurone die nächst homologen Proteine. Sowohl Caldendrin als auch Calneurone finden sich prominent in Neuronen des Gehirns und der Retina. Biochemische Analysen zeigen, dass Caldendrin eng mit dem spezialisierten Zytoskelett der Postsynapse, der so genannten postsynaptischen Dichte (PSD), assoziiert ist, während Calneurone am Golgi anreichern.

In der vorgelegten Arbeit wurde zunächst die Interaktion von Caldendrin mit seinem synaptischen Bindungspartner Jacob näher charakterisiert. Auf der Beobachtung aufbauend, dass Jacob ausschließlich nach Stimulation von N-Methyl-D-Aspartat (NMDA)-Rezeptoren in den Zellkern transloziert und die Anreicherung von Jacob im Zellkern zu deutlichen Veränderungen in der Morphologie der Nervenzellen führt, wurde der Jacob-Signalweg in Neuronen genauer charakterisiert. Im Gegensatz zu Jacob findet sich Caldendrin vor allem prominent im subsynaptischen Zytoskelett, wo es über eine  $\text{Ca}^{2+}$ -abhängige Bindung ein nukleäres Lokalisierungssignal (NLS) in Jacob maskiert. Die hierzu notwendigen  $\text{Ca}^{2+}$ -Konzentrationen werden vermutlich nur in dendritischen Spine-Synapsen unterhalb der postsynaptischen Membran erreicht, so dass Caldendrin Jacob nur nach Aktivierung synaptischer NMDA-Rezeptoren in der Synapse fixiert. Der Kerntransport von Jacob erfolgt über den klassischen Importin-Transportweg und erfordert das Vorhandensein des NLS in Jacob. Die kompetitive Bindung von Caldendrin an Jacob ist spezifisch, Calmodulin kann die mit dem NLS überlappende IQ-Domäne von Jacob nicht binden. Jacob ist im Zellkern funktionell an den Transkriptionsfaktor CREB gekoppelt und spielt unter pathophysiologischen Bedingungen eine prominente Rolle beim späten neuronalen Zelluntergang nach exzitotoxischer Schädigung. Da Jacob unter Bedingungen neuronaler Erregung in den Zellkern wandert, die auch die CREB-kontrollierte Genexpression blockieren (in der Literatur als CREB shut-off pathway bezeichnet), wurde nachfolgend untersucht, welche Konsequenzen die Präsenz von Jacob im Zellkern für die Aktivierung von CREB hat. Eine gezielte Überexpression von Jacob im Zellkern hatte eine drastische Abnahme von transkriptionell aktiven CREB unabhängig von den eingesetzten Stimulationsbedingungen zur Folge. Diese Beobachtung führte zu der Hypothese, dass Jacob Bestandteil des CREB 'shut-off pathways' ist.

Im zweiten Teil der Arbeit wurde eine neue Subfamilie von neuronalen Calcium-Sensor Proteinen, die so genannten Calneurone, identifiziert und charakterisiert. Calneurone gehören zur Calmodulin-Superfamilie und weisen hohe Ähnlichkeit zu dem synaptischen  $\text{Ca}^{2+}$ -Sensor Caldendrin auf. Calneurone finden sich prominent am Trans-Golgi-Netzwerk (TGN), wo sie mit dem Enzym Phosphatidylinositol 4-OH kinase III $\beta$  (PI-4K $\beta$ ) interagieren. Diese Interaktion führt zu einer Inhibition der enzymatischen Aktivität von PI-4K $\beta$ . PI-4K $\beta$  ist wesentlich an der Produktion von Phosphatidylinositol 4,5-Bisphosphate (PI(4,5)P<sub>2</sub>) am TGN beteiligt und PI(4,5)P<sub>2</sub> ist ein essentielles Phospholipid für den Transport von Vesikeln aus dem TGN. Die Interaktion von Calneuronen mit PI-4K $\beta$  wird über Kalzium reguliert. Interessanterweise binden nicht nur Calneurone PI-4K $\beta$ , sondern auch das Calcium-Sensor Protein NCS-1. Im Gegensatz zur Calneuron-Bindung erfordert die Interaktion mit NCS-1 erhöhte Kalzium-Konzentrationen und führt zur Aktivierung von PI-4K $\beta$ . Die differentielle Bindung beider Kalzium-Bindungsproteine konstituiert einen molekularen Schalter, der über eine Kalziumschwelle den Transport von Vesikeln aus dem TGN reguliert.



# **1 Introduction**

## **1.1 Neuronal calcium signaling**

### ***1.1.2 The role of calcium as a second messenger***

The Calcium ion ( $\text{Ca}^{2+}$ ) is of central importance in cellular physiology because of its enormous versatility that is due to an extensive  $\text{Ca}^{2+}$ -tool kit involved in assembling intracellular signaling systems with different spatial and temporal dynamics (Berridge, 1998).  $\text{Ca}^{2+}$  is particularly suitable for this role because of its chemical properties and a very high concentration gradient of free chelatable  $\text{Ca}^{2+}$  between the extracellular fluid (1,5-2 mM / Jones et al., 1987) and the cytosol (less than 0,1  $\mu\text{M}$  at resting conditions / Ferris et al., 1992) that covers about four orders of magnitude. The cytosolic  $\text{Ca}^{2+}$  concentration is tightly regulated by binding and chelation of the ion by various  $\text{Ca}^{2+}$ -binding proteins and by transport of the ion across plasma and intracellular membranes. Several channels, transport ATPases, uniporters, and antiporters in the plasma membrane, endoplasmic and sarcoplasmic reticulum, and mitochondria are responsible for the transport of  $\text{Ca}^{2+}$  (Berridge, 1998). The complex regulation of these transport systems is the subject of an increasing number of investigations. In neurons  $\text{Ca}^{2+}$  plays an important role in regulating a wide variety of processes that are essential not only for specific neuronal functions like neurotransmitter release, synaptic plasticity and activity-dependent gene transcription, but also for endoplasmic reticulum (ER) and Golgi trafficking (Hardingham et al., 2001; Chen et al., 2002; Burgoyne et al., 2004; Dolman et al., 2006; Hay, 2007).

### ***1.1.2 Sources and processes regulated by $\text{Ca}^{2+}$***

Increases in intracellular  $\text{Ca}^{2+}$  concentrations can result from entry of  $\text{Ca}^{2+}$  into the cell through voltage-dependent or receptor-operated channels. Alternately, a rise in intracellular  $\text{Ca}^{2+}$  can be due to release mainly from ER but also from the Golgi and mitochondria (Sayer, 2002, Dolman et al., 2006). Owing to the restraints of space and with respect to the topic of this thesis, only the  $\text{Ca}^{2+}$  dynamics of the ER and Golgi and the role of  $\text{Ca}^{2+}$  in Golgi trafficking as well as in activity dependent gene transcription will be described in more detail.

### *1.1.2.1 Endoplasmic reticulum*

The ER extends throughout the neurons as a continuous tubules system of membranes connected with each other (Voeltz et al., 2002). As it was shown by electron microscopy, on immunostainings with specific protein markers as well as by live imaging studies with fluorescent dyes the ER in the cell soma is organized as cisternae and cisternae organelles (Voeltz et al., 2002.). The ER in axons consists of parallel tubules, which are in continuity with the presynapse where they are tightly associated with mitochondria (Aihara et al., 2001). The ER is also present along dendrites as a continuous network which finally terminates in mature spines, in the so called spine apparatus – a structure of not yet clearly defined function and consisting of tightly packed membrane stacks with dense material in between (Bhatt et al., 2009).

The ER can contribute to the dynamics of neuronal signaling by acting either as a source or as a sink for  $\text{Ca}^{2+}$  (Miller et al., 1991; Simpson et al., 1995). It plays an active role in neuronal  $\text{Ca}^{2+}$  signaling due to presence of Inositol 1,4,5-triphosphate receptors (IP3Rs) and ryanodine receptors (RYRs). Both receptors are capable to release  $\text{Ca}^{2+}$  stored inside the ER upon ligand binding. These receptors were found on the surface of somatic and dendritic cisternae as well as within synaptic terminals (Hoesch et al., 2002). IP3Rs and RYRs are sensitive to  $\text{Ca}^{2+}$  and display the phenomenon of “calcium induced calcium release” (CICR). CICR is a mechanism by which  $\text{Ca}^{2+}$  influx can stimulate  $\text{Ca}^{2+}$  release from internal stores. It was first demonstrated in 1975 by Fabiato & Fabiato in muscle cells but later on also shown in neurons (Marrion & Adams, 1992; Kuba, 1994; Verkhratsky & Shmigol, 1996; Cohen et al., 1997; Berridge, 1998). Binding of  $\text{Ca}^{2+}$  to RYRs activates a  $\text{Ca}^{2+}$ -permeable channel allowing  $\text{Ca}^{2+}$  to exit from the ER and to enter the cytosol. The  $\text{Ca}^{2+}$  concentration within the ER lumen is very high (100-300  $\mu\text{M}$ ) as compared to that of the surrounding cytoplasm (around 100 nM / Mogami et al., 1998). The maintenance of a high  $\text{Ca}^{2+}$  concentration within the ER lumen is essential for a number of vital cellular processes including protein synthesis, protein processing and  $\text{Ca}^{2+}$  signal generation. The release of  $\text{Ca}^{2+}$  from ER induces oscillations in free intracellular  $\text{Ca}^{2+}$  concentrations (also called  $\text{Ca}^{2+}$  waves). These oscillations largely result from an influx of  $\text{Ca}^{2+}$  into the cytosol from the ER, followed by an efflux of  $\text{Ca}^{2+}$  from the cytosol back to the ER (Ashby et al., 2001). Comparing the structure and function of neuronal ER and the plasma membrane Berridge (1998) suggested the concept of a ‘neuron-within-a neuron’ with the main idea that neuronal  $\text{Ca}^{2+}$  signaling depends upon a binary membrane system. The plasma membrane integrates external stimuli

and generates fast propagating action potentials using voltage-dependent  $\text{Na}^+$  and  $\text{Ca}^{2+}$  channels whereas the ER system monitors internal signals and produces in response to these signals slowly propagating  $\text{Ca}^{2+}$  signals via IP3Rs and RYRs. Finally, these two membranes are tightly interacting in functional terms and are together able to regulate neuronal processes like excitability, associativity (association of synaptic input), neurotransmitter release, synaptic plasticity and gene transcription.

#### *1.1.2.2 The Golgi apparatus*

The Golgi apparatus is responsible for receiving, sorting and processing secretory and membrane proteins and lipids that are needed for cell growth and function. In neurons, like in all other eukaryotic cells, the Golgi apparatus is composed of membrane-bound stacks known as cisternae (Mollenhauer & Morre, 2005). It occupies a perinuclear position, extends into the major dendrite and is also present at the dendritic branching points as Golgi outposts (Horton et al., 2005). The cisternae stack has five functional regions: the cis-Golgi network, cis-Golgi, medial-Golgi, trans-Golgi, and trans-Golgi network (Horton & Ehlers, 2003). Vesicles from the endoplasmic reticulum fuse with the cis-Golgi network and subsequently progress through the stack to the trans-Golgi network, where they are packaged and sent to the required destination. Each region contains different enzymes, which selectively modify the contents depending on their destination. The trans-Golgi network is the sub-compartment from which vesicles leave the Golgi. Changes in  $\text{Ca}^{2+}$  concentration within the Golgi lumen or in the adjacent cytosol regulate Golgi function. Moreover, the Golgi system is by itself a  $\text{Ca}^{2+}$  store containing release and sequestration apparatuses (Dolman & Tepikin, 2006). The concentration of  $\text{Ca}^{2+}$  in the Golgi lumen is around 0.3 mM in unstimulated cells and therefore a large gradient exists between the internal side of the Golgi and the cytosol (Pinton et al., 1998; Vanoevelen et al., 2004). Production of Inositol 1,4,5-triphosphate (IP3) activates IP3Rs on the Golgi membrane resulting in  $\text{Ca}^{2+}$  release from the Golgi complex (Pinton et al., 1998). Moreover,  $\text{Ca}^{2+}$  is known to regulate vesicular trafficking along the secretory pathway (Burgoyne & Clague, 2003). For instance,  $\text{Ca}^{2+}$  acting via Calmodulin regulates intra-Golgi transport (Porat et al., 2000). Cytosolic  $\text{Ca}^{2+}$  gradients have also been postulated to regulate the assembly and disassembly of coat proteins responsible for vesicular trafficking between Golgi stacks and the release of vesicles from the trans-Golgi network (Hay, 2007). Moreover, cytosolic  $\text{Ca}^{2+}$  transients activate a broad spectrum of downstream effectors and many of them also localize to the Golgi apparatus (Taverna et al., 2002; Haynes et al., 2005; Hay, 2007).

### 1.1.2.3 $Ca^{2+}$ is a regulator of secretory processes

$Ca^{2+}$  is known to regulate vesicular trafficking along the secretory pathway (Hay, 2007). Importantly,  $Ca^{2+}$  chelation was shown to inhibit both anterograde and retrograde transport of vesicles and  $Ca^{2+}$  is thought to be a fundamental trigger for vesicle trafficking in the secretory pathway. In recent years, there is number of studies demonstrating a role of  $Ca^{2+}$  in different steps of this process (Fig. 1).

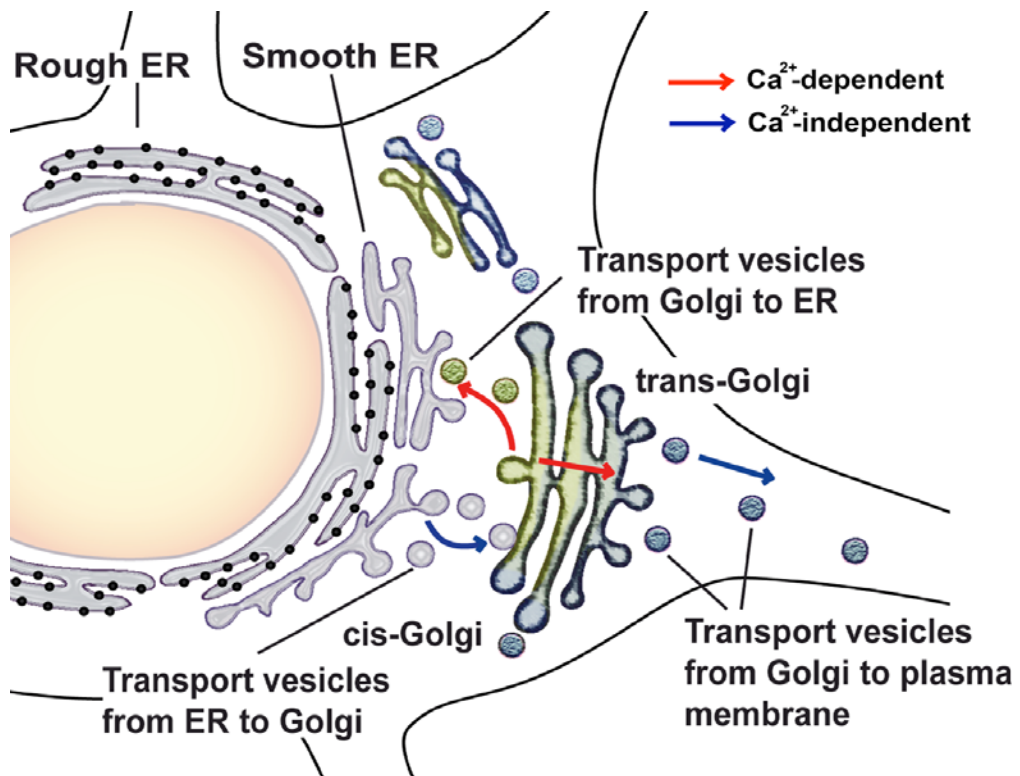


Figure 1.  $Ca^{2+}$  regulates different steps in the secretory pathway. Red arrows indicate  $Ca^{2+}$  sensitive processes, blue arrows –  $Ca^{2+}$  insensitive processes.

Proteins and lipids are initially synthesized in the ER. The export from the ER defines the first step of the pathway and is mediated by the recruitment of the COP II protein coats and the subsequent budding of COP II-coated vesicles. The coat proteins are responsible for the initial sorting and the preferential recruitment of cargo and exclusion of resident ER proteins (Aridor et al., 1998). Budded COP II vesicles fuse with each other and with already fused vesicles to form the polymorphic tubular structures called vesicular tubular clusters (VTCs). This step was shown to be  $Ca^{2+}$  independent (Hay, 2007). VTCs integrate the anterograde ER-to-Golgi complex and the retrograde recycling transport pathways. During their limited life span, VTCs undergo maturation by the selective recycling and acquisition

of specific proteins and the sequential exchange of specific molecules. For instance, COP II coats exchange for COP I coats on VTCs. Porat and Elazar (2000) have convincingly demonstrated that the association of the COP I coat on those vesicles that are targeted back to ER is  $\text{Ca}^{2+}$  dependent. VTCs accumulate in the peri-Golgi region and are connected to the cis-Golgi network. Intra-Golgi trafficking is regulated by  $\text{Ca}^{2+}$  via Calmodulin (CaM / Porat & Elazar, 2000). Cargos subsequently progress through the stack to the trans-Golgi network (TGN), where they are packaged and sent to the required destination.

These processes in the TGN are also  $\text{Ca}^{2+}$ -sensitive due to the  $\text{Ca}^{2+}$ -dependent regulation of one of the key enzymes involved – Phosphatidylinositol 4-OH kinase III $\beta$  (PI-4K $\beta$ ). PI-4K $\beta$  phosphorylates Phosphatidylinositol (PI) at position 4 and produces Phosphatidylinositol 4'-monophosphate (PI(4)P). Lipid rafts are enriched in PI(4)P and the phosphoinositide is needed for clathrin-independent vesicle formation and it has been proposed to participate in sorting at the TGN (McNiven et al., 2006). PI-4K $\beta$  activity is positively regulated by neuronal calcium sensor-1 in a  $\text{Ca}^{2+}$ -dependent manner (Haynes et al., 2005). Hence, the trafficking of vesicles that were budding off from the TGN is  $\text{Ca}^{2+}$  independent whereas the fusion of cargo vesicles with the plasma membrane is again a  $\text{Ca}^{2+}$ -dependent process due to the  $\text{Ca}^{2+}$  sensitivity of SNARE proteins (Hilfiker et al., 1999).

#### *1.1.2.4 Synaptic plasticity*

Synaptic plasticity is the mechanism of use-dependent change of synaptic strength and it is postulated to be a basis for learning and memory (Baudry, 1998). Long-term potentiation (LTP) and long-term depression (LTD) are the best-studied examples of synaptic plasticity processes. Both LTP and LTD can be generated by the same neuron via transient  $\text{Ca}^{2+}$  signals that differ in their timing and amplitude. LTP is triggered by high frequency, short lasting  $\text{Ca}^{2+}$  elevations when local  $\text{Ca}^{2+}$  concentration can reach to micromolar levels in spine synapses (Conti & Lisman, 2002), whereas LTD is generated by longer lasting transients but a  $\text{Ca}^{2+}$  concentration that is usually below the micromolar range (Holthoff & Tsay, 2002). During LTP induction N-methyl D-aspartate receptors (NMDARs) as well as L-type voltage-dependent calcium channel (VDCC), play a crucial role in local synaptic  $\text{Ca}^{2+}$  increase. High-resolution measurements of  $\text{Ca}^{2+}$  in dendritic spines show how  $\text{Ca}^{2+}$  can encode the precise relative timing of presynaptic input and postsynaptic activity and generate long-term synaptic modifications of opposite polarity (Hirsch & Crepel, 1992; Holthoff & Tsay, 2002; Stosiek et al., 2003).

#### 1.1.2.5 Gene transcription

It is widely believed that synaptic plasticity is established at individual synaptic sites. On the other hand, it is also a common belief that synapse-to-nucleus communication and changes in gene expression are required for long-term memory formation and long-lasting changes in synapto-dendritic cytoarchitecture. In this context the NMDARs controlled gene expression is of particular importance (Hardingham et al., 2001). However, it is essentially unclear how the NMDAR  $\text{Ca}^{2+}$  signal is transduced to the nucleus and how changes in gene expression feed back to alter or sustain synaptic integrity and function.

There are number of ways by which the activated synapses then can subsequently transfer information about the  $\text{Ca}^{2+}$  influx through NMDARs and L-type VDCC to the nucleus. The classical view mainly considers the  $\text{Ca}^{2+}$  ion itself as the key regulator of plasticity-related gene expression (Hardingham et al., 2001). Within this framework synaptic NMDARs and L-type VDCC induce dendritic  $\text{Ca}^{2+}$  waves that are integrated in the soma and elicit by yet unknown mechanism, nuclear  $\text{Ca}^{2+}$  waves that are in turn instrumental in the control of gene expression (Bito & Takemoto-Kimura, 2003). An alternative non-competing hypothesis suggests that synapto-nuclear protein messengers translocate to the nucleus in response to synaptic  $\text{Ca}^{2+}$  influx and are subsequently involved in transcriptional regulation.  $\text{Ca}^{2+}$  waves crucially involve the activity of the ER (Berridge, 1998). Thus, the initial influx of  $\text{Ca}^{2+}$  via NMDARs and L-type VDCC in activated synapses or as the result of action potential propagation induce secondary responses in the ER and the Golgi complex generating  $\text{Ca}^{2+}$  oscillations that can spread along the axon and dendrites and potentially reach the nucleus where it initiates a cascade of signaling events that results in the expression of genes that can promote dendritic growth, synapse development, and neuronal plasticity (Yeckel et al., 2007).

NMDARs play an important role in transcriptional regulation of gene expression not only because they provide the initial  $\text{Ca}^{2+}$  trigger but also due to their association with a large number of signaling molecules like CaM, Calcium/calmodulin-dependent protein kinase II (CaMKII), Calcineurin, Tiam1, and proteins involved in Ras/MAP kinase signaling, including H-Ras, c-RAF1, MEK1/2, and ERK1/2, each of which has been implicated in the regulation of activity-dependent gene transcription (Hardingham et al., 2001). An important target of the NMDAR regulated gene expression is the transcription factor cyclic-AMP response element binding protein (CREB). CREB controls the expression of a large number of genes (for example c-fos, BDNF, NGF, Arc/Arg1.3, Homer,  $\alpha$ CaMKII)

implicated in cell differentiation, survival and plasticity (Impey & Goodman, 2001; Impey et al., 2004). One of the pathways for CREB activation utilizes CaM. CaM is one of the most abundant  $\text{Ca}^{2+}$  binding proteins that is present in all cellular compartments including the nucleus (Deisseroth et al., 1998). CaM interacts in the  $\text{Ca}^{2+}$  bound state with CaMKIV and CREB is one of the nuclear substrates of CaMKIV. CaMKIV phosphorylates CREB at a crucial serine at position 133 and this phosphorylation event renders CREB transcriptionally active (Wu et al., 2001).

## **1.2 Calcium binding proteins**

### ***1.2.1 Types of calcium binding proteins***

Principally  $\text{Ca}^{2+}$  signals are transduced by specific  $\text{Ca}^{2+}$ -binding proteins (CaBPs). Numerous intracellular CaBPs belong to the EF-hand super-family. These proteins are characterized by the presence of one or more EF-hand motifs which are high-affinity  $\text{Ca}^{2+}$  binding sites. Intracellular EF-hand bearing CaBPs are thought to serve two general functions, i.e. they can have buffering functions to limit the intracellular free  $\text{Ca}^{2+}$  concentration and  $\text{Ca}^{2+}$ -sensing functions to modulate activities of enzymes, ion channels or cell surface receptors (Sokalet al., 2000; Haeseleer et al., 2002, Lee et al., 2002; Haeseleer et al., 2004; Haynes et al., 2004). In the latter case, CaBPs change their conformation upon  $\text{Ca}^{2+}$  binding triggering the target interaction. The prototype of a ubiquitously expressed  $\text{Ca}^{2+}$ -sensor protein is CaM. CaM is the ancestor of a large family of  $\text{Ca}^{2+}$ -sensor proteins and includes in the nervous system of vertebrates the Caldendrin/CaBP1-5 and neuronal calcium sensor proteins (Seidenbecher et al., 1998; Haeseleer et al., 2002, Burgoyne, 2007). These proteins usually exhibit a  $\text{Ca}^{2+}$ -dependent conformational change which opens a target binding site. The second group is represented by Calbindin D9k, Parvalbumin and Calretinin. They usually have a lower  $\text{Ca}^{2+}$  binding affinity and do not undergo  $\text{Ca}^{2+}$  dependent conformational changes (Baimbridge et al., 1992; Camp & Wijesinghe, 2009). EF-hand proteins can contain from two to twelve copies of the EF-hand motif (Krebs & Michalak, 2007). The abbreviation comes from their structure: an  $\alpha$ -helix - E, loop, and a second  $\alpha$ -helix - F (Fig. 2). Usually a  $\text{Ca}^{2+}$  ion is bound in the loop under physiological conditions; however, 30% of all known EF-hands do not bind  $\text{Ca}^{2+}$  and are therefore cryptic (Krebs & Michalak, 2007). Usually the complete EF-hand domain is 29-34 amino acids long (Myosin, CaM). In the canonical  $\text{Ca}^{2+}$  binding loop of the EF-hand (12 amino acids) the  $\text{Ca}^{2+}$  ion is coordinated by seven oxygens in a pentagonal bipyramidal configuration (Fig. 2).

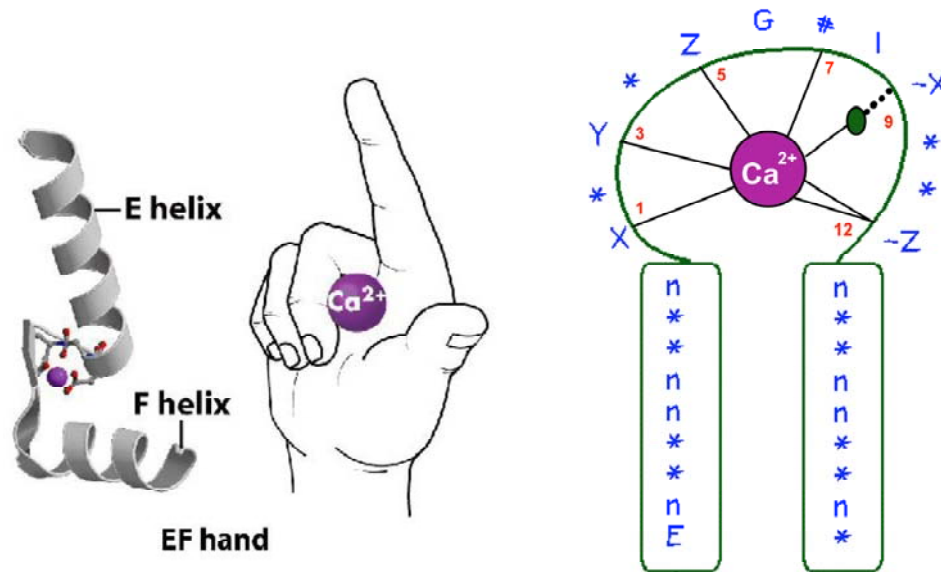


Figure 2. EF-hand. The consensus sequence for the EF-hands: E = glutamate; n = hydrophobic residue; \* = any residue; X = first calcium ligand; Y = second calcium ligand; Z = third calcium ligand; G = glycine; # = fourth calcium ligand, provided by a backbone carbonyl; I = isoleucine (although other aliphatic residues are also found at this position); -X = fifth calcium ligand; -Z = sixth and seventh calcium ligands, provided by a bidentate glutamate or aspartate residue. Modified from <http://structbio.vanderbilt.edu>

The six residues involved in the binding are in position 1, 3, 5, 7, 9 and 12; these residues are denoted by X, Y, Z, -Y, -X and -Z (Kretsinger & Nockolds, 1973). The invariant Glu or Asp at position 12 provides two oxygens for binding  $\text{Ca}^{2+}$  (bidentate ligand). Usually Asp or Asn are found at X and Y; Asp, Asn, or Ser at Z; the carbonyl oxygen of a variety of residues is a -Y; -X is more variable but usually Asp, Asn, or Ser. Despite their similar structure EF-hands might be very different in their  $\text{Ca}^{2+}$  binding affinity and extent of  $\text{Ca}^{2+}$  dependent conformational change (Krebs & Michalak, 2007). Another distinction that can be applied to EF-hands is their on-off rate of  $\text{Ca}^{2+}$  binding. A fast on-rate might be limited only by the speed of ion diffusion whereas the equilibrium dissociation constant might be variable due to the off-rate of different EF-hands, which largely depends on the amino acid at position 9 (Krebs & Michalak, 2007). In recent years, it was also shown that many  $\text{Ca}^{2+}$  binding proteins can bind magnesium cation ( $\text{Mg}^{2+}$ ) with an affinity much lower than the affinity of these proteins for  $\text{Ca}^{2+}$ .  $\text{Mg}^{2+}$  is hexagonally coordinated in the EF-hand loop but the conformation changes induced by binding are relatively small compared to  $\text{Ca}^{2+}$ . Due to high concentration of free  $\text{Mg}^{2+}$  in the cell (up to 2 mM) as compared to  $\text{Ca}^{2+}$ , most of those  $\text{Ca}^{2+}$ -binding proteins that show considerable affinity for  $\text{Mg}^{2+}$  will always be in  $\text{Mg}^{2+}$ -bound form (Aravind et al., 2008). Therefore this binding is termed structural,



indicating that it is essential for the physiological function of the protein. Thus, EF-hands that are specific for  $\text{Ca}^{2+}$  are called regulatory sites whereas those that are able to bind both  $\text{Ca}^{2+}$  and  $\text{Mg}^{2+}$  - are called structural sites.

### ***1.2.2 Neuronal calcium sensor proteins***

Neurons are excitatory cells that exhibit a highly dynamic range of free intracellular  $\text{Ca}^{2+}$  concentrations. At resting state free neuronal intracellular  $\text{Ca}^{2+}$  concentrations are estimated to be between 40-100 nM. Upon  $\text{Ca}^{2+}$  influx via L-type VDCCs or NMDARs or from intracellular stores local  $\text{Ca}^{2+}$  concentrations in postsynaptic microdomains can reach up to 15-30  $\mu\text{mol}$  (Hardingham et al., 2001; Bengtson et al., 2009; Franks & Sejnowski, 2002; Sabatini et al., 2002) and in presynaptic compartments via N- and P/Q-type VDCCs even up to hundred  $\mu\text{mol}$  (Llinas et al., 1996). This observation serves as the basis for the concept of  $\text{Ca}^{2+}$  nano- and microdomains suggested by Augustine et al. (2003). At presynaptic terminals this local evaluation of  $\text{Ca}^{2+}$  is for example involved in vesicle exocytosis and fast neurotransmitter release (Oheim et al., 2006). Postsynaptic  $\text{Ca}^{2+}$  concentrations in spine-synapses can easily reach the micromolar range without accompanying changes in the adjacent dendrite. This is due to the shape of the very narrow spine neck that serves as a diffusion barrier (Augustin et al., 2003). Thus, different types of  $\text{Ca}^{2+}$  signals in neurons are covering the wide range of physiological functions. This broad spectrum is mediated by the characteristics and properties of the different neuronal  $\text{Ca}^{2+}$  binding proteins.

Neuronal calcium sensor (NCS) proteins play multiple and divergent roles in neuronal signaling. Members of this family closely resemble the structure of their common ancestor Calmodulin with four EF-hand  $\text{Ca}^{2+}$ -binding motifs (Fig. 3). Despite their relatively high degree of similarity NCS proteins are thought to serve highly specialized functions in neurons. It is generally believed that the specificity with respect to their target interactions is brought about by either a restricted subcellular localization, differences in  $\text{Ca}^{2+}$ -binding affinities or modifications of their EF-hand structure that might provide a unique interface for protein interactions (Lewit-Bentley & Réty, 2000). The ancestral  $\text{Ca}^{2+}$  sensor CaM has four functional EF-hands with a global  $\text{Ca}^{2+}$  binding affinity of 5-10  $\mu\text{M}$  (Burgoyne, 2007).

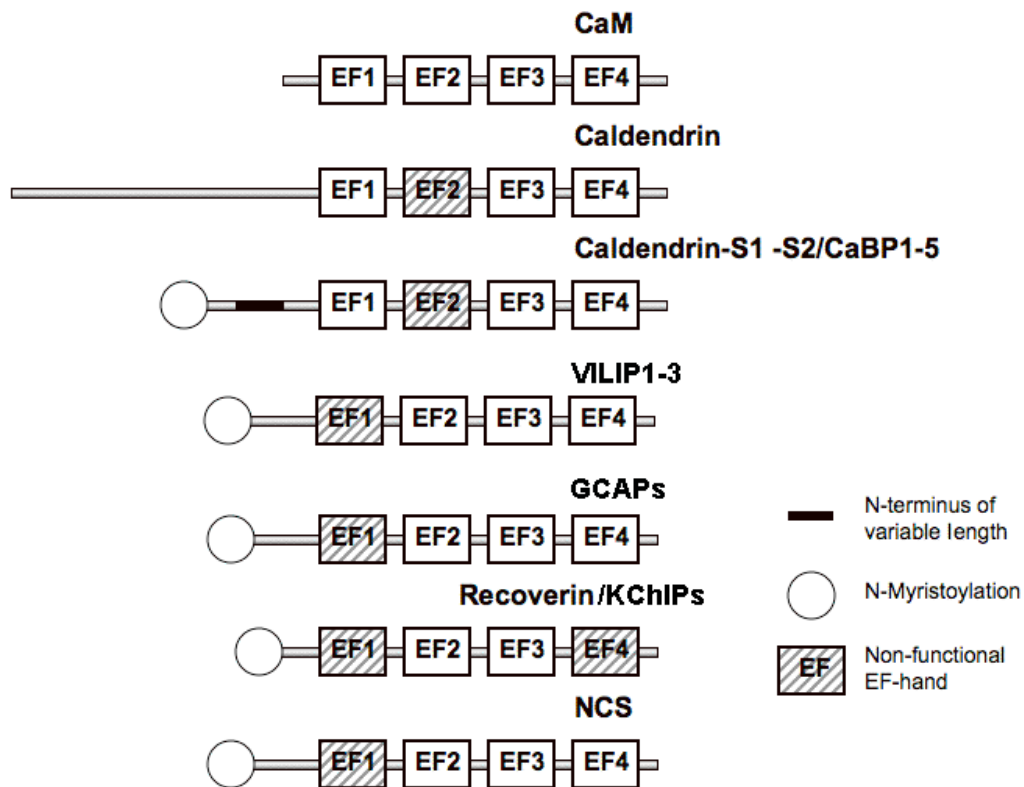


Figure 3. Schematic diagram depicting the EF-hand organization of different calcium sensor proteins that are abundantly expressed in brain and retina. N-terminal myristoylation is depicted as a round circle, nonfunctional EF-hand motif as a filled box, and N- or C-terminal extensions are represented in the appropriate proteins. CaM, VILIP1-3, GCAPs and NCS-1 represent for Calmodulin, Visinin-like proteins 1-3, Guanylate Kinase Associated Protein and Neuronal Calcium Sensor-1 respectively.

NCS proteins have like all members of the CaM superfamily a similar EF-hand organization with 4 EF-hands from which one or two of them are however non-functional in all other members apart from CaM. According to their EF-hand organization and sequence similarity, NCS proteins can be divided in different families including NCSs, Caldendrin S1-S2/CaBB1-5, VILIPs, GCAPs and Recoverin/KChIPs.

#### 1.2.2.1 NCS-1/Frequenin: Its role for regulation of PI-4K $\beta$ activity and Golgi trafficking

NCS-1 was cloned as Frequenin (Frq1) from *D. melanogaster* T(X:Y) V7 mutants. The phenotype of these mutants is associated with an enhancement of activity-dependent facilitation of neurotransmission implicating a function of the protein in the regulation of neurotransmitter release (Rivosecchi et al., 1994). Frq1/NCS-1 can be N-myristoylated and thereby attached to membranes. However the protein does not exhibit a Ca<sup>2+</sup>-myristoyl switch, a process first described for Recoverin and then other myristoylated NCS proteins (Ames et al., 1997). In the absence of Ca<sup>2+</sup>, the myristoyl group is buried in the N-terminal protein domain, surrounded on all sides by alpha helices that form a hydrophobic pocket.

The binding of  $\text{Ca}^{2+}$  induces a conformational change that extrudes the myristoyl and exposes some hydrophobic amino acids on the surface. This enables the molecule to bind to the lipid bilayers of intracellular membranes (Tanaka et al., 1995; Ames et al., 1997). NCS-1 contains 4 EF-hands while the first EF-hand is cryptic (Fig. 2). NCS-1 is a high affinity calcium sensor (global calcium affinity around 100 nM / Aravind et al 2008) and NCS-1 was shown to regulate numerous cellular processes (Fig. 3). Knock down of NCS-1a, one of the two closely related NCS-1 genes in zebrafish, abolishes formation of the semicircular canals of the inner ear (Blasiolo et al., 2005). Changes in neuronal function are seen in *D. melanogaster*, in which overexpression of the NCS-1 orthologue Frq1 resulted in increased facilitation of neurotransmission (Fig. 4 / Pongs et al., 1993). In *C. elegans*, a knockout of NCS-1 impaired learning and memory (Gomez et al., 2001). NCS-1 is expressed highly in all brain regions and also in many non-neuronal cell types (Burgoyne, 2007).

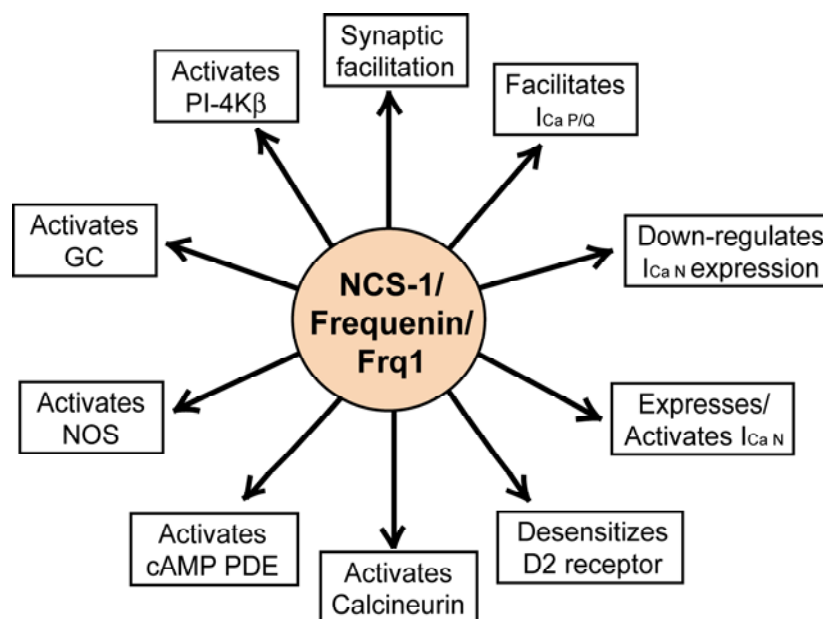


Figure 4. Overview reported/proposed functions of Frq1/NCS-1 proteins. GC – Guanylyl Cyclase; NOS – Nitric oxide synthase; cAMP PDE – cAMP phosphodiesterase, I<sub>Ca</sub> –  $\text{Ca}^{2+}$  current (P/Q or N-type). Modified from Stockebrand&Pongs, 2006.

An important advance in the understanding of NCS-1 function was the discovery that Frq1 is essential for survival in yeast due to its ability to activate Pik1, one of the two phosphatidylinositol-4-OH kinases (Hendricks et al., 1999). It was subsequently shown that the vertebrate orthologue NCS-1 can activate the closely related mammalian enzyme PI-4K $\beta$  (Fig. 4), and thereby increase the production of PI(4)P and facilitate Golgi to plasma

membrane trafficking (Balla & Balla, 2005). The lab of Robert D. Burgoyne has shown that NCS-1 localizes, in a  $\text{Ca}^{2+}$ -independent manner, at the Golgi whereas it interacts in a  $\text{Ca}^{2+}$ -dependent manner with the GTPase ADP-ribosylation factor 1 (ARF1), leading to the recruitment of PI-4K $\beta$  to the Golgi and the modification of membrane trafficking (Haynes et al., 2005; Haynes et al., 2007). On the other hand, data from the lab of Tamas Balla suggest that the activation of PI-4K $\beta$  by NCS-1 is  $\text{Ca}^{2+}$ -independent (Zhao et al., 2001). To date, NCS-1 is the only NCS protein known to interact with PI-4K $\beta$  whereas other members of this family, like Recoverin (Hendricks et al., 1999) apparently do not modulate PI-4K $\beta$  activity.

#### *1.2.2.2 The Caldendrin/CaBP1-5 gene family*

The postsynaptic density (PSD) of spinous excitatory synapses is characterized by an electron-dense filamentous meshwork of cytoskeletal proteins that are thought to be crucially involved in the topological organization of synaptic signaling pathways (Kennedy et al., 2005). In a search for protein components of the PSD a  $\text{Ca}^{2+}$  sensor protein subsequently called Caldendrin was identified, that was highly abundant in the somato-dendritic compartment of mainly principal neurons in brain regions with a laminar organization like cortex or hippocampus (Seidenbecher et al., 1998). Caldendrin harbors a bipartite structure with an N-terminus not related to entries in public databases that is highly basic, and a C-terminal part that resembles the EF-hand-structure of CaM with four EF-hands from which the second one is cryptic (Fig. 3 / Seidenbecher et al., 1998; Laube et al., 2002). With respect to its C-terminal part Caldendrin is the closest homologue of CaM expressed in brain, and it turned out to be the founding member of an entire gene family termed CaBPs by Haeseleer and colleagues (Haeseleer et al., 2000; Haeseleer et al., 2002). The family derives from five different genes that give rise to a number of differently spliced isoforms. In case of Caldendrin two shorter isoforms were identified termed Caldendrin S1 and S2 (Laube et al., 2002) or L-CaBP1 or S-CaBP1 (Haeseleer et al., 2000). These isoforms arise by usage of an alternative exon downstream of exon 1 of the Caldendrin gene, which harbors an alternative start codon and thereby generates an N-terminus that is shorter than that of the long form. Another splice variant derives from the insertion of a third exon located further downstream of exon 2 (Laube et al., 2002). All Caldendrin / CaBP family members share the same EF-hand organization while their N-termini vary considerably in length and structure (Fig. 3). The functional implication of this variability is at present unclear, but it is conceivable that the different N-termini might be important for the

subcellular distribution of the proteins. It should also be noted in this regard that CaBPs, but not Caldendrin, can be N-terminal myristoylated, which could provide a lipid anchor to cellular membranes (Fig. 3).

Surprisingly, apart from Caldendrin all other family members are very low abundant in the brain, although they could be localized to neuronal cells in retina (Haeseleer et al., 2000, Sokalet al., 2000; Haeseleer et al., 2004). Thus, it seems that the Caldendrin promoter is unique within the gene family driving expression in mainly principal neurons like pyramidal cells. During the primary characterization of the protein a number of other interesting features could be revealed. In brain, Caldendrin is highly enriched in the PSD fraction and immunolocalized to dendritic spines and the dendritic shaft (Seidenbecher et al., 1998; Laube et al., 2002; Bernstein et al., 2003). The protein occurs as two protein isoforms of 33 kDa and 36 kDa, which derive from the same primary translation product. Upon subcellular fractionation of rat brain proteins, a significant amount of the 33 kDa isoform is found in both, the soluble as well as the detergent-insoluble particulate fraction. In contrast, the 36 kDa protein isoform is tightly associated with the cortical cytoskeleton and extraction conditions for the 36 kDa isoform from the particulate fraction are similar to those of core components of the PSD (Seidenbecher et al., 1998; Laube et al., 2002). Both its unique bipartite structure and the differential association with subcellular compartments suggest that Caldendrin serves functions different from those of known NCS proteins. Previous work suggests that this function might be related to the organization of the postsynaptic scaffold (Seidenbecher et al., 1998; Laube et al., 2002; Smalla et al., 2003) as well as the control of NMDAR-activated morphogenetic signaling to the nucleus (Dieterich et al., 2008). Of particular interest is also the observation that the association of Caldendrin with the PSD is stimulus-dependent and that enhanced synaptic activity leads to higher Caldendrin-levels in the PSD and a recruitment to the postsynapse *in vivo* and *in vitro* (Smalla et al., 2003, Schultz et al., 2004; Dieterich et al., 2008).

During the course of its functional characterization a number of potential interaction partners for Caldendrin and its shorter splice isoforms were identified that constitute  $\text{Ca}^{2+}$  channels and it has been therefore hypothesized that Caldendrin might be a multifunctional regulator of intracellular  $\text{Ca}^{2+}$  levels (Seidenbecher et al., 2002). Interactions of Caldendrin / CaBP1 have been reported with transient receptor potential channels (TRPC / Kinoshita-Kavada et al., 2005; Kreutz et al., 2006),  $\text{Ca}_v2.1$ ,  $\text{Ca}_v1.2$   $\text{Ca}^{2+}$  channels (Zhou et al., 2004; Lee et al., 2005) as well as with the IP3Rs (Haynes et al., 2004; Zhou et al., 2005). The

functional consequences of Caldendrin binding to these channels range from a facilitation of presumably postsynaptic L-type-  $\text{Ca}_v1.2$  channels (Lee et al., 2002) and thereby increased synaptic  $\text{Ca}^{2+}$  influx to an inhibition of IP3-induced  $\text{Ca}^{2+}$  release through IP3Rs (Haynes et al., 2004; Zhou et al., 2005). Interestingly the interaction of Caldendrin with  $\text{Ca}^{2+}$  channels in most cases is  $\text{Ca}^{2+}$ -independent (i.e. IP3Rs,  $\text{Ca}_v2.1$  and presumably  $\text{Ca}_v1.2$  channels). Based on these findings, it was proposed that Caldendrin depending upon its activity-dependent localization to different subcellular microdomains like the synapse might trigger different target interactions. Binding to L-type VDCC at the synapse will probably lead to increased  $\text{Ca}^{2+}$  currents following synaptic activation and thereby can indirectly promote Caldendrin's association with the PSD. In contrast, low synaptic activity and in consequence low dendritic  $\text{Ca}^{2+}$  levels might shift the balance of caldendrin binding to a preferential interaction with the IP3Rs, which is more prominently localized to the smooth ER in dendrites than in spine synapses. Binding to the IP3Rs will thereafter further reduce intracellular  $\text{Ca}^{2+}$  levels. Thus, Caldendrin will potentially trigger different target interactions in a manner that is controlled by synaptic activity and its subcellular localization and in consequence could even amplify existing differences in synapto-dendritic  $\text{Ca}^{2+}$  signaling within a neuron. Interestingly, this in turn could possibly also feed back to Caldendrin's own  $\text{Ca}^{2+}$ -dependent target interactions in the synapse and to its suggested role in synapse-to-nucleus communication.

#### *1.2.2.3 Jacob is a Caldendrin interaction partner in the synapse*

In a search for other interaction partners of the C-terminal half of Caldendrin with particular interest to find synaptic proteins, a yeast two hybrid (Y2H) screen from rat brain cDNA library was performed. One of the specific Caldendrin-binding partners was a novel protein termed Jacob. During its primary characterization we have found that Jacob is prominently present in cortical and limbic brain regions and displays considerable overlap with the distribution of Caldendrin. Jacob is present in the PSD as well as associated with highly purified nuclear fractions. The Jacob gene contains 16 exons and can be alternatively spliced to form up to 12 different isoforms. The longest and most abundant one is 532 amino acids long (Fig. 5). Analysis of the primary structure of Jacob revealed a putative N-terminal myristoylation site (confirmed later by experiments) and several potential phosphorylation sites for a variety of protein kinases including ERK1/2 kinases, cdk5, protein kinase C (PKC), cAMP-/cGMP-dependent protein kinases and protein tyrosine kinases (Fig. 5). In addition, Jacob harbors a well-conserved bipartite nuclear localization signal (NLS). The

NLS of Jacob is functional and responsible for NMDAR-dependent nuclear translocation of Jacob (Dieterich et al., 2008). Interestingly, this NLS is part of an incomplete IQ motif - a protein-protein interaction region characteristic for CaM binding (Dieterich et al., 2008). The IQ motif was first characterized in myosins by Cheney and Mooseker (1992). Proteins that contain IQ motifs typically bind CaM in the absence of  $\text{Ca}^{2+}$ , although there are some exceptions. The IQ domain is approximately 25 amino acids in length and is widely distributed in nature. The motif consists of the consensus sequence [I,L,V]QxxxRGxxx[R,K], which forms an amphiphilic seven-turn  $\alpha$ -helix capable of binding CaM. Proteins found to contain at least one IQ domain include myosins, voltage-operated channels, several neuronal growth proteins, phosphatases, sperm surface proteins, Ras exchange proteins, spindle-associated proteins and a RasGAP-like protein (Krebs & Michalak, 2007). In previous work the interaction region between Caldendrin and Jacob was mapped using a Y2H approach. It turned out that indeed the first two EF-hands of Caldendrin and the NLS in Jacob are essential for the interaction to happen. In further experiments it was shown that the Caldendrin-Jacob interaction is  $\text{Ca}^{2+}$ -dependent and deletion of the first six basic residues of the NLS led to significantly reduced Caldendrin binding in pull down assays (Dieterich et al., 2008).

#### *1.2.2.4 The identification of Calneurons*

Taken together the evidence so far points to an important role of Caldendrin in many aspects of neuronal  $\text{Ca}^{2+}$  signaling and it was therefore rather surprising that the shorter Caldendrin splice isoforms and the other CaBP family members that share the same EF-hand organization and show a high degree of homology are only prominent in retina. A search in public databases, however, revealed several EST- and cDNA clones from brain tissue that show significant similarity to the first two EF-hands of Caldendrin / CaBPs and CaM. Further analysis of these clones disclosed the existence of two highly homologous proteins, the sequence of one of which has been published previously under the name of Calneuron (Wu et al., 2001). Based on our initial characterization we decided to introduce the name Calneuron for both proteins to indicate that they are CaBPs prominently present in neurons and constitute a new subfamily of CaM-like calcium sensors closely related to but distant from Caldendrin/CaBPs.

### ***1.2.3 Aims of the study***

(i) To extend the characterization of Caldendrin – one of the most unique neuronal calcium sensors and its interaction partner Jacob in terms of the cellular function of this interaction.

(ii) To provide a functional characterization of the novel subfamily of neuronal calcium sensor proteins of Calneurons, and to learn more about their role in neuronal Ca<sup>2+</sup> signaling.



## 2 Materials and methods

### 2.1 Materials and production of materials

#### 2.1.1 Chemicals

All chemicals were obtained from Roche, Calbiochem, Clontech, Gibco Life Technologies, Invitrogen, Merck, Roth, Serva and Sigma-Aldrich.

#### 2.1.2 Enzymes and kits

Table 1. Enzymes and kits.

Name	Supplier
Restriction enzymes	New England Biolab
Taq DNA polymerase	Fermentas
Pfu-Turbo DNA polymerase	Startagene
Klenov DNA polymerase	Amersham
Alcaline phosphatase from calf intestin	Roche
T4 ligase	Invitrogene
RNase H	New England Biolab
$\alpha$ -Chymotrypsin	Sigma-Aldrich
Aprotinin	Sigma-Aldrich
dNTPs	Invitrogene
Primers/Oligomers	Invitrogene
Nucleospin PCR cleanup gel extraction Kit	Macherey-Nagel
Quik mutagenesis kit	Stratagene
pGEM®-T Easy Vector System	Promega
Champion™ pET-SUMO TA Cloning kit	Invitrogene
mMESSAGE mMACHINE® High Yield Capped RNA Transcription Kit	Ambion
hGH-Sensitiv ELISA	Mediagnost
PI(4)P mass strip kit	MoBiTec
Thrombin Cleavage Capture Kit	Novagene

#### 2.1.3 cDNA constructs

cDNA constructs and vector systems used in this study are described in the supplementary Table 1 and 2. The novel calcium binding proteins Calneuron-1/CaBP8 (accession number XM344102) and Calneuron-2/CaBP7 (accession number AY841152) were cloned in our lab from a rat brain cDNA (produced by Dr. P. Landgraf) into pGEM-Teasy plasmid and subsequently subcloned into the other vectors either directly or by a PCR approach. The new Caldendrin constructs were subcloned by cutting out the insert with compatible restriction sites from existing vectors or by PCR with Caldendrin full length in pRC as the template. NCS-1 was subcloned into pEGFP-N1 vector from a pEYFP-N1 construct obtained from Dr. A. Jeromin.

For RNAi treatment, oligonucleotides with the sense/antisense sequence (19–21 bp) linked by a 9- or 10-bp–long stemloop sequence were obtained from Biomers. Caldendrin

sRNAi (5' TCC TGG CGG AGA CAG CAG ATA 3'/bp 665–685 of Caldendrin cDNA) and Caldendrin scrambled (5' AGA ATC CTA AGA CAA GTG CAG 3'). Forward and reverse oligos were annealed, phosphorylated, and cloned using the BamHI and HindIII restriction sites into the pRNAT-H1.1/Neo vector (Genscript) for plasmid-based RNAi knockdown. 29-mer shRNA constructs against Calneuron-1 in pRS-GFP and scrambled controls were generated by Origene (ams Biotechnology, Abingdon, UK). After RNAi construct validation (by immunostaining and immunoblots) the most efficient sequence (5'-GCA-GCC-AAC-CAG-ATC-CTG-CGG-AGC-GGC-AT-3') and scrambled control (non-effective GFP shRNA) were selected for further experiments.

#### ***2.1.4 Cloning of Jacob constructs into a Semliki Forest Virus vector and production of viral particles***

For transfection of adult neurons in primary culture with Jacob constructs a Semliki Forest Virus (SFV / Invitrogene, Karlsruhe, Germany) was used. Jacob was cloned into pSFV1 using SmaI site of pSFV and blunt ligation. pSFV1 was digested with SmaI at 25°C overnight and dephosphorylated by Alkaline Phosphatase for 1 h at 37°C. A Jacob-GFP insert was cut out from a pEGFP-N1 vector with EcoRI/NotI and blunt ends were created by a filling in reaction with nucleotides using dNTPs and Klenow polymerase. The plasmid was ligated with the insert overnight. After transformation of bacteria single colonies were isolated and plasmid DNA was purified by a standard miniprep method. The orientation of the insert was checked by restriction with BamHI (this site is present in front of the insert in pSFV1 and also between Jacob and GFP), positive clones were sequenced and amplified by a maxiprep. pSFV-Δ-Myr-Jacob-GFP or pSFV-GFP and pSFV-Helper constructs were linearized with at SpeI site and in vitro transcribed with mMACHINE® High Yield Capped RNA Transcription Kit according to the manufacturers manual. RNA was checked by agarose gel and co-transfected with Lipofectamine 2000 (Invitrogene, Karlsruhe, Germany) into packaging CHO-K1 cells. Media was collected 24, 48 and 72 hrs after transfection and particles were concentrated by ultracentrifugation in a 10% sucrose gradient. Aliquots of inactive virus were stored at -80°C. Shortly before infection SFV particles were activated with α-Chymotrypsin (10 mg/ml) for 45 min at room temperature, then the reaction was terminated with the trypsin inhibitor Aprotinin (0,5 mg/ml) and the virus could then be used for infection of primary neuronal cultures within the next 3 days. The efficiency of infection was optimized on CHO-K1 cells or cortical primary neurons by

titration of virus and counting the number of cells expressing GFP for each construct individually.

### **2.1.5 *In situ hybridization (oligonucleotides)***

*In situ* hybridization was performed exactly as described previously (Laube et al., 2002). Oligonucleotide sequences for Calneurons were as follows: Calneuron-1 [antisense: 5'-gcc aac tgc tca ctg tgc ctg cctg cag aca gag atc gg-3' / sense control: 5'-ccg atc tct gtc tgc agg cag cga cag tga gca gtt ggc-3']; Calneuron-2: [antisense: 5'-gcg ctg ctc cga cag cag gtt ggg cac ggt gta ga-3' / sense control: 5'-tct aca ccg tgc cca acc tgc tgt cgg agc agc gc-3']. In control experiments adult rat brain sections were either treated prior to hybridization with RNase H or hybridized with the corresponding sense controls.

### **2.1.6 *Generation of Calneuron-specific antibodies***

Full length recombinant MBP-Calneuron-1 and MBP-Calneuron-2 were produced and purified from bacteria using amylose resin (a purification procedure is described below) and sent to Biogenes (Berlin, Germany) for the production of polyclonal antibody. Each protein was injected 3 times (1<sup>st</sup>, 4<sup>th</sup> and 14<sup>th</sup> days) to 2 different rabbits. Over a 6-month period serum samples were collected and analyzed for the presence of Calneuron-specific antibodies by immunoblot with injected antigens and brain homogenates. Both rabbits produced antibodies recognizing the recombinant protein but only one of them for Calneuron-1 as well as for Calneuron-2 was detecting the endogenous protein. After 6 months immunoserum was collected and stored at -80°C. For the western blot experiments and immunostaining the antiserum was additionally purified with his-SUMO-Calneuron-1 or preincubated with MBP to remove the antibody against MBP. 300 µg of recombinant his-SUMO-Caln-1 were loaded on a SDS-PAGE. After electrophoresis and blotting the nitrocellulose membrane was stained with ponceau and dried. The bands corresponding to Calneuron were cut out, blocked with blocking buffer for 1.5 hrs at RT and incubated with 1 ml of antiserum overnight at 4°C. On the next day the pieces of membrane were extensively washed with wash buffer and antibodies were eluted with glycine elution buffer. The low pH of eluted probes was immediately adjusted to 7.4, mixed with 50% Glycerol and the recovered antibodies were finally stored at -20°C.

### 2.1.7 Antibodies used for IB, IF and IPs

The primary and secondary antibodies used for immunoblots (IB), immunofluorescence (IF) and immunoprecipitations (IP) are presented in the tables below.

Table 2. List of the primary antibodies with the dilutions used.

Antibody	Supplier	Species	Applications and Dilutions tested	Remarks
Calneuron-1	Generated in the lab/Biomers	rabbit polyclonal	IB 1:500 IF 1:100 IP	
Calneuron-2	Generated in the lab/Biomers	rabbit polyclonal	IB 1:500 IF 1:100 IP	
Calneuron-1	Abnova, Tebu-bio, Taiwan	mouse polyclonal	IB 1:1000-2000 IF 1:500	Good for IF
Calneuron-2/CABP7	Abnova, Tebu-bio, Taiwan	MaxPab mouse polyclonal antibody	IB 1:1000	Does not work for IF
Caldendrin	Generated in the lab/ Dr. Pineda Antibody-Service	guinea pig	IB 1:2000 IF 1:200	
Caldendrin	Generated in the lab/ Dr. Pineda Antibody-Service	rabbit (Farlchen)	IB 1:2000 IF 1:200 IP	
NCS-1	Santa Cruz Biotechnology Inc., Santa Cruz, California, USA	rabbit polyclonal	IB 1:1000 IF 1:100 IP	
PI-4K $\beta$	Transduction Laboratories, Heidelberg, Germany	mouse monoclonal	IB 1:5000 IF 1:500	
SNAP25	Transduction Laboratories, Heidelberg, Germany	mouse monoclonal	IF 1:100	
Syntaxin-6	Synaptic Systems, Goettingen, Germany	rabbit polyclonal	IB 1:1000 IF 1:500	
TGN38	Novus Biologicals; Littleton, UK	mouse monoclonal	IF 1:100-1:500	Very good for IF
GM130	Abcam, Cambridge, UK	rabbit polyclonal	IF 1:500	A very good golgi marker
Calreticulin	Upstate biotechnology, Lake Placid, NY, USA	rabbit polyclonal	IF 1:200	Fuzzy staining
Piccolo	Obtained from Dr. A. Fejtova	Guinea pig	IF 1:800	Very good for IF
GFP	BabCO/Covance, Berkeley, California, USA	mouse monoclonal	IB 1:2000	Only IB
GFP	Abcam	rabbit polyclonal	IB 1:2000	
Synaptophysin	Stressgene, Hines Drive, USA	Mouse monoclonal	IF 1:100	
$\beta$ -Cop	Sigma, Saint Louis, Missouri, USA	mouse monoclonal	IF 1:200	
$\beta$ -Actin	Sigma, Saint Louis,	mouse	IB 1:4000	Antibody also work at

	Missouri, USA	monoclonal		RT – 3 hrs incubation
MAP2	Sigma, Saint Louis, Missouri, USA	Mouse monoclonal	IF 1:800	Antibody also work at RT – 3 hrs incubation
CREB	Zymed (Invitrogene), Carlsbad, CA, USA	Mouse monoclonal	IB 1:2000	
pCREB	Upstate biotechnology, Lake Placid, NY, USA	rabbit polyclonal	IB 1:1000 IF 1:100	Very good for IF, require BSA blocking for IB
Jacob (jac2gp2)	Generated in the lab	guinea pig	IB 1:2000	Recognize low MW isoforms
JB150	Generated in the lab/ Dr. Pineda Antibody-Service	rabbit polyclonal	IB 1:2000 IF 1:250 IP	Recognize high MW isoforms, very good for IF
Karyopherin $\alpha$ /Rch-1 (Importin $\alpha$ 1)	BD Biosciences, Heidelberg, Germany	mouse monoclonal	IB 1:1000 IF 1:100	
6x-his	Cell Signaling, Frankfurt am Main, Germany	mouse monoclonal	IB 1:2000	Gives high background staining

Table 3. List of the secondary antibodies with dilutions used.

Antibody	Supplier	Species	Applications and Dilutions tested
immunoglobulins-HRP linked secondary antibody	DakoCytomation, Denmark	mouse	IB 1:5000
immunoglobulins-HRP linked secondary antibody	DakoCytomation, Denmark	Guinea pig	IB 1:5000
immunoglobulins-HRP linked secondary antibody	Cell Signaling, NEB, Frankfurt am Main	rabbit	IB 1:5000
Alexa Fluor 488	Molecular Probes Europe BV, Leiden, The Netherlands	rabbit	IF 1:1000
Alexa Fluor 568	Molecular Probes Europe BV, Leiden, The Netherlands	mouse	IF 1:1000
Alexa Fluor 488	Molecular Probes Europe BV, Leiden, The Netherlands	Guinea pig	IF 1:1000
Cy <sup>TM</sup> 5-conjugated AffiniPure goat	Dianova, Hamburg, Germany	rabbit	IF 1:1500
Cy <sup>TM</sup> 5-conjugated AffiniPure goat	Dianova, Hamburg, Germany	mouse	IF 1:1500

### 2.1.8 Common buffers and cell culture media

Common buffers and cell culture media used in the study are listed in Supplementary Table 3 and 4. Some specific buffers are described directly in the methods.

### 1.2.9 Prokaryotic and eukaryotic cell lines.

Cell line	Supplier	Application
<i>E.coli</i> XL1-BlueMRF	Stratagene	Electrocompetent bacteria; pDNA amplification
<i>E.coli</i> BL21(DE3)	Invitrogene	Chemically competent bacteria; protein production

COS-7 cells		Eukaryotic protein production, transfections and immunocytochemistry
CHO-K1	Invitrogene	Packaging cell line for Semliki Forest Virus
PC12		hGH release assay

### **1.2.10 Animals**

In this work Wistar rats from the Leibniz Institute for Neurobiology (Magdeburg, Germany) animal facilities were used. All animal housing and experimental procedures were authorized and approved by the Institutional State and Federal Government regulations (Land Sachsen-Anhalt, Germany).

## **2.2 Methods**

### **2.2.1 Cell culture, transfections and immunocytochemistry**

Hippocampal and cortical neurons were isolated at embryonic day 18, plated and cultured as described previously (Dieterich et al., 2008). For overexpression and knock down studies neurons were transfected with 1 µg of total pDNA and 1 µl of Lipofectamine 2000 per 12 mm coverslip according to the manufacturers protocol. At the proper stage depending upon the experiment neurons were fixed with 4% paraformaldehyde (PFA) for 10 min, washed 3 times with phosphate buffered saline (PBS), permeabilized with 0,25% TritonX-100 in PBS for 10 min, washed again and blocked for 1 hour in blocking buffer containing 2% Glycine, 2% BSA, 0,2% Gelatine, 50 mM NH<sub>3</sub>Cl (pH 7,4). Primary antibody were diluted in the blocking buffer and incubated overnight at 4°C. After extensive wash the secondary antibody (also in blocking buffer) were applied for 1.5 hours at RT in darkness. Coverslips were washed then again with PBS 3 times for 10 min and 1 time with water and fixed on the slides with Mowiol (Merck, Darmstadt, Germany). COS-7 cells were grown on coverslips for immunocytochemistry or in cell culture flasks (75 cm<sup>2</sup>) for protein production in DMEM medium for 24 hours after seeding. Transfection was done using 0,7 µg of pDNA and 2 µl of PolyFect reagent per 12 mm coverslip or 12 µg of pDNA and 40 µl of Polyfect according to the manufacturers protocol (Qiagen, Hilden, Germany). Cells were harvested or fixed 48 hours after transfection. Immunofluorescence stainings of COS-7 were done with the same protocol as described for the primary neurons. CHO-K1 cells were cultured in F12 media and used for the production of SFV particles.

### **2.2.2 Stimulation of primary hippocampal neurons**

Synaptic or extrasynaptic stimulation primary hippocampal neurons were done at DIV16-18 according to the protocol from Hardingham et al. (2002). Following concentrations of agonists and antagonists were used: NMDA (50  $\mu$ M), Ifenprodil (10  $\mu$ M), Biccuculine (50  $\mu$ M), 4-AP (2,5 mM), MK-801 (10  $\mu$ M), Anysomycin (7,5  $\mu$ M). For the pCREB stainings after different types of stimulation 1  $\mu$ M of tetrodotoxin (TTX) was added to cultures 12 hours before stimulation to reduce endogenous synaptic activity and “set” the pCREB at the same level in all neurons. All of the drugs were added directly to the medium, and during the incubation the neurons were kept in the 5% CO<sub>2</sub> incubator.

### **2.2.3 Confocal laserscan microscopy**

Images were taken with 63x oil objective as z-stacks (300 nm z step for COS-7 cells and 126 nm for high resolution images of neurons used for quantifications) using a Leica DMRXE microscope (Wetzlar, Germany) equipped with a Krypton-Argon-Ion laser (488/568/647 nm) and an acousto-optic-tunable filter (AOTF) for selection and intensity adaptation of laser lines. Maximum intensity projections were calculated from each fluorescence channel of the image-stack and analyzed with ImageJ software (<http://rsb.info.nih.gov/ij>). For 3D reconstruction and volume rendering Imaris software (Version 6.2, Bitplane) was applied.

### **2.2.4 Immunoblotting**

For protein detection standard western blot protocols were applied (Seidenbecher et al., 2004). Briefly, protein samples were solubilised in SDS-loading dye, denaturated for 5 minutes at 95°C and loaded on a SDS-PAGE. The protein amount loaded varied from 10 to 40  $\mu$ g of protein depending upon the experiment. Gels were blotted on a nitrocellulose membrane, stained with ponceau for 10 min and then blocked for 1.5 hrs at room temperature (RT) with 5% low fat milk in TBS-T buffer. When using Calneuron-1, -2 or Caldendrin antibodies 5% BSA fraction V in TBS-T buffer was used for blocking in order to reduce background. After blocking primary antibody diluted in TBS-A buffer were applied and the membrane was incubated overnight at 4°C on a shaker. After extensive washing with TBS and TBS-T buffers secondary antibody diluted in 5% milk in TBS-T buffer were added for 1.5 hrs at the RT. Protein bands were detected by chemiluminescence with standard ECL solution (Pierce).

### **2.2.5 Subcellular fractionation and microsomal preparation**

Subcellular fractionation was performed as described earlier (Smalla et al., 2003). The detail scheme of this preparation with the buffers used can be found in Supplementary Scheme 1 and Supplementary Table 6. For immunoblot analysis of subcellular fractions 25 µg protein were loaded per lane, equal protein loading was ensured by measuring the protein concentration with AmidoBlack and by densitometric measurements of equivalent lanes on a Coomassie brilliant-blue stained SDS-PAGE using a GS-800 gel-scanner and Quantity-One software (Bio-Rad; Hercules, USA). The microsomal fraction obtained during subcellular fractionation was further extracted with lysis buffer (10 mM Tris-HCl, 150 mM NaCl, 1% Triton X-100, 2 mM dithiothreitol (DTT), protease inhibitor cocktail Complete™ (Roche); pH 7.5). The complexes from the microsomal extract were analyzed on a gel filtration column. The first preparation was done at low Ca<sup>2+</sup> conditions due to the presence of 1 mM of EDTA in the homogenization buffer in order to check whether calcium might play a role in the association of NCS-1 and Calneurons with PI-4Kβ in vivo. The microsomal preparation was subsequently repeated using Ca<sup>2+</sup> and also under Ca<sup>2+</sup>-free conditions. Briefly, rat brains were homogenized in cold TBS buffer (10 mM Tris-HCl, 150 mM NaCl, pH 7.5) containing 2 mM of CaCl<sub>2</sub> and 1 mM of MgCl<sub>2</sub> or 2 mM of EGTA and 1 mM of MgCl<sub>2</sub> in a ratio 1 g of tissue in 15 ml of buffer. After 10 min centrifugation at 1000xg the supernatant was collected. The pellet (P1; nuclei and cell debris) was re-suspended in the corresponding buffers and centrifuged second time for 10 min at 1000xg. Supernatant fractions from the first and second centrifugation step (S2) were mixed and centrifuged for 15 min at 12.000xg (also see Suppl. Scheme 1). Supernatants were removed and the pellet washed with the same homogenization buffers. The P2 (crude membrane) fraction was re-homogenized in extraction buffer containing additionally 1% TritonX-100, incubated on ice for one hour and then centrifuged at 100.000xg for 1h. The pellets (P3) obtained after this step which represent the microsomal fraction were re-suspended in a double volume of the Ca<sup>2+</sup> or Ca<sup>2+</sup>-free TBS buffer and stored at -80°C.

### **2.2.6 Gel filtration**

For the separation of microsomal complexes by molecular weight gel filtration experiments were performed. 500 µl of microsomes containing approximately 6 mg of protein were re-suspended in 5 ml of lysis buffer, incubated for 30 min on ice and subsequently centrifuged at 100.000xg for 1hour. From the remaining supernatant 2 ml



(about 2.5 mg of protein) were separated on a HR16/60 HiLoad Superdex200 gel filtration column (Amersham Biosciences/GE Healthcare) implemented in a FPLC system (Amersham Biosciences/GE Healthcare) and calibrated according to manufacturers instructions using a gel filtration calibration kit (Gel Filtration HMW Calibration Kit, Amersham Biosciences/GE Healthcare). For further analysis 1.5 ml fractions were collected. The first 20 fractions represented the void volume of the column and were discarded. Fractions from number 20 to 80 were precipitated with acetone overnight at -20°C, washed with ice-cold 70% ethanol and lyophilized. Dry pellets were solubilized in 50 µl SDS-PAGE loading buffer and analyzed by western blot analysis using different antibodies. In the first preparation 7 µl of every second fraction were loaded on the gel and checked with PI-4Kβ, Calneuron-1 and 2, NCS-1 and Syntaxin 6 antibodies (the latter one was applied as the proof for an enrichment of Golgi proteins). On the second run the gel filtration was performed in the same manner but all buffers contained 2 mM of CaCl<sub>2</sub> and 1 mM of MgCl<sub>2</sub> or 2 mM of EGTA and 1 mM of MgCl<sub>2</sub>. The same blots were processed with different antibodies.

### ***2.2.7 Co-immunoprecipitation***

COS-7 cells transfected with Calneuron-1-GFP, Calneuron-2-GFP, NCS-1-GFP or GFP were harvested and washed with ice-cold 1xTBS buffer. 500 µl of lysis buffer was added to the pellet from each flask and samples were incubated for 30 min on ice. After centrifugation for 20 min at 100.000xg the supernatant was collected and incubated with 5 µg of rabbit Calneuron-1, Calneuron-2, Caldendrin, NCS-1 antiserum or control rabbit IgG at 4°C for 2 hrs. 50 µl of protein A-sepharose beads were added to the reaction tube and incubated further overnight at 4°C. Then the beads were washed 3 times with 1 ml of the same buffer following centrifugation at 500xg, and were then finally eluted with 30 µl of 2xSDS sample buffer and immunoblotted using mouse GFP and PI-4Kβ antibodies. For co-immunoprecipitation of endogenous proteins 1g of total brain tissue from adult rats was homogenized in 10 ml of cold lysis buffer, incubated for 30 min on ice and then centrifuged at 100.000xg for 1h. All proteins of interest were detectable in the soluble fraction. Co-immunoprecipitation was done as described above from 500 µl of this supernatant.

### ***2.2.8 Bacterial expression and purification of recombinant proteins***

Glutathione S-transferase (GST) alone or fusion proteins of Caldendrin-C-terminus-GST, GST-PI-4Kβ were expressed in BL21(DE3) bacteria. 4-8 hrs after induction the

recombinant fusion proteins were isolated from the bacterial lysates. After French press and sonication in 1x TBS buffer containing 1% TritonX-100 the proteins were purified from the soluble fraction by glutathione agarose chromatography. Columns with sepharose bound Caldendrin-C-terminus-GST, GST-PI-4K $\beta$  or GST were extensively washed with Ca<sup>2+</sup>-free (treated with Chelex100, Bio-Rad) TBS buffer and aliquots of these beads were used for pull down assays. For PI-4K $\beta$  activity the enzyme was cleaved from the GST tag with thrombin according to the manufacturers manual.

Untagged Caldendrin, Calneuron-1 and myristoylated NCS-1 (myr-NCS-1) were purified from the BL21 bacterial strain after expression with pET21 vectors (for NCS-1 and Caldendrin) and pTrcHis2B (for Calneuron-1) using hydrophobic columns (Aravind et al., 2008). The expression yield of Calneuron-2 in both of these vectors was not sufficient for its purification by this technique. Myristoylated NCS-1 was prepared by co-transformation of N-myristoyl transferase in a pBB131 vector. After induction of protein expression with 0,5 mM IPTG, bacteria were incubated at 37°C overnight in the presence of myristic acid (10 mg/l) and sodium myristate (30 mg/l). NCS-1 was purified using a phenyl-sepharose fast flow matrix (Pharmacia, Munich, Germany) by binding of bacterial extract to the column in the presence of 2 mM Ca<sup>2+</sup> and 1 mM Mg<sup>2+</sup> in TBS buffer and eluting the protein with the 2-5 mM EGTA buffer. After elution from the column the EGTA containing buffer was exchanged by Chelex100 treated 1xTBS buffer (10 mM Tris-HCl, 150 mM NaCl, 2 mM DTT and protease inhibitor; pH 7,5) and proteins were concentrated by centrifugation on Amicon Ultra columns (10 kDa pore size, Millipore, Schwalbach, Germany). Further purification steps included gel filtration with UV-detection and purity was finally cross-checked using SDS-PAGE electrophoresis with subsequent Coomassie staining and immunoblotting. Then samples were concentrated up to 1 $\mu$ g/ $\mu$ l, aliquoted and stored at -80°C. Calneuron-1 and -2 were expressed with a maltose binding protein (MBP) tag using pMAL-c2X vector according to the manual (NEB, Frankfurt am Main, Germany) and purified with amylose resin (NEB, Frankfurt am Main, Germany). Cleavage of the tag was not successful due to instability of the proteins. His-SUMO-Calneuron-1 and -Caldendrin were expressed in the BL21(DE3) bacterial strain and purified with ProBond resin according to the manual. Proteins were eluted with a 250-700 mM gradient of imidazole and then undergone buffer exchange (buffers were selected depending upon the experiment) and the subsequent decalcification procedure. Information regarding expression and purification of bacterial proteins is summarized in Table 4.

Table 4. Bacterially expressed recombinant proteins and conditions for induction and purification.

Protein	Plasmid	Resistance	Tag	Induction temp. C°	Induction time, hrs	Purification method	Detergents	Expression yield
Calneuron-1	pMAL-C2X	Amp	MBP	37	4-6	Amylose resin	none	middle
Calneuron-1	pTrcHis2B	Amp	none	25-37	8	Phenyl sepharose	Sodium Sarcosyl	low
Calneuron-1	pET-SUMO	Kana	His-SUMO	37	4-6	ProBond resin	None, 0.5% TritonX-100 can be used	high
Calneuron-2	pMAL-C2X	Amp	MBP	37	4-6	Amylose resin	none	high
Calneuron-2	pTrcHis2B	Amp	none	20-37	6-8	Phenyl sepharose	Sodium Sarcosyl, goes to inclusion bodies	low
Caldendrin	pGHEB	Amp	GST	37	4	Glutathione sepharose	1% Triton-X-100	high
Caldendrin-C-terminus	pET21	Amp	none	18	ON	Phenyl sepharose	8 M Urea	middle
Caldendrin-N-terminus	pET-SUMO	Kana	His-SUMO	37	4-6	ProBond resin	none	high
Caldendrin full length	pET-SUMO	Kana	His-SUMO	37	4-6	ProBond resin	none	high
Myr-NCS-1 co-expressed with N-myristoyl transferase	pET21 and pBB131	Amp	none	37	ON	Phenyl sepharose	none	high
PI-4K III b	pGEX	Amp	GST	25-37	6-8	Glutathione sepharose	1% Triton-X-100	low
GST	pGEX	Amp	GST	37	4	Glutathione sepharose	1% Triton-X-100	high
MBP	pMAL-C2X	Amp	MBP	37	4	Amylose resin	none	high

Amp- ampicillin; Kana-kanamycin, ON-overnight

### 2.2.9 Isothermal titration calorimetry (ITC)

ITC measurements with Caldendrin, Calneurons and myr-NCS-1 were performed using a Microcal Omega Titration Calorimeter (VP-ITC). Samples were centrifuged and degassed prior to titration. All titrations were carried out at 30°C in 50 mM Tris-HCl buffer, pH 7.2 containing 100 mM KCl. Proteins samples were prepared in Chelex-treated 50 mM Tris pH 7.4, 100 mM KCl and 0.5 mM DTT buffer. Protein solutions were exchanged with the above buffer using Millipore ultrafiltration columns (3 and 10 kDa). In case of titration

of proteins with  $\text{Ca}^{2+}$ , the protein samples were titrated until saturation. Stock solutions of  $\text{CaCl}_2$  or  $\text{MgCl}_2$  were prepared in the same buffer. A typical titration consisted of injecting 1.5  $\mu\text{l}$  aliquots of 2 mM  $\text{CaCl}_2$  solution into 1.45 ml of the protein solution at a concentration of 20-50  $\mu\text{M}$ . In a separate run, aliquots of ligand solution were injected into the buffer solution (without the protein), in order to subtract the heat of dilution. All experiments were repeated two or three times with different protein preparations and curve fitting was performed using the software Origin (version 7) supplied by Microcal.

#### ***2.2.10 Steady-state fluorescence studies***

Intrinsic fluorescence spectra were recorded on a Hitachi F-4500 fluorescence spectrophotometer with proteins in the concentration range of 0.1 mg/ml. Fluorescence measurements were made in the correct spectrum mode of the instrument using excitation and emission slit widths of 5 nm each. Titrations were performed by adding increasing concentrations of the ligand till saturation was attained. Tryptophan fluorescence was recorded between 300-450 nm with the excitation wavelength set at 295 nm.

#### ***2.2.11 8-Anilino-1-naphthalene sulfonic acid binding***

ANS-binding experiments were performed by mixing the protein solution with 1-anilino-8-naphthalene-sulfonate (ANS; 100  $\mu\text{M}$  / Sigma-Aldrich, Munich, Germany). Fluorescence spectra were recorded by excitation at 365 nm in the correct spectrum mode on a fluorescence spectrofluorometer (model F-4500, Hitachi; see above).  $\text{Ca}^{2+}$  was successively added to the protein ANS complex and the fluorescence was recorded. The spectra were corrected for ANS fluorescence in buffer without protein.

#### ***2.2.12 Pull-down assays***

To prove the protein interactions recombinant GST-CDD, GST-PI-4K and GST were produced in bacteria as described above. GST-Importin- $\alpha$ 1 was obtained from Biotech (Jena, Germany). GFP- or myc-tagged Jacob constructs were heterologously overexpressed in COS-7 cells and proteins were extracted with lysis buffer (see above) 48 hrs after. Calneuron-1-GFP, Calneuron-2-GFP, NCS-1-GFP, CDD-GFP, or GFP overexpressed in COS-7 cells were extracted with lysis buffer in the presence of 2 mM  $\text{CaCl}_2$  and 1 mM  $\text{MgCl}_2$  ( $\text{Ca}^{2+}$ -buffer) or 2 mM EGTA and 1 mM  $\text{MgCl}_2$  ( $\text{Ca}^{2+}$ -free buffer). Bacterially produced recombinant proteins were immobilized on sepharose beads (for each experiment

not more than 10 µg depending upon the molecular weight) were washed with the corresponding buffers and incubated overnight at 4 °C with 500 µl of the COS-7 cell extract. After triple washing with the same buffers protein complexes were eluted with 30 µl of 2xSDS sample buffer and detected on western blots with a mouse monoclonal GFP antibody.

### **2.2.13 Competition pull-down assays**

Competition pull-down assays for the *in vitro* binding to PI-4Kβ-GST were performed with untagged Calneuron-1 (or his-SUMO-Calneuron-1 in another set of experiments) and myristoylated NCS-1. All proteins were decalcified with Chelex100 and used in equimolar amounts. The experiments were repeated 3-5 times for each protein combination (PI-4Kβ-GST + Calneuron-1, PI-4Kβ-GST + NCS-1 and PI-4Kβ-GST + Calneuron-1 + NCS-1) in the presence of either 2 mM EGTA (no Ca<sup>2+</sup>), or 200 nM, 500 nM and 1 µM CaCl<sub>2</sub> in the pulldown buffer (1 mM MgCl<sub>2</sub>, 10 mM Tris-HCl, 150 mM NaCl, 2 mM DTT and protease inhibitor cocktail; pH 7.5). Incubation was done either overnight at 4 °C (for the experiment with untagged Calneuron-1; unspecific binding to GST control was subtracted for quantification) or for 1 h at RT (for his-SUMO-Calneuron-1; unspecific binding was also subtracted for quantification). After incubation and washing probes were eluted with 20 µl of 2x SDS sample buffer and loaded on SDS-PAGE gels. On every gel the different amounts of recombinant Calneuron-1 or NCS-1 up to the level used in the assay were loaded in separate lanes to quantify the efficiency of binding using the rabbit Calneuron-1 or rabbit NCS-1 antibody. To further analyse the dynamic of these complexes the triple amount of myristoylated NCS-1 was added to the reaction with equimolar amounts of PI-4Kβ and Calneuron-1 (NCS-1:Calneuron-1 is 3:1) in the presence of 2 mM EGTA or 1 µM CaCl<sub>2</sub>. Other buffer components were constant as in the previous reactions. The experiment was repeated three times and intensity of the bands on immunoblots were analyzed by ImageJ (NIH).

### **2.2.14 Surface plasmon resonance analysis**

Binding studies for Calneuron-1, PI-4Kβ and myr-NCS-1 were carried out using the Biacore 2000 instrument and sensor chip CM5 (Biacore AB, GE Healthcare, Uppsala, Sweden) at 25 °C. His-SUMO-Calneuron-1 was coupled to the carboxymethylated dextran matrix of a sensor chip cell according to the manufacturers instructions. After equilibrating

the sensor chip with flow buffer HBS-P (10 mM Hepes pH 7.4, 150 mM NaCl, 0.005% Surfactant P20) at a flow rate of 5  $\mu$ l/min, the Dextran matrix was activated with a 7-minute pulse of 50 mM N-hydroxysuccinimide/200 mM N-ethyl-N'-(dimethylaminopropyl)-carbodiimide at a flow rate of 5  $\mu$ l/min. Subsequently his-SUMO-Calneuron-I was immobilized at the surface of the sensor chip cell by injecting a 7-minute pulse of ligand solution (20  $\mu$ g/ml of His-SUMO-Calneuron-1 in 10 mM Sodium acetate pH 4.5). Finally the excess of reactive groups on the chip surface was deactivated with a 7-minute pulse of 1 M ethanolamine hydrochloride pH 8.5, at a flow rate of 5  $\mu$ l/min. For binding studies including GST-PI-4K $\beta$  (or GST control) and myr-NCS-1 the purified proteins were diluted at the indicated concentrations in the continuous flow buffer HBS-P containing various Ca<sup>2+</sup> and/or Mg<sup>2+</sup>-concentrations. Each analytic run was performed at 20  $\mu$ l/min flow rate under the following conditions: 1 min equilibration of the chip with the indicated analysis buffer. Afterwards the analyte was injected in a 3-min pulse (association time) followed by a 3-min pulse with analysis buffer alone (dissociation time). Individual runs were finished with the regeneration of the chip matrix using a 2-min pulse of 50 mM NaOH at a flow rate of 5  $\mu$ l/min and a terminating 5-minutes pulse with flow buffer in order to equilibrate the chip surface again. For the final graph the binding of GST control alone of with NCS-1 was subtracted from the corresponding GST-PI-4K $\beta$  values. For estimation of binding of NCS-1 to GST-PI-4K $\beta$  in presence or absence of Mg<sup>2+</sup> and different Ca<sup>2+</sup> concentrations myr-NCS-1 was directly coupled to the sensor chip and GST-PI-4K $\beta$  was injected as described above. The molar binding activities were calculated based on the equation from Catimel et al. (1997).

#### **2.2.15 PI-4K $\beta$ activity assays**

The PI-4K $\beta$  activity assay was carried out in a final volume of 120  $\mu$ l containing 50 mM Tris (pH 7.5), 20 mM MgCl<sub>2</sub>, 1mM EGTA, 0.5 mg/ml BSA, 80  $\mu$ g of substrate (PI) in micelles containing 0.4% Triton X-100 and ATP (mixture of 500  $\mu$ M cold ATP and 2  $\mu$ Ci ATP-P<sup>32</sup>). The reactions were carried out in Ca<sup>2+</sup>-free conditions (2 mM EGTA) or in the presence of 2 mM CaCl<sub>2</sub>. 8  $\mu$ M of wortmanine was used to inhibit the kinase activity in control experiments. Reactions were initiated by adding the ATP mixture, the reaction mix was incubated at room temperature for 30 min and terminated by adding 3 ml of a chloroform/methanol/0.6N HCl (200:100:0.75 v/v%) mixture. The labeled phospholipids were extracted with 1.5 ml of chloroform/methanol/0.6 N HCl (3:48:47, v/v/v%). The

organic phase was transferred into a scintillation vial. After evaporation, 5 ml of the scintillation fluid containing 1.3 mM POPOP and 22 mM PPO in Toluene were added and radioactivity was measured by a liquid scintillation counter. The blank value was subtracted and data were represented as the percentage of basal kinase activity (100%) with or without  $\text{Ca}^{2+}$ .

#### **2.2.16 PI(4)P assay**

The PI(4)P assay was carried out with a PI(4)P mass strip kit (MoBiTec, Goettingen, Germany) in COS-7 cells. 75 cm<sup>2</sup> flasks were transfected and after 48 hrs cells were harvested with cold 1xTBS buffer, homogenized and centrifuged at 1000xg for 10 min at 4°C. The pellet fraction was resuspended in 150 µl of TBS and 5 µl were taken for immunoblotting with anti-β-Actin (loading control) and anti-Syntaxin 6 (Golgi marker control). The remaining pellet was used for PI(4)P extraction according to the protocol from the manufacturer. Briefly the pellet was washed twice with cold 5% TCA /1 mM EDTA buffer by centrifugation and then neutral lipids were extracted by MeOH:CHCl<sub>3</sub> (2:1). The obtained pellet was homogenized in CHCl<sub>3</sub>:MeOH:12 N HCl (40:80:1) for the acetic lipid extraction. The supernatant was collected, then organic and aqueous phases were separated by adding CHCl<sub>3</sub> and 0,1 N HCl. The organic phase was transferred into a fresh tube and lyophilized. Dry lipids were reconstituted with 10 µl of CHCl<sub>3</sub>:MeOH:H<sub>2</sub>O (1:2:0,8) and 2 µl were spotted onto a PI(4)P Strip. Strips were dried, blocked with 3% BSA and incubated with PI(4)P detector solution for 1 h at RT. After extensive wash with 1xPBS the strip was incubated for 45 min with Secondary detector solution supplied with a kit, washed again and incubated with Tertiary Detector solution for another 45 min. After the final wash the signals on the membrane were detected by chemiluminescence. Films were scanned and the optical density of the spots was analyzed by ImageJ.

#### **2.2.17 hGH release assay**

PC12 cells were plated on collagen-coated 6 well plates and co-transfected 24 hrs later with pXGH5 (2 µg/well) encoding human Growth Hormone (hGH) and pEGFP-Calneuron-1 (2.5 µg/well), pEGFP-Calneuron-2 (2 µg/well) or pEGFP control vector (1.5 µg/well) using Lipofectamine (Invitrogen, Karlsruhe, Germany). hGH release was determined 48 hrs after transfection. PC12 cells were washed twice with stimulation buffer, incubated for 10 min in 1 ml of  $\text{Ca}^{2+}$ -free stimulation buffer (containing 2 mM EGTA) to measure the basal

release or with 1 ml of stimulation buffer containing 30  $\mu$ M ATP. The supernatant was collected, and the cells were harvested in the same volume of stimulation buffer. The amount of hGH secreted into the buffer or the total amount present in the cells was measured using hGH Elisa kit from Meddiagnost (Reutlingen, Germany). The basal release in control pXGH5 – pEGFP-C1 transfected cells was taken as 100% and the amount of secreted hGH was normalized to its total level and expressed as a percentage of control.

### **2.2.18 VSV-G trafficking assay**

To test the role of Calneurons in Golgi trafficking COS-7 cells were transfected with GFP-tagged vesicular stomatitis virus glycoprotein (VSV-G) alone or co-transfected with VSVG-GFP and untagged Calneurons in pcDNA3.1 and grown for 24 hrs. 7.5  $\mu$ M of Anisomycin (Sigma-Aldrich, Munich, Germany) was added to stop new protein synthesis when the experiment was started. Then temperature was shifted to 40°C for 30 minutes. This time point was chosen because in the case of co-transfection with Calneuron constructs already at the basal level majority of VSVG-GFP were observed at the Golgi. Thereafter the temperature was reduced to 32°C and cells were subsequently fixed after 0, 60, 90 and 120 min, stained with rabbit Calneuron-1 or Calneuron-2 antibodies to confirm the double transfection and processed for confocal laser scanning microscopy. Images were taken as the 300 nm z-stack using 63x-objective and 1.5 confocal zoom and constant data acquisition settings. The maximal projection of each stack was analyzed in ImageJ. A region of interest corresponding to plasma membrane was selected and intensity of fluorescence was calculated as a mean grey value (represented as 255 different gray values). An average background signal measured on empty areas close to the transfected cells was subtracted.

### **2.2.19 $Ca^{2+}$ imaging**

To control whether the change of temperature in the VSV-G trafficking assay affects the  $Ca^{2+}$ - levels in the cell as it was reported previously we performed  $Ca^{2+}$ -imaging experiments. COS-7 cells, cultured on glass coverslips were loaded 24 hrs after plating with Fura-2 by incubation at 35°C for 30–60 min with Fura-2 acetoxymethyl ester (5  $\mu$ M) dissolved in HPPS (120 mM NaCl, 5.3 mM KCl, 0.8 mM MgSO<sub>4</sub>, 1.8 mM CaCl<sub>2</sub>, 11.1 mM glucose, 20 mM Hepes, pH7.4). After washing with fresh HPPS, coverslips were transferred to a small experimental chamber on the stage of an upright microscope (Axioskop FS, Zeiss, Oberkochen, Germany) and continuously superfused with HPPS at 35°C for 10–20 min to



allow de-esterification of the dye. The temperature of the bath solution was controlled with a solution in-line heater (Warner Instruments, Hamden, CT, USA). A monochromator (VisiChrome, Visitron Systems, Puchheim, Germany) was used to excite Fura-2 fluorescence at 358 and 380 nm. Fluorescence light was collected by a water-immersion objective (LUMPLFL 40x W, Olympus, Hamburg, Germany) and images were acquired with a cooled CCD camera (Pentamax, Princeton Instruments, Trenton, NJ, USA) after passing a 400 nm dichroic and a 510 – 560 nm long-pass filter (Zeiss). Acquisition rate was 0.3 – 1 Hz in order to minimize photobleaching of Fura-2. Data acquisition was performed by Metafluor software (Universal Imaging, Downingtown, PA, USA). For off-line analysis and processing of fluorescence images the Image J software (NIH) was used.

### ***2.2.20 FRAP experiments***

Fluorescence recovery after photobleaching (FRAP) experiments were carried out using a confocal laser scanning microscope (Leica DMRXE confocal microscope; Wetzlar, Germany). 5-7 DIV cortical neurons were transferred 24 hrs after transfection with mCherry-Synaptophysin and GFP or Calneuron-1-GFP and 72 hrs after transfection for the Calneuron 1 shRNA into a recording chamber with ACSF (125 mM NaCl, 2,5 mM KCl, 2 mM MgSO<sub>4</sub>, 2 mM Ca<sup>2+</sup>, 10 mM glucose, 30 mM Hepes, pH 7.3) at 37°C. A 488-nm laser line was used to monitor the GFP channel and a 568-nm line for both imaging of mCherry and photobleaching. A 63x oil objective and 2x confocal zoom were used. Pictures were taken every 5 min as a z-stack (300 nm z-step) with a resolution of 524x524 pixels. The first five images were recorded before bleaching to establish a baseline and to ensure that the neurons on the coverslip have stabilized responses in the recording chamber. Then, the first 15-20 µm segment of the longest neurite (axon) was bleached with the maximal laser power for 5–8 min (12x zoom) due to the high photo-stability of mCherry, followed by 1 h of post-bleach recordings at the same conditions as for the baseline. After the bleaching 100 µM ATP was added for 3 min to increase intracellular Ca<sup>2+</sup> levels and to stimulate Golgi trafficking in the case of Caln-1-GFP or GFP transfection. For the BAPTA experiments cells were pre-incubated with 10 µM of BAPTA-AM for 1 h at 37°C in serum free medium. Images were analyzed with ImageJ (NIH). Z-stacks were processed as maximal projections and a 10 µm initial segment of the bleached neurite was selected as the region of interest (ROI). In each experiment, the ROI was analyzed at all time points and the mean grey value (represented as 255 different gray values) was calculated. Data were normalized to the

photo-bleaching during the image acquisition by introducing the “bleaching coefficient” (unrelated area with the background fluorescence monitored during the experiment after the neurite was bleached, initial fluorescence intensity was taken as 1 and each change of the intensity was calculated as the proportion). For the evaluation of % of FRAP the initial fluorescence was taken as 100% and data were graphically plotted. The differences between fluorescence intensity after bleaching at time point 0 min and time point 60 min were taken as % of recovery.

### ***2.2.21 Life imaging experiments***

For the line analysis of vesicle trafficking the same groups as described above were studied. For the BAPTA-AM experiments cells were preincubated for 1 h at 37°C. Coverslips were transferred to an experimental chamber on the stage of an upright microscope (Zeiss AxioScope FS, Oberkochen, Germany). Cells were continuously superfused with HEPES-buffered ACSF at 35°C. mCherry fluorescence was excited at 575 nm. Excitation light was directed onto the specimen via a 60x objective and a 580 nm dichroic. Emission was filtered with a 590 nm long-pass filter. Images were acquired every 30s (exposure times 200-500 ms) via a water-immersion objective (LUMPLFL 60x W, Olympus, Hamburg, Germany) and a cooled CCD camera (Pentamax, Princeton Instruments, Trenton, NJ, USA). Data acquisition was performed by Metafluor software (Universal Imaging, Downingtown, PA, USA). For off-line analysis and processing of fluorescence images the ImageJ software was used.

### ***2.2.22 Analysis of Golgi complexes and PTVs in primary neurons***

Transfected primary cortical neurons were fixed at DIV5 and stained with trans-Golgi network markers (Syntaxin-6, TGN38), the endosomal/Golgi marker  $\beta$ -Cop or the cis-Golgi marker GM150 in combination with PI-4K $\beta$  or different presynaptic markers (SNAP25, Piccolo, Synaptophysin). For analysis of co-localization images were scanned with a confocal microscope (see above) as 300 nm z-stacks (63x oil objective) and calculated as maximum intensity projections using the ImageJ software (see above). The size of the Golgi complex was analyzed 24 hrs after transfection with Calneuron-1-GFP and GFP-Calneuron-2, NCS-1-GFP or GFP constructs and 72 hrs after introduction of the Calneuron-1 shRNA. Images were scanned as 126 nm z-stacks (63x oil objective and 4x confocal zoom) and analyzed using Imaris image analysis software. The Syntaxin-6 channel was reconstructed as

3D with the same parameters for all groups and then the volume, total surface area and the number of TGN clusters was measured. For the analysis of Piccolo Bassoon transport vesicles (PTVs) number MAP2 was used as a dendritic marker and Piccolo as a marker of PTVs. The longest MAP2 negative neurite was identified as the axon. For quantitative analysis 50  $\mu\text{m}$  stretches were taken 30  $\mu\text{m}$  away from the cell body to exclude the axon initial segment, scanned as z-stack (63x oil objective, 2x zoom) and then transferred to the maximal projection as described above. The GFP channel was adjusted to saturation level and inverted to a binary image, which was then used to calculate the total area of the axonal segment. Subsequently the Piccolo-immunofluorescence was also converted to a binary image with the same threshold for all groups. Only the area overlapping with the GFP image was analyzed. Data are presented as the ratio between the area covered by PTVs (Piccolo positive) and the total area of the axon (GFP positive). GFP transfected neurons were taken as control (set to 100%) and percentage deviations were calculated. For analysis of PTVs size and intensity of fluorescence for Piccolo on PTVs, the mask created from the binary Piccolo image was applied to the original not modified Piccolo channel. The size and fluorescence intensity of ROI was measured.

### ***2.2.23 Structural Modeling***

The 3D structures were generated using automated homology modeling on Swiss Modeller Server (<http://swissmodel.expasy.org/SWISS-MODEL.html>) with a high confidence score. The model generated was visualized and corrected using the SETOR program (Evans, 1993) on a Silicon Graphics machine. The structure is generated with suitable targets and energy minimization was performed on the developed model. The quality of the model and robustness was evaluated by performing molecular dynamics using the InsightII program. EF-hand structures of Calneurons and Caldendrin have been modeled using coordinates from the calcium saturated structure of human CaM (protein data bank, pdb entry: 1c1l (Chattopadhyaya et al., 1992) and the  $\text{Ca}^{2+}$  free CaM-like skin protein CLSP (Babiniet al., 2006).

### ***2.2.24 Statistical Analysis***

Statistical analyses were performed with the paired Student's *t* test and the Mann-Whitney U-test when applicable using Excel or Prism software (Prism Computational Sciences, Inc. Madison. USA).

### 3 Results

#### 3.1 Jacob is a Caldendrin binding partner in brain and competes with Importin- $\alpha$ for an overlapping binding site

Based on its EF-hand organization, a unique bipartite structure with a highly basic N-terminal part that doesn't share homology with any other protein and its restricted subcellular localization, it can be expected that Caldendrin has a function in neurons that is associated with specific binding partners that are different than those of CaM. To test this hypothesis a number of screens for interaction partners were initiated some years ago in our lab. Part of these efforts was a Y2H screen using the C-terminal part of Caldendrin containing the four EF-hands as bait (Doctoral thesis of Dieterich DC, 2003; Dieterich et al., 2008). Among the proteins that came out of this screen were eight independent clones that contained the sequence of an uncharacterized gene product that was subsequently named Jacob (see above).

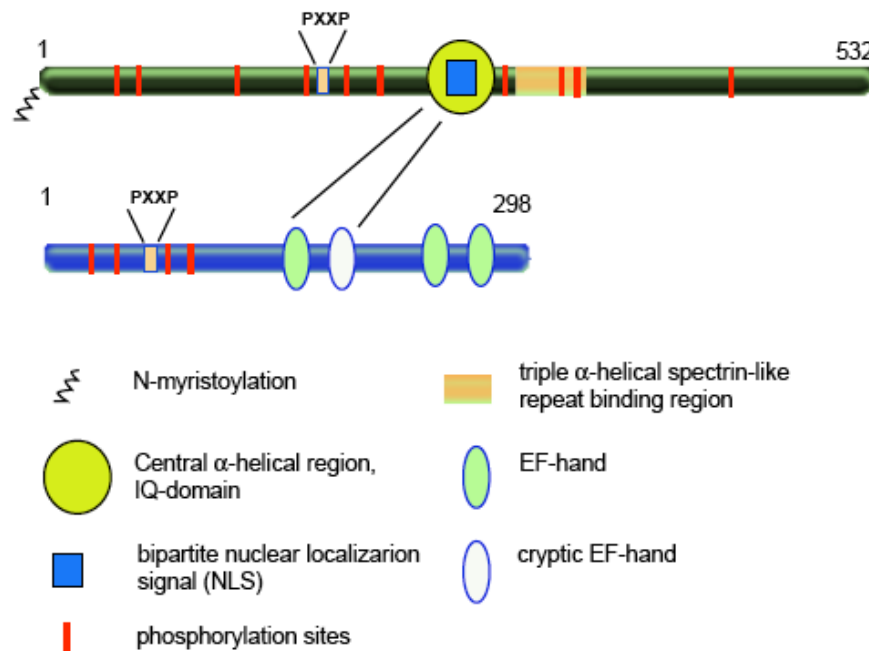


Figure 5. Primary structure of Jacob (upper) and Caldendrin (lower). The main features cDNAs are depicted: N-myristoylation, PXXP motif, bipartite NLS, central  $\alpha$ -helical region, number of predicted phosphorylation sites and EF-hands.

The interaction regions of Jacob and Caldendrin were mapped in detail in Y2H studies and confirmed by pull-down assays and analysis of deletion mutants. According to these experiments the EF-hands 1 and 2 of Caldendrin are critical for an interaction with Jacob. Strikingly, in Jacob, we could map the Caldendrin binding region to the central  $\alpha$ -helical

region that harbors the bipartite NLS (Fig. 5). Deletion of the first six basic residues of the NLS led to significantly reduced Caldendrin binding (Dieterich et al., 2008). In pull-down assays using recombinant proteins Caldendrin binds Jacob only in the presence of  $\text{Ca}^{2+}$ . To check if this  $\text{Ca}^{2+}$  dependency also holds true under *in vivo* conditions co-immunoprecipitation experiments were performed with extracts of rat brain proteins either in the in presence of 100  $\mu\text{M}$   $\text{Ca}^{2+}$  or 5 mM EGTA ( $\text{Ca}^{2+}$  - free conditions / Fig. 5A).

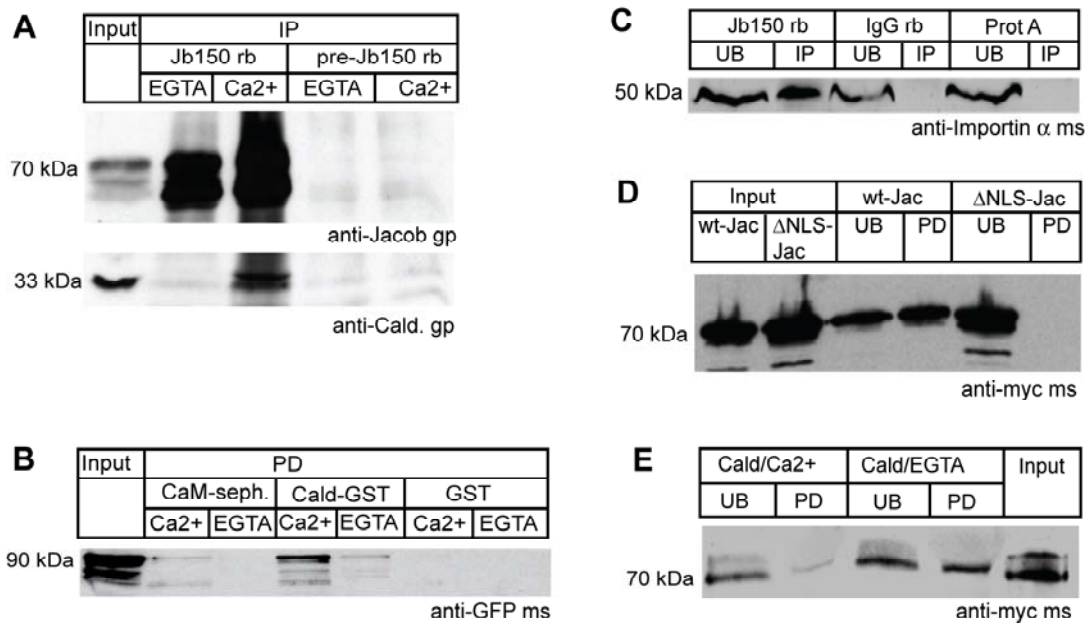


Figure 6. (A) Caldendrin co-immunoprecipitates with Jacob from a rat brain extract in a  $\text{Ca}^{2+}$  -dependent manner. Rabbit anti-Jacob bound to protein A sepharose specifically precipitates Jacob independent from the conditions used (5 mM of EGTA or 100  $\mu\text{M}$   $\text{Ca}^{2+}$  in the precipitation buffer). Rabbit IgG was used as a negative control (upper panel). Caldendrin was only detected in the precipitate in the presence of  $\text{Ca}^{2+}$  (lower panel). (B) WT-Jacob-GFP does not bind to CaM in a pull-down assay. Jacob binding to CaM or Caldendrin-GST sepharose was tested in the presence of 100  $\mu\text{M}$   $\text{Ca}^{2+}$  or 2 mM EGTA. GST sepharose was used as the control. WT-Jacob-GFP was detected by western blotting with a GFP antibody. (C) Immunoprecipitation of Importin- $\alpha$ 1 from a soluble rat brain protein fraction with a Protein-A sepharose-coupled Jacob antibody (JB-150). Importin- $\alpha$ 1 was only found in the immunoprecipitate (IP) of the Protein-A sepharose coupled Jacob-antibody, whereas it remained in the unbound fraction in the IgG and Protein-A sepharose control. (D) GST-Importin- $\alpha$ 1 pull-down of myc/his-tagged wt- and  $\Delta\text{NLS}$ -Jacob extracted from transfected COS-7 cells. Only wt-Jacob, but not  $\Delta\text{NLS}$ -Jacob, is found in the pull-down, indicating that the presence of the NLS is essential for the Importin- $\alpha$ 1/Jacob interaction. (E) GST-Importin- $\alpha$ 1 pull-down of myc/his-tagged WT Jacob in the presence of equimolar amounts of recombinant Caldendrin C-terminus. Pull-down of Jacob is attenuated in the presence of 2 mM  $\text{Ca}^{2+}$ , but not in the presence of 2 mM EGTA. PD, pull-down fraction; UB, unbound material; Cald – Caldendrin; CaM – Calmodulin; rb. rabbit; gp, guinea pig; ms, mouse.

In agreement with the pull-down assay data Caldendrin was eluted only from the Jacob antibody beads treated with  $\text{Ca}^{2+}$  whereas the amount of Jacob protein precipitated by the antibody was not significantly affected by  $\text{Ca}^{2+}$  (Fig. 6A). Proteins that contain IQ motifs

typically bind CaM that in turn is much more abundant than Caldendrin. To exclude that Jacob's IQ motif might be a CaM binding site for Jacob expressed in eukaryotic cells, GST-pull-down assays were performed with Jacob expressed in COS-7 cells. Strikingly, there was almost no binding of Jacob-GFP to CaM observed at any  $\text{Ca}^{2+}$  concentration tested (Fig. 6B) and CaM also could not compete with Caldendrin for binding to Jacob (Dieterich et al., 2008). Thus, the interaction of the IQ motif in Jacob is Caldendrin specific and  $\text{Ca}^{2+}$  dependent *in vitro* and *in vivo*.

The transport of proteins from the cytosol through the nuclear pore complex into the nucleus depends on the binding of Importins to a specific NLS within the cargo. Within this scheme Importin- $\alpha$  functions as an adapter molecule by binding both the NLS-bearing protein and Importin- $\beta$ . Since structural modelling suggested that Caldendrin-binding will potentially mask Jacob's NLS we therefore decided to address this prediction more directly by first confirming an interaction of Jacob with Importin- $\alpha$ . Co-immunoprecipitation experiments from brain extract have shown that Jacob might interact with Importin- $\alpha$ 1 (Fig. 6C). In further pull-down experiments we found specific binding of myc-his tagged wt-Jacob but not of the  $\Delta$ NLS Jacob mutant to GST-Importin- $\alpha$ 1 (Fig. 6D). The binding of GST-Importin- $\alpha$  1 was not affected by the presence or absence of  $\text{Ca}^{2+}$  (data not shown). We next investigated whether the binding of Importin- $\alpha$  can be competed by equimolar amounts of recombinant Caldendrin. Indeed, these studies revealed a competition between Caldendrin and Importin- $\alpha$ 1 for binding to Jacob in the presence of  $\text{Ca}^{2+}$ . Interestingly, no competition was seen in the presence of EGTA suggesting that elevated  $\text{Ca}^{2+}$ -levels are needed for Caldendrin to mask the NLS in Jacob (Fig. 6E).

### **3.2 Importin-bound Jacob translocates to the nucleus after stimulation of NR2B-containing NMDARs**

An elegant recent study from Kelsey Martin's lab (Thompson et al., 2004) established a role of the classical Importin-mediated nuclear import for synapse-to-nucleus communication. In this study an NMDA receptor-dependent translocation of Importin- $\alpha$ 1 and - $\alpha$ 2 from distal dendrites to the nucleus was observed. Under resting conditions, however, dendritic importins are largely immobile. Potential cargos associated with this translocation are at present unknown. Jacob is found to be localized both at synapses and the nucleus and harbors a bipartite NLS, which is bound by Importin- $\alpha$  and masked in a  $\text{Ca}^{2+}$ -

dependent manner by Caldendrin. We therefore tested whether increased NMDA receptor activity will alter the intracellular localization of Jacob. For this purpose we stimulated hippocampal primary cultures with NMDA for 3 min and quantified the Jacob immunoreactivity (IR) fluorescence signal intensity of 4'-6-Diamidino-2-phenylindole (DAPI) counterstained neuronal nuclei. Jacob IR increased significantly in neuronal nuclei within 30 min after NMDA receptor activation (Fig. 7A and B) with highest levels after 2 hrs. Nuclear Jacob IR returned to control levels within 4 hrs (Dieterich et al., 2008). As previously reported (Thompson et al., 2004) Importin- $\alpha$ 1 accumulated in the nucleus in a similar time frame. Interestingly, no recruitment of Caldendrin to the nucleus was observed (data not shown).

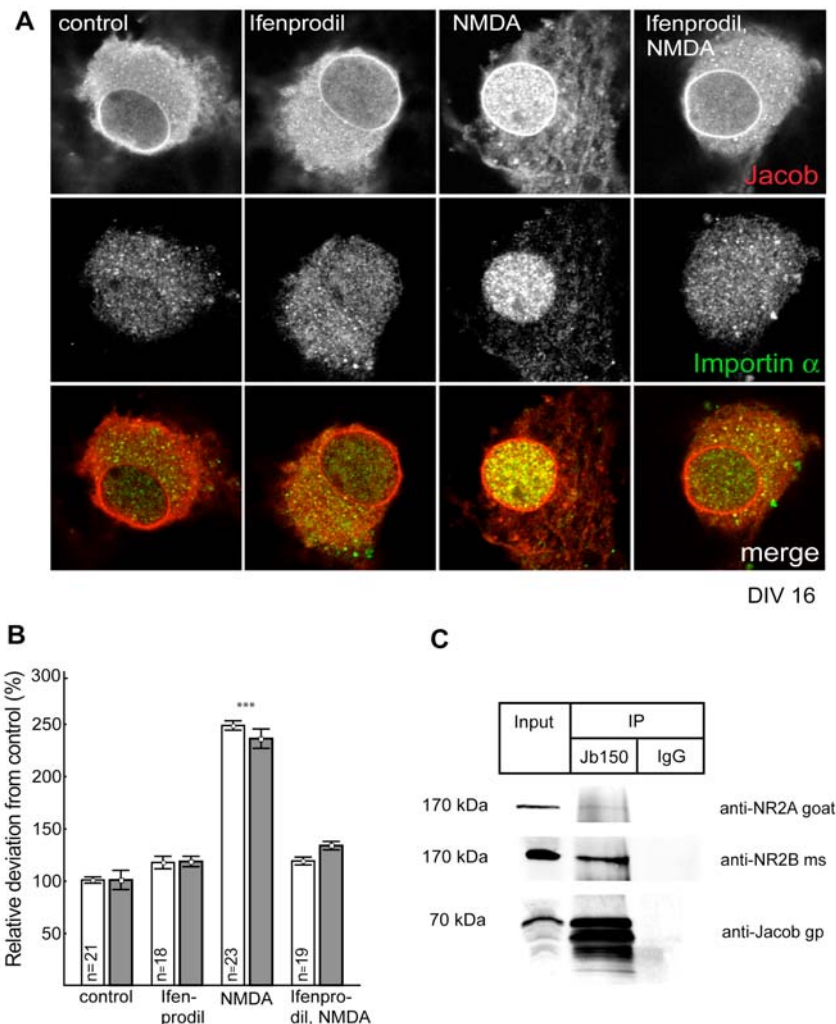


Figure 7. Jacob and Importin- $\alpha$ 1 translocate into the nucleus upon NR2B-containing NMDARs stimulation. (A-B) Blockage of nuclear Jacob and Importin-1 trafficking after bath application of NMDA (100  $\mu$ M for 3 min) in the presence of the NR2B antagonist ifenprodil (5  $\mu$ M). Cultures were fixed 30 min after NMDA stimulation. \*\*\*,  $p < 0.001$ . (C) NR2BRs co-immunoprecipitates with Jacob from a Triton-X-100 soluble rat brain fraction. There is only minor amount of NR2A containing NMDARs can be observed in immunoprecipitate. Protein-A sepharose-coupled Jacob antibody (JB-150) or rabbit IgG control were used.

Using quantitative fluorescence time-lapse microscopy of hippocampal primary neurons transfected with wt-Jacob-GFP or the  $\Delta$ NLS-mutant we found that the presence of the NLS is essential for the nuclear translocation of Jacob. Glutamate stimulation of wt-Jacob-GFP transfected cultures kept in the presence of anisomycin resulted in an increase of somatic and nuclear GFP-fluorescence with a time-course comparable to that of the endogenous protein. The nuclear accumulation of Jacob-GFP, however, was not seen in neurons transfected with the  $\Delta$ NLS-mutant Jacob-GFP construct (Dieterich et al., 2008) suggesting that the presence of the binding site for Importin- $\alpha$  is a prerequisite for Jacob's nuclear accumulation. Importantly, concomitant to the nuclear accumulation of wt-Jacob the GFP-fluorescence decreased in proximal and distal dendrites, an effect, which was absent in  $\Delta$ NLS-mutant Jacob-GFP transfected neurons. This indicates that the presence of the NLS and the interaction with Importin- $\alpha$  are not only important for the nuclear import but are already crucial for Jacob's transport from dendrites to the nucleus (Dieterich et al., 2008).

To learn more about the role of Caldendrin for the extra-nuclear retention of Jacob and to understand the apparently contradictory findings (i.e. NMDAR activation with subsequent  $\text{Ca}^{2+}$ -influx leading to Jacob's nuclear import and concomitantly Caldendrin binding preventing this process at high synapto-dendritic  $\text{Ca}^{2+}$ -levels) we analyzed the transport process of Jacob in more detail using confocal laserscan microscopy. NMDA receptors are situated both at synaptic and extrasynaptic sites (Rumbaugh&Vicini, 1999; Tovar&Westbrook, 1999). Bath application of NMDA is considered to affect preferentially but not exclusively extrasynaptic NMDARs (Hardingham et al., 2001; Hardingham et al., 2002). The latter ones are less efficiently coupled to steep intracellular  $\text{Ca}^{2+}$ -release than their synaptic counterparts (Sala et al., 2000; Köhr, 2006).

To differentiate between these two populations we indirectly stimulated hippocampal cultures by incubation with the A-type of gamma-amino butyric acid receptor ( $\text{GABA}_A$ -receptor) antagonist bicuculline. The blockade of inhibitory synapses leads to an increased release of glutamate at synaptic sites, and as expected an increased accumulation of Jacob and Importin- $\alpha$  in the nucleus (Dieterich et al., 2008). This effect, however, was much less distinct as compared to the bath application of glutamate.

A co-incubation with the non-competitive NMDAR antagonist MK-801 attenuated the nuclear accumulation of Jacob and Importin- $\alpha$ 1 to levels indistinguishable from control conditions (Dieterich et al., 2008). Since MK-801 is an irreversible open channel blocker we took advantage of this fact to differentiate between synaptic and extrasynaptic NMDARs.



After removal of the drug following stimulation of synaptic glutamate receptors we applied NMDA to the bath solution to exclusively activate extrasynaptic NMDARs. Interestingly, this regimen induced a marked nuclear translocation of Jacob and Importin- $\alpha$ 1 that was more prominent than the accumulation after stimulation of synaptic NMDARs (Dieterich et al., 2008).

Synaptic NMDARs contain predominantly the NR2A-subunit while their extrasynaptic counterparts contain mainly the NR2B-subunit (Halpain et al., 1998). To prove the hypothesis that the nuclear translocation of Jacob and Importin- $\alpha$ 1 requires activation of NR2B-containing NMDARs we repeated the experiments outlined above in the presence of the NR2B specific antagonist ifenprodil. Intriguingly, we found that after bath application of NMDA, Jacob's and Importin- $\alpha$ 1 nuclear import could be completely blocked in the presence of ifenprodil (Fig. 7A and B). These results show that the nuclear import of Jacob and Importin- $\alpha$ 1 requires signaling via the largely extrasynaptically localized NR2B-containing NMDARs. Finally, in support of the notion that largely NR2B containing NMDARs are associated with Jacob we found in co-immunoprecipitation experiments using a Jacob antibody NR2B immunoreactivity from a Triton-X-100 soluble rat brain extract. There was only a minor amount of NR2A containing NMDARs in this precipitate probably due to the existence of hetero-trimeric NMDARs (Fig. 7C).

### **3.3 Caldendrin binding targets Jacob outside the nucleus only after synaptic NMDAR stimulation**

These data led to the hypothesis that only if synapto-dendritic  $\text{Ca}^{2+}$ -levels reach a critical range like after sustained synaptic activity, Caldendrin will block Jacob's nuclear import. However, not all synapses are Caldendrin immunopositive (Laube et al., 2002), and probably therefore after synaptic stimulation one can still see some translocation of Jacob into the nucleus. To check this hypothesis we transfected a GFP-Caldendrin construct into hippocampal primary neurons at DIV 7. Expectedly, overexpression of Caldendrin blocked the increase of endogenous nuclear Jacob immunoreactivity after synaptic stimulation at DIV 16, indicating that the interaction with Caldendrin masks the NLS of Jacob (Fig. 8A and B). However, after stimulation of extrasynaptic NMDARs, overexpression of Caldendrin attenuated Jacob's nuclear import much less efficiently (Fig. 8A and B). We therefore checked whether RNAi knockdown of Caldendrin affects the nuclear trafficking of Jacob differentially after synaptic and extrasynaptic NMDA receptor stimulation. We

generated four different RNAi constructs and checked their efficiency in COS-7 cells by co-transfection of each RNAi sequence in pRNAi vector with different amount of untagged Caldendrin in pRC vector. The most efficient sequence was used for the transfections of hippocampal primary culture where it also induced the reduction of endogenous Caldendrin (Fig. 9A and B).

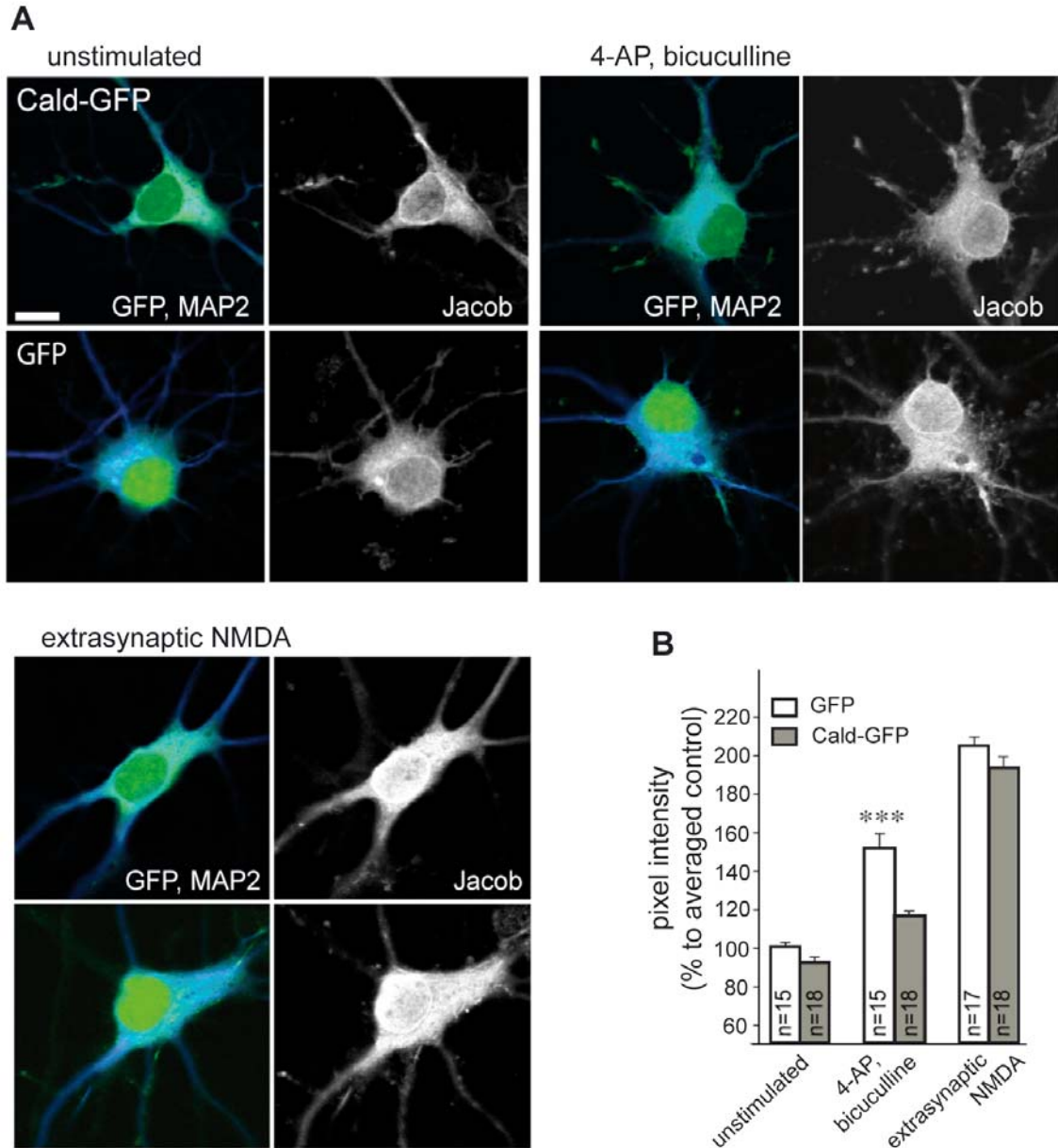


Figure 8. Caldendrin targets Jacob outside the nucleus. (A) Nuclear Jacob immunofluorescence following Caldendrin overexpression (upper panel) and in GFP control transfections (lower panel). Depicted are unstimulated neurons (first two rows), neurons 30 min after bicuculline stimulation, and neurons after stimulation of extrasynaptic NMDARs. Transfections were done at DIV13, stimulation experiments at DIV16. Scale bar indicates 10  $\mu$ m (B) Quantitative analysis of nuclear Jacob immunofluorescence as percent deviation from unstimulated GFP control transfections. \*\*\*,  $p < 0.001$ . Error bars represent the SEM

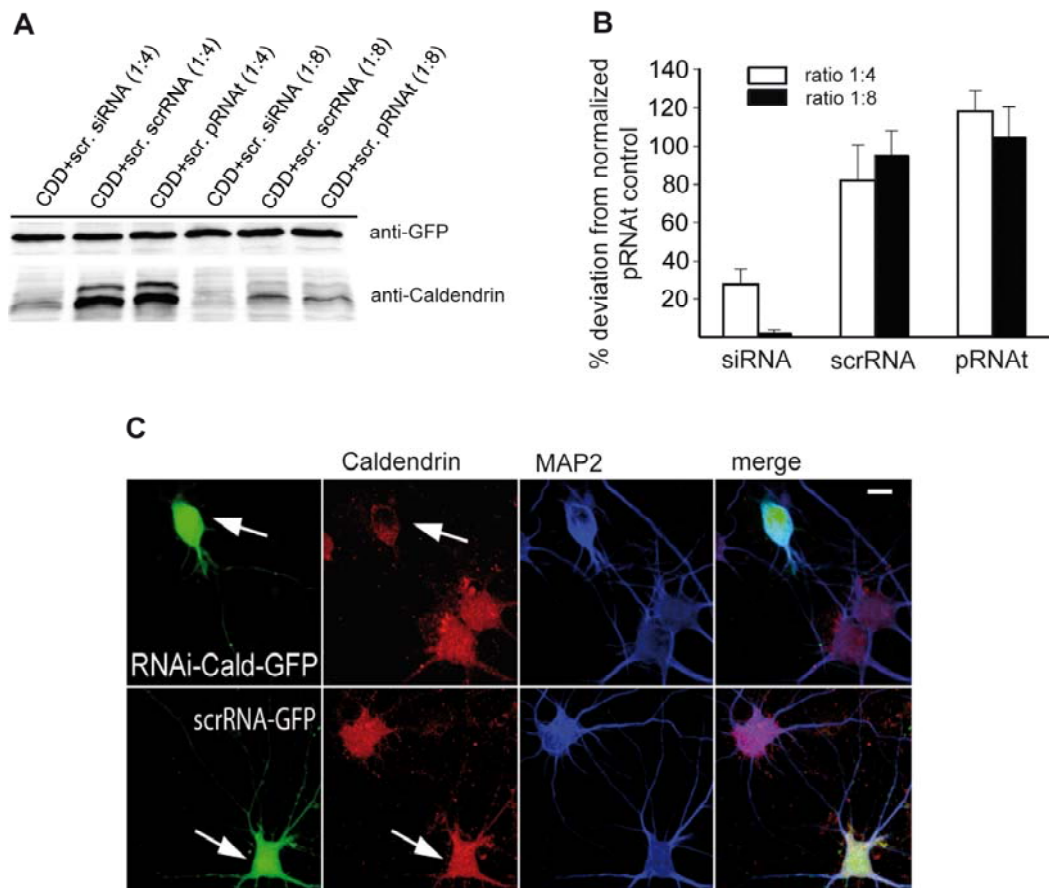


Figure 9. Validation of Caldendrin RNAi-GFP construct. (A) COS-7 cells double transfected with RNAi for Caldendrin or the scrambled construct and Caldendrin without tag in a ratio of 4:1 or 8:1. 72 hours later cells were harvested and protein levels were checked by immunoblotting with GFP and Caldendrin antibodies. (B) Quantification of Caldendrin knock down in COS-7 cells. (C) Caldendrin staining (red) is clearly reduced after transfection of hippocampal primary neurons with a RNAi-GFP construct (GFP-positive cells are indicated with arrows, upper panel) as compared to nontransfected cells from the same culture or neurons infected with the scrRNA-GFP construct (see arrow in the lower panel). Blue channel: MAP2 staining. Transfection was done at DIV10, fixation at DIV16. Scale bar is 10  $\mu$ m.

We transfected hippocampal primary neurons with Caldendrin RNAi-GFP construct or the corresponding scrambled control on DIV 5 and again applied differential stimulation protocol for synaptic and extrasynaptic NMDARs. We found that the nuclear immunofluorescence for Jacob was significantly increased in cells with reduced Caldendrin levels after enhancing synaptic activity with bicuculline (Fig. 10A and B), whereas the Caldendrin knock down had no effect on Jacob's nuclear import after activation of extrasynaptic NMDARs. This points to a regulatory function of this protein-protein interaction in nuclear trafficking of Jacob after enhanced synaptic activation that is related to the competitive accessibility of the NLS of Jacob for either Caldendrin or Importin- $\alpha$  binding.

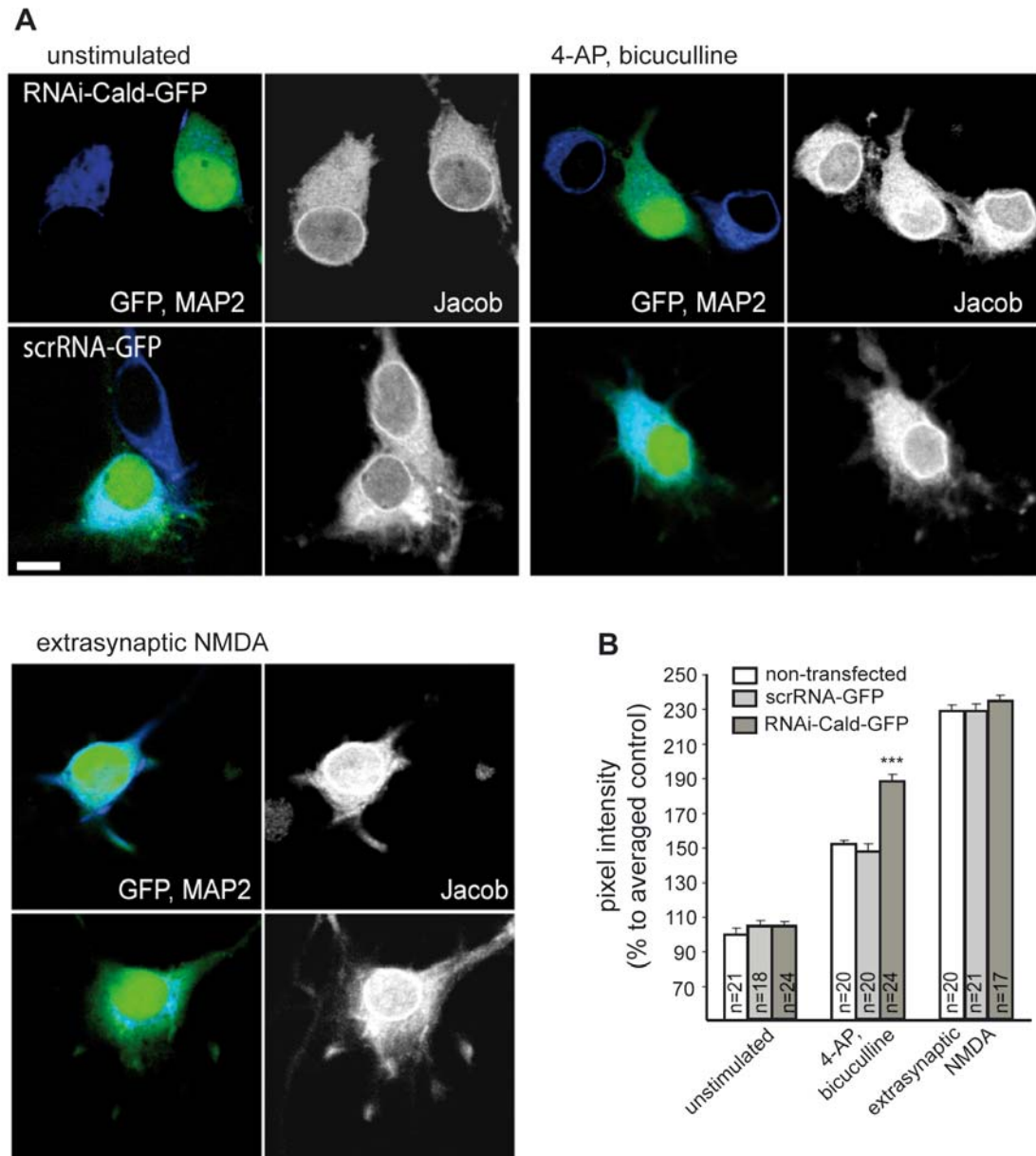


Figure 10. (A) Synaptic and extrasynaptic stimulation of hippocampal primary neurons (DIV16). Cultures were transfected with a Caldendrin RNAi-GFP construct (upper panel) or scrambled scrRNA-GFP construct (lower panel) at DIV5. Depicted are a transfected and a nontransfected neuron. Scale bar is 10  $\mu$ m. (B) Quantitative analysis of nuclear Jacob immunofluorescence after Caldendrin knockdown (RNAi-Cald-GFP), in scrambled controls (scrRNA-GFP) or non-transfected cells as percent deviation from unstimulated controls. \*\*\*,  $p < 0.001$ . Error bars represent the SEM.

### 3.4 Jacob is part of the CREB shut-off pathway

The predominant  $\text{Ca}^{2+}$ - and NMDA receptor activated signaling pathways to the nucleus in neurons funnel through the activation of the transcription factor CREB (West et al., 2002; Deisseroth et al., 2003). Previous work has shown that extrasynaptic NMDA receptor activation results in a dephosphorylation of CREB at Ser133 (pCREB) that renders it transcriptionally inactive and, therefore, constitutes a CREB shut-off signal (Hardingham et al., 2002; Noguchi et al., 2005). We could replicate this finding in our cell culture system (Fig. 11A and B).

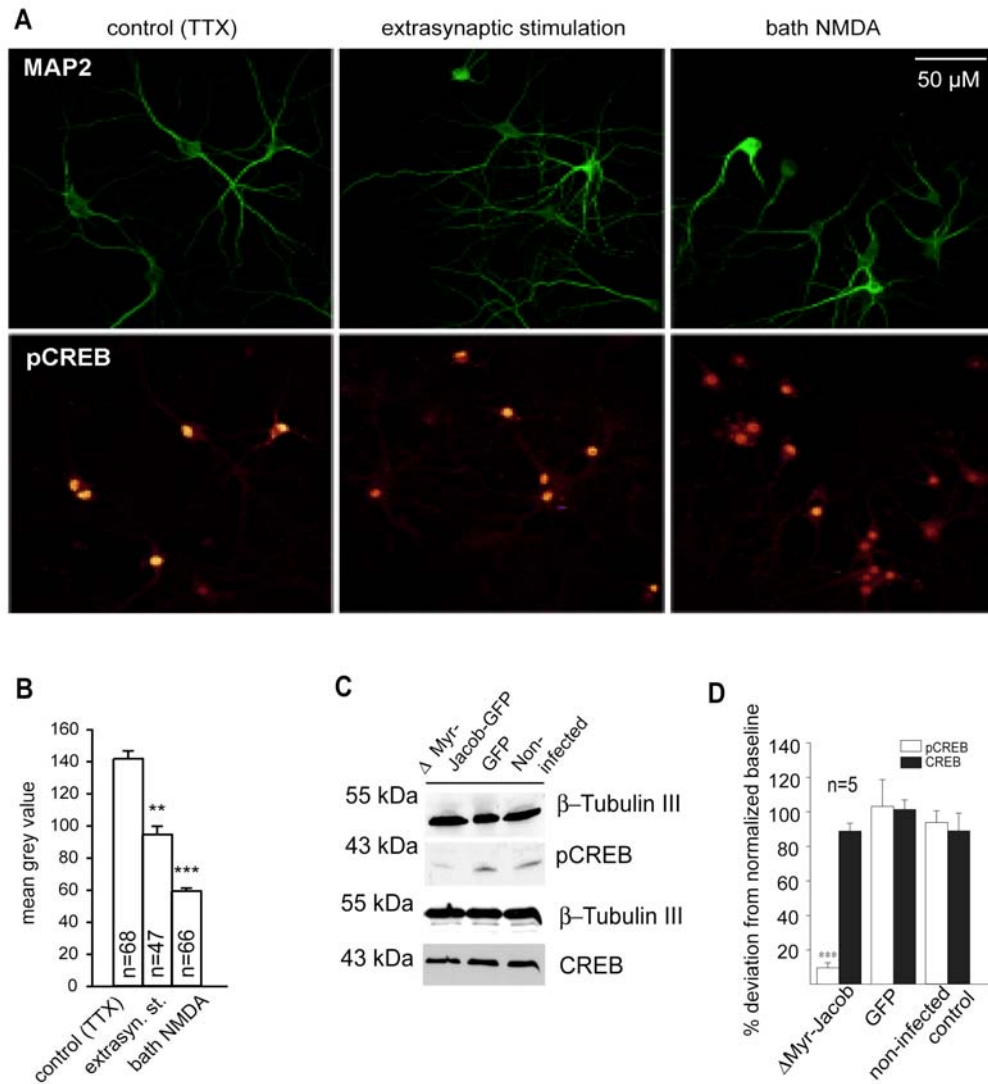


Figure 11. Nuclear Jacob regulates the phosphorylation of CREB. (A) Extrasynaptic stimulation (hippocampal neurons, DIV18) as well as bath application of NMDA (100  $\mu\text{M}$ , 3 min) reduces level of pCREB in the nucleus. MAP2 is included as a neuronal marker and also as an indicator for a living cells (B) Quantification of pCREB level upon different stimulations. (C) Overexpression of  $\Delta$ Myr-Jacob-EGFP using a Semliki Forest Virus vector significantly reduced the level of pCREB at resting conditions in comparison to EGFP-infected and noninfected cortical primary neurons. The diagram (B) represents the data from four to five independent experiments normalized to  $\beta$ -Tubulin III. Total CREB levels were not affected by infection of the cultures. \*\*\*,  $p < 0.001$ , \*\*,  $p < 0.01$ . Error bars represent the SEM.

Since Jacob is targeted efficiently to neuronal nuclei after extrasynaptic NMDA receptor activation, we next addressed the question whether the presence or absence of Jacob in the nucleus affects the phosphorylation of CREB at this crucial residue. As a first proof of principle, we explored whether the nuclear overexpression of the myristoylation mutant of Jacob ( $\Delta$ Myr-Jacob-GFP construct) significantly reduced the levels of pCREB in hippocampal primary neurons as compared to untransfected or GFP-transfected controls under resting conditions (Dieterich et al., 2008). Similarly, infection of cortical primary cultures with a Semliki Virus expressing  $\Delta$ Myr-Jacob-GFP leads to drastically reduced pCREB levels as evidenced by quantitative immunoblotting while the total CREB levels were not affected (Fig. 11C and D).

To more rigorously test the hypothesis that Jacob is part of the CREB shut-off we induced a knock-down of nuclear Jacob using plasmid based RNAi constructs targeting exon 6 containing isoforms of the protein and subsequently stimulated extrasynaptic NMDA receptors with the protocol outlined above. We found that nuclear knock down of Jacob completely abolished the reduction of pCREB observed after stimulation of extrasynaptic NMDA receptors (Dieterich et al., 2008). These data point to a critical role of Jacob for survival of hippocampal primary neurons after triggering the CREB shut-off pathway.

### **3.5 The primary structure of Caldendrin and Calneurons**

Taken together the evidence so far points to an important role of Caldendrin in many aspects of neuronal  $\text{Ca}^{2+}$  signaling and it was therefore rather surprising that the shorter Caldendrin splice isoforms and the other CaBP family members that share the same EF-hand organization and show a high degree of homology are only prominent in retina. A search in public databases, however, revealed several EST- and cDNA clones from brain tissue that show significant similarity to the first two EF-hands of Caldendrin/CaBPs and CaM. Further analysis of these clones disclosed the existence of two highly homologous proteins from which the sequence of one of them has been previously published under the name of Calneuron (Wu et al., 2001), whereas the other was termed CaBP7 (Haeseleer et al., 2002). Based on our initial characterization (see below) we decided to introduce the name Calneuron for both proteins to indicate that they are  $\text{Ca}^{2+}$  binding proteins prominently present in neurons and constitute a new subfamily of CaM-like calcium sensors closely related to but distant from Caldendrin/CaBPs. We cloned Calneuron-1 (Accession number: XM344102) and -2 (Accession number: AY841152) using RT-PCR from rat brain cDNA

and a subsequent alignment of their amino acid sequence revealed that they are highly homologous to each other (Fig. 11A). Calneuron-1 encompasses an open reading frame of 219 amino acids and Calneuron-2 of 215 amino acids with an overall identity of 63% between both of them (Fig. 12A). They have a short N-terminal region flanking the EF-hands but interestingly, they also possess a 38 amino acid long extension of its C-terminus as compared to Caldendrin (Fig. 12). This extension is uncommon in neuronal calcium sensor proteins and a unique feature of the Calneuron structure. CaM, the archetypal calcium sensor, consists of two canonical EF-hand domains tethered by a flexible linker. As depicted in Figure 3, Caldendrin has only three functional EF-hands, i.e. 1, 3 and 4, whereas EF-hand 2 does not bind  $\text{Ca}^{2+}$ . In Calneuron-1 and -2 only the first two EF-hands fulfill the criteria for a canonical  $\text{Ca}^{2+}$  binding EF-hand. Based on sequence comparison, it appears that there is a deletion of three residues in EF-hand 3 of Calneurons, and Asp is replaced by Ser at the +x coordinate position (first coordinating residue of the loop) in EF-hand 4 which makes both of them most likely incapable to chelate  $\text{Ca}^{2+}$  or other cations (Fig. 2 and Fig. 12). Interestingly, the presence of an Asp at the -z coordinating position in EF-hand 1 (12<sup>th</sup> residue of the EF-hand loop) of Caldendrin decreases its specificity for  $\text{Ca}^{2+}$  and it has been shown that it most likely exists in a constitutively  $\text{Mg}^{2+}$  bound form (Burgoyne et al, 2004). This is at variance with calneurons that have a Glu at this position and it can therefore be expected that their two functional EF-hands are high-affinity  $\text{Ca}^{2+}$  binding sites.

Moreover, the organization of functional EF-hands is unique for Calneurons and does not match those of other neural calcium sensor proteins (Fig. 12). The presence of non-functional EF-hands is a common feature of NCS proteins (Fig. 3) and it is thought to play an important structural role for the dynamics and specificity of their target interactions. It can be therefore concluded that the C-terminal non-functional EF-hand like structures might be significant for their cellular function. Interestingly, databank entries show that the amino acid sequence of Calneuron-1 and -2 is 100% identical between human, rat and mouse. This high degree of conservation clearly supports the idea that also the c-terminal half of Calneurons has some functional significance related to its structure. Of particular interest is the observation that in contrast to all CaBP family members as well as all to the closely related NCS proteins, Caldendrin and Calneurons lack a N-myristoylation motif that can provide a lipid anchor for membrane attachment (Fig. 12). In conjunction with a bootstrap analysis of neighbor joining distances (data not shown), which showed that although Caldendrin, CaBPs and Calneurons are closely related the phylogenetic tree also indicates that Calneurons



constitute a new subfamily of CaM-related EF-hand calcium sensors with a unique EF-hand organization (Fig. 16B).

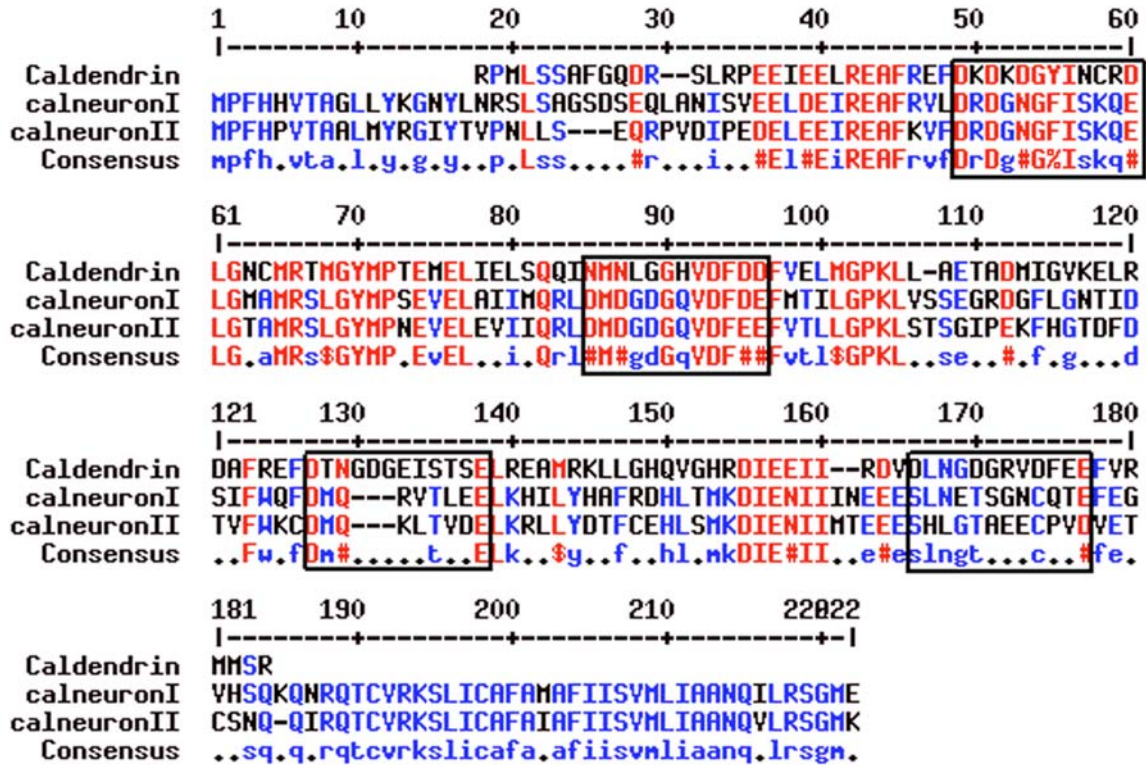


Figure 12. Alignment of the amino acid sequence of Caldendrin and Calneuron-1 and -2. Sequences were aligned using the MultAlin program (<http://bioinfo.genotoul.fr/multalin/>). Putative EF-hand motifs (EF1 – EF4) are represented as boxes. Amino acids in red are identical in all three proteins, amino acids in blue only in Calneuron-1 and -2. \$ is anyone of LM; % is anyone of FY; # is anyone of NDQEBZ.

### 3.6 Comparative modeling of Caldendrin and Calneurons EF-hand structures

We next looked more closely into the predicted 3D structure of Calneurons in comparison to those of Caldendrin. The 3D structure of Caldendrin is not yet known though the resonance assignments of apo, Mg<sup>2+</sup> and Ca<sup>2+</sup> bound forms of CaBP1 by NMR have been completed (Wingard et al., 2005). Using the Swiss Modeller server (Swede et al., 2003) we first generated a structural model of Caldendrin (Fig. 13A).



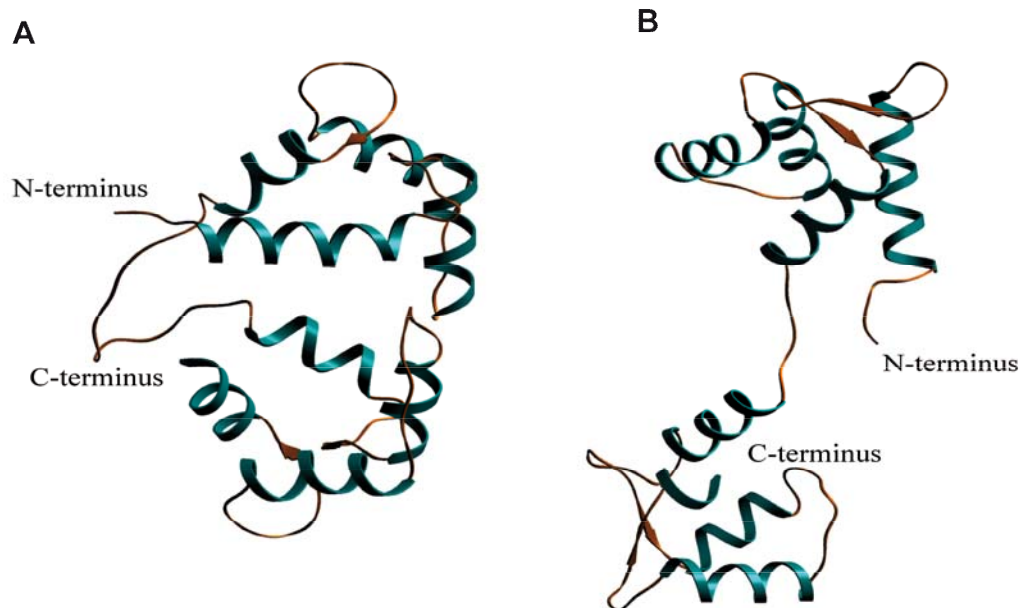


Figure 13. Predicted structure of (A) Caldendrin (from amino acid 155 to 298) and (B) Calneuron-1 (from amino acid 1 to 219). The structures were generated by automatic homology modeling using the Swiss Modeler Server <http://swissmodel.expasy.org/SWISS-MODEL.html>, and visualized using the SETOR program on a Silicon Graphics Work station. The model is represented in the form of secondary structures showing helix,  $\beta$ -strand and coiled-coil conformations.

The topology of Caldendrin appears different than the CaM structure since it does not show the typical CaM-like dumb-bell shaped topology, though it has a two-domain structure. Unlike CaM, which in the region joining both domains forms a long central helix, Caldendrin appears to be more in a coiled-coil conformation in this region (Fig. 13A). Calneuron-1 is predicted to have a more CaM like topology (Fig. 13B). Interestingly, however, also in Calneuron-1 the CaM-like central linker region seem to be different and might exhibit a more coiled-coil structure. As mentioned above, Calneuron-1 has two functional EF-hands (EF-hand 1 and 2) located in the N-terminal domain whereas both non-functional EF-hands (3 and 4) are located at the C-terminal domain. Though non-functional, both of these EF-hands have typical helix-loop-helix conformations, which will, however, not bind  $\text{Ca}^{2+}$ . The intrinsic specificity of the CaM-fold is determined by each of the dumb-bell shaped halves and the various arrangements of the two halves upon target peptide binding.  $\text{Ca}^{2+}$ -free EF hands sterically allow the complete closure of the concave hydrophobic target peptide binding pocket build by one double EF hand domain. The saturation of  $\text{Ca}^{2+}$  ions fixes the flexibility of both EF hand loops and shifts the equilibrium towards the open state. Mutated EF hand loops not capable to bind  $\text{Ca}^{2+}$  may exhibit either all time flexibility or stiffness depending on the type of residue mutation or deletion.

Interestingly, Caldendrin and Calneurons show both types of mutated EF hands. In Caldendrin, the flexibility of the mutated second EF hand is increased by a mutation of a  $\text{Ca}^{2+}$  binding aspartate to glycine. The third EF hand in Calneurons is in part deleted and mutated with hydrophobic side chains to make a short stiff conformation of the helix-loop-helix motif. The fourth EF hand remains flexible, which may be moderated by  $\text{Ca}^{2+}$  ions as three glutamic acids and in Calneuron-1 an additional aspartate are located within this loop. In consequence, both double EF hand domains of Caldendrin and Calneurons may bind to target peptides, using different protein dynamics. The first domains of Calneurons and the second domain of Caldendrin exhibit similar  $\text{Ca}^{2+}$ -dependent binding properties as CaM, while the remaining domains require a high-affinity binding peptide, which forces the domain to take up an open conformation.

Interestingly, while looking more closely at the EF-hand structure, it appears that the calcium-binding pockets in Calneurons differ in cavity sizes thereby influencing the affinity for  $\text{Ca}^{2+}$  (Fig. 13). Leu48 (Calneuron-1) at the beginning of the EF-hand 1 loop is replaced by Phe45 (Calneuron-2), which fills up the cavity due to its large side chain (Fig. 14).

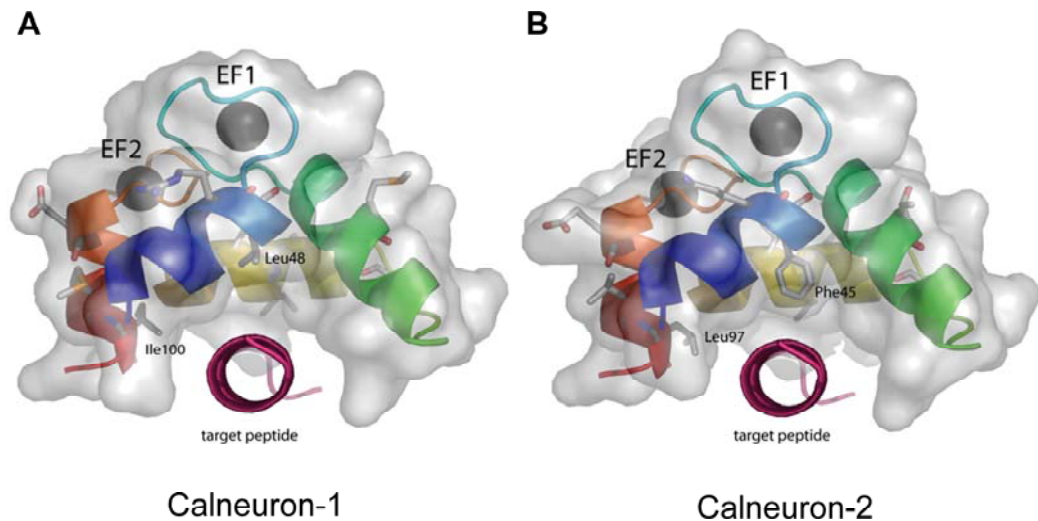


Figure 14. Differences in the target peptide binding pockets of EF-hand 1 and 2 in Calneurons. The target helical peptide binds to the  $\text{Ca}^{2+}$  activated open hydrophobic pocket. The binding pocket differs by two residues, only. Calneuron-2 pocket is filled with three more atoms maintained by Phe45 as compared to Leu48 in Calneuron-1. The other differences between both proteins are located within the EF hand connecting residues and on the surface of the domain.

Therefore Calneuron-2 may preferentially bind to helices having a shorter hydrophobic side chain anchor (Fig. 14B). The surface charge distribution is comparable in all three proteins. Notable differences are seen at the tip of the linking loop between the two EF-hands. Ser73 and Ala78 of Calneuron-1 are replaced by Asn70 and Glu75 in Calneuron-2, respectively.

Larger sequence deviations are also on the concave surface and as mentioned the helix, which joins the second double EF-hand domain. In Calneurons and CaM, the second EF-hand is more dependent on pH and it is likely, that the second EF-hand undergoes a larger conformational change at low  $\text{Ca}^{2+}$  concentrations. Interestingly, there is a tyrosine residue at the tip of the linking loop between EF-hand 1 and EF-hand 2 (Calneuron-1: Tyr70, Calneuron-2: Tyr67) and a corresponding Tyr was also noted for Caldendrin (Seidenbecher et al., 2002). The influence of this residue on the binding specificity for target interactions is unknown.

### **3.7 Caldendrin and Calneurons are abundant in brain**

To initially address the important question whether Calneurons like Caldendrin show prominent expression in brain, we performed *in situ* hybridization studies to localize Calneuron transcripts in rat brain sections (Fig. 15A).

These studies revealed that Calneuron-1 and -2 mRNA is indeed present in rat brain with an expression pattern that exhibits partial overlap with those of Caldendrin. Calneuron-1 transcripts have a widespread distribution with intense hybridization signals in the cerebellum but are also present in many other brain regions like cortex and hippocampus where high levels of Caldendrin transcripts are found (Fig. 15A). This is in contrast to the expression of Calneuron-2, which is restricted to the CA3 region of the hippocampus, entorhinal cortex, the antero-dorsal and antero-ventral thalamus as well as the inferior and superior colliculus (Fig. 15A). We next generated antibodies to Calneuron-1 and -2 to perform immunoblots and immunocytochemical stainings of hippocampal primary neurons.

Subcellular fractionation studies of rat brain homogenates showed that Calneurons are present in all fractions including membrane-containing fractions like microsomes (Golgi membranes) and light membrane fraction (ER and Golgi) (Fig 15B). In contrast to Calneurons and NCS-1, Caldendrin is also tightly associated with the specialized cytoskeleton of the synapse, the postsynaptic density protein fraction (PSD) that was also demonstrated previously (Seidenbecher et al., 1998; Dieterich et al., 2008).

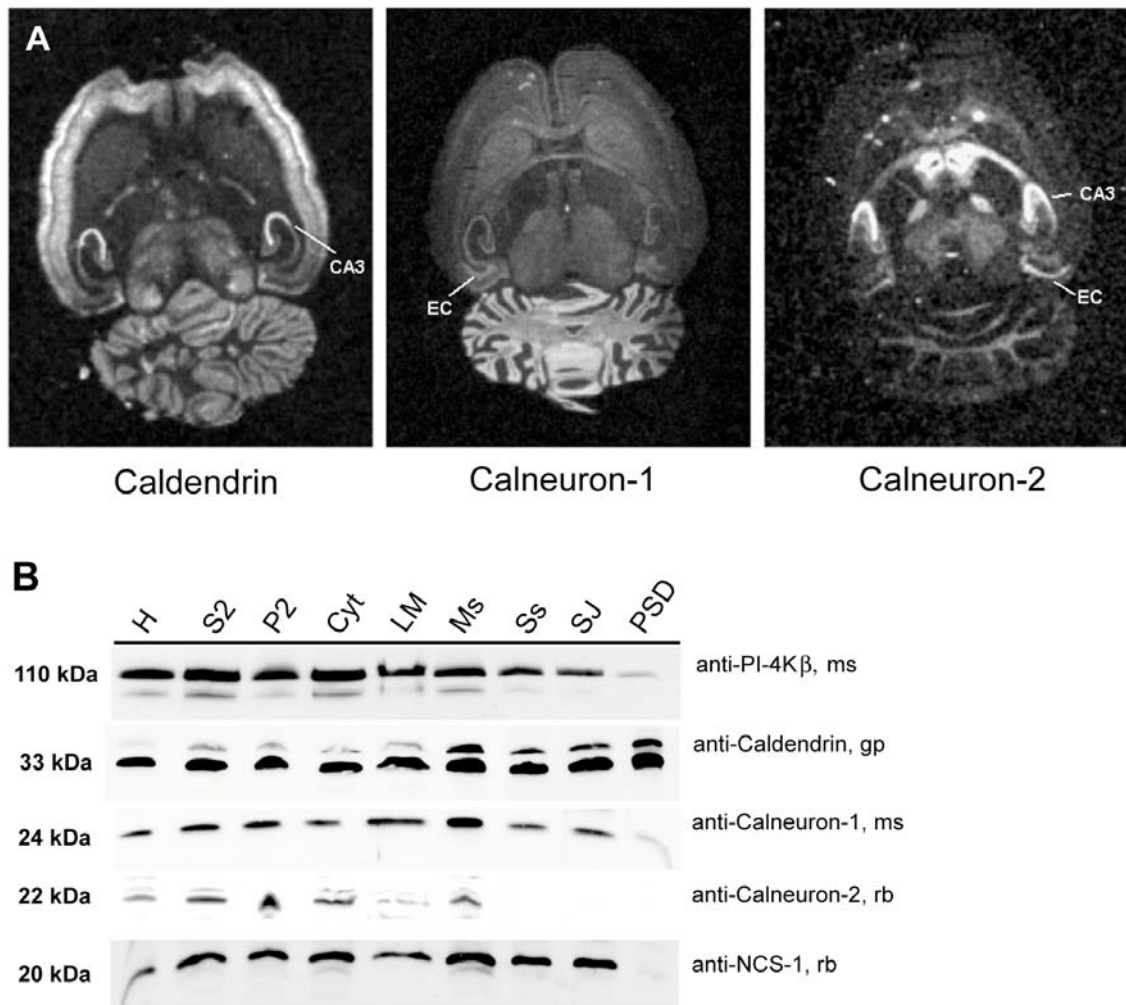


Figure 15. (A) *In situ* hybridization of horizontal adult rat brain sections with oligonucleotide probes specific for Caldendrin and Calneurons. CA3, cornu ammonis 3 of the hippocampus; EC, entorhinal cortex (B) Subcellular fractionation of rat brain protein homogenates. H, homogenate; S2, 13.000xg supernatant after removal of cell debris and nuclei; P2, corresponding pellet; Cyt, cytosol fraction; LM, light membranes; MS, microsomes – Golgi containing fraction; Ss, synaptosomes; SJ, synaptic junctions; PSD, postsynaptic density fraction. Equal amounts of protein (20  $\mu$ g) were loaded in each lane. The same blots were incubated with several different antibodies. ms, mouse; gp, guinea pig; rb, rabbit.

### 3.8 Calneurons are localized at the Golgi apparatus and associate with PI-4K $\beta$ *in vivo*

During their initial characterization we realized that, when expressed as GFP-fusion proteins in COS-7 cells, Calneuron-1 and -2 consistently accumulated at cellular structures counterstained with the Golgi marker Syntaxin-6 (Fig. 16A). This is in contrast to the localization of Caldendrin expressed in COS-7 cells and this highly restricted localization was also not observed with NCS-1-GFP construct (Fig. 16A). It is to be noted that a considerable overlap exists between the GFP-Calneuron-1 and -2 fluorescence and the

immunofluorescence of endogenous PI-4K $\beta$  (Fig. 16A). Confocal laserscans also revealed overlap in the distribution of endogenous Calneurons with PI-4K $\beta$  and Syntaxin 6 in neuronal cells that was again stronger than those of Caldendrin and NCS-1 (Fig. 17A).

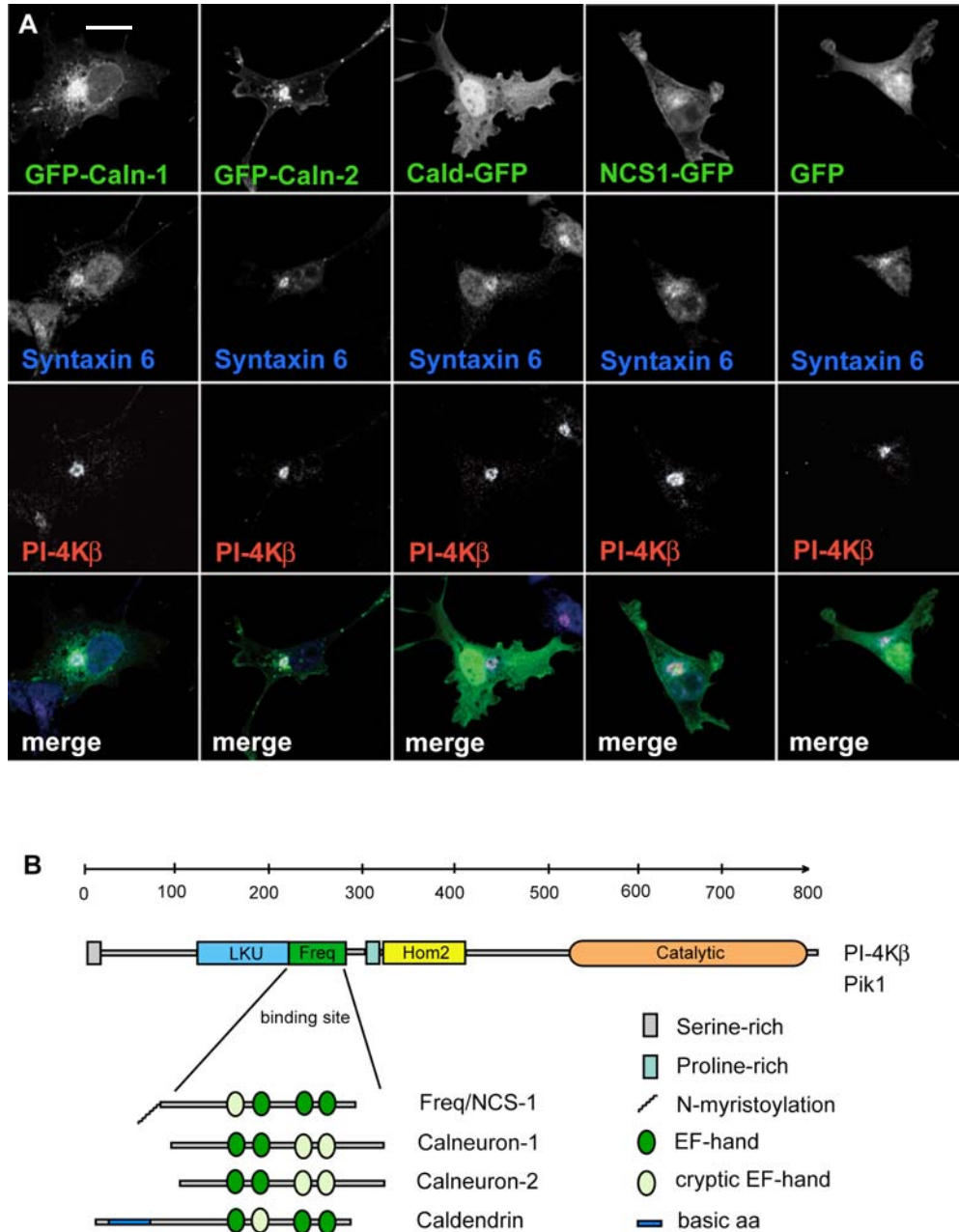


Figure 16. (A) Over-expression of Calneuron-1, -2, Caldendrin, NCS-1 GFP-fusion constructs and a GFP-control in COS-7 cells. Syntaxin-6 (blue) immunofluorescence staining was used as a trans-Golgi network marker. Please note that Calneurons as compared to NCS-1 and Caldendrin are particularly abundant at the Golgi. Importantly, they show a very good co-localization with PI-4K $\beta$  (red) on confocal laserscans. Scale bar is 20  $\mu$ m. (B) Primary structure of Caldendrin, Calneurons, NCS-1 and PI-4K $\beta$ . Shown is a schematic representation as predicted from their cDNA sequences. The main sequence features including EF-hand structures, N-myristoylation, the lipid kinase unique (LKU) and catalytic domain as well as the Frq1/NCS-1 binding site (Freq) in PI-4K $\beta$  are depicted.



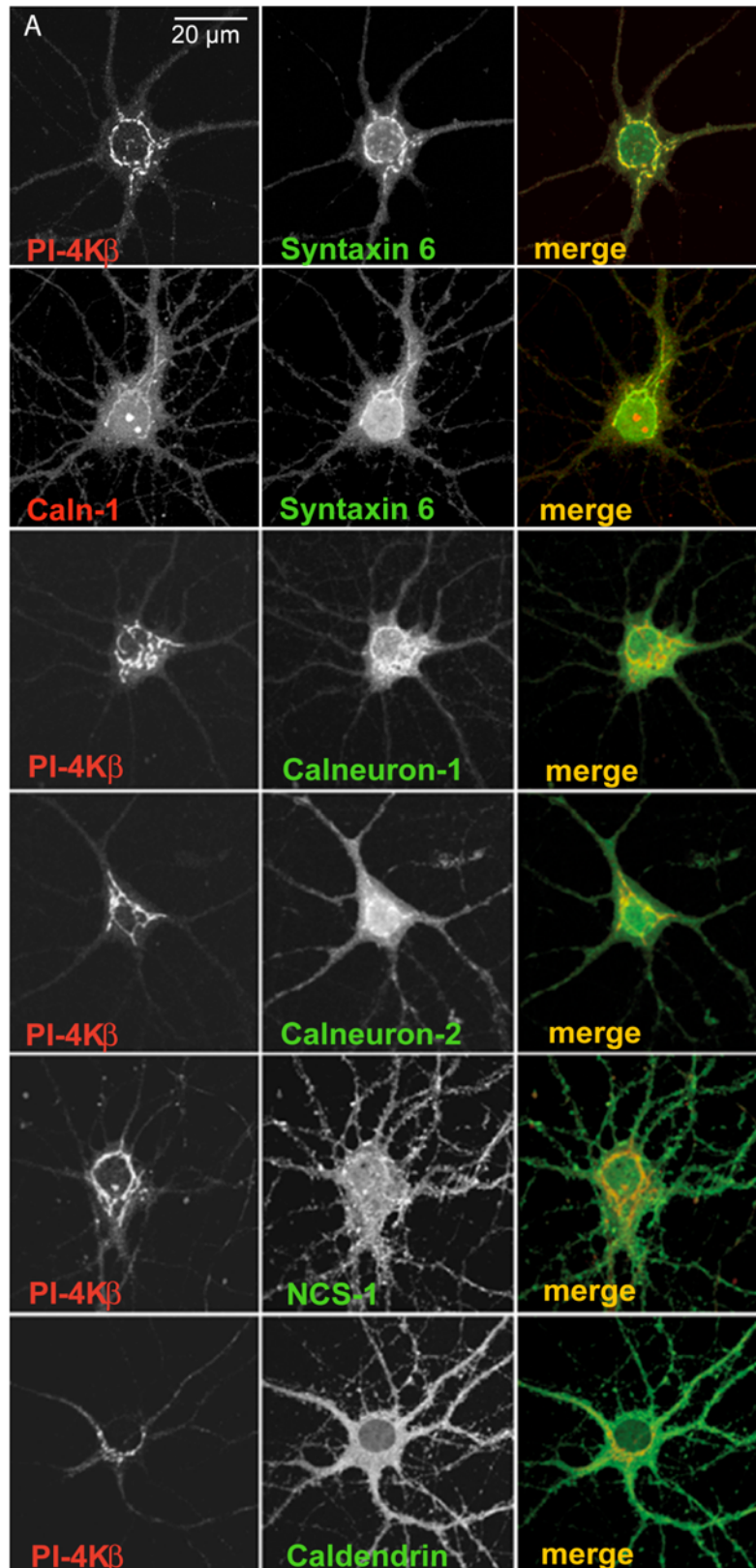


Figure 17. Distribution of endogenous Calneurons in comparison to NCS-1 and Caldendrin. (A) Note that in hippocampal primary neurons Calneurons are much more restricted to the Golgi complex and show a much better overlap with PI-4K $\beta$  than Caldendrin and NCS-1. Syntaxin 6 co-staining is used as a Golgi marker. Scale bar is 20  $\mu\text{m}$ .

Studies so far showed that the calcium sensor NCS-1 via its N-terminal myristoylation associates in a  $\text{Ca}^{2+}$ -independent manner with Golgi membranes (McFerran et al., 1999; O'Callaghan et al., 2002) where it interacts with PI-4K $\beta$  (Hendricks et al., 1999; Zhao et al., 2001). This interaction appears to be an evolutionary highly conserved mechanism that has evolved already in yeast (Hendricks et al., 1999, Huttner et al., 2003). Yeast null mutant strains of Frq1, the Drosophila (Pongs et al., 1993) / yeast orthologue (Hendricks et al., 1999) of NCS-1, as well as those of the yeast PI-4K $\beta$  orthologue Pik1 are not viable pointing to the essential role of both proteins in Golgi-to-plasma membrane trafficking (Flanagan et al., 1993; Hendricks et al., 1999; Strahl et al., 2003; Strahl et al., 2005). This is, however, at variance with the situation in mammalia where NCS-1 seems to be more diffusely distributed in neurons with considerable amounts of the protein localized outside of the Golgi (Bourne et al., 2001; Taverna et al., 2002). Moreover, its binding to PI-4K $\beta$  seems to be of lower affinity as compared to the yeast proteins (Zhao et al., 2001). It is therefore likely that the regulation of Pik1 and PI-4K $\beta$  differs substantially with the latter one being more susceptible to modulation via  $\text{Ca}^{2+}$  transients at the Golgi (Haynes et al., 2005). To date NCS-1 is the only NCS protein known to interact with PI-4K $\beta$  whereas other members of this family, like Recoverin (Hendricks et al., 1999) or KChIP (Strahl et al., 2003), apparently do not modulate PI-4K $\beta$  activity.

To check if Calneurons like NCS-1 also can associate with PI-4K $\beta$  we performed a number of interaction studies. First we tested whether rabbit polyclonal Calneuron-1 and -2 and NCS-1 antibody can be suitable for immunoprecipitation experiments. In co-immunoprecipitation experiments from COS-7 cell extracts after over-expression of GFP-Calneuron-1, -2 or -NCS-1 significant amount of corresponding proteins can be seen in IP fractions on the immunoblots with GFP mouse antibody. We also could detect the presence of PI-4K $\beta$  in precipitates from the corresponding lysates of cells transfected with the different GFP-  $\text{Ca}^{2+}$ -binding protein fusion constructs but not in GFP-controls (Fig. 18A). Further evidence that endogenous Calneurons are in the same complex with PI-4K $\beta$  *in vivo* came from co-immunoprecipitation experiments. PI-4K $\beta$  immunoreactivity could be detected in precipitates obtained with Calneuron-1 and -2 antibodies, but not after precipitation with control IgG (Fig. 18B).

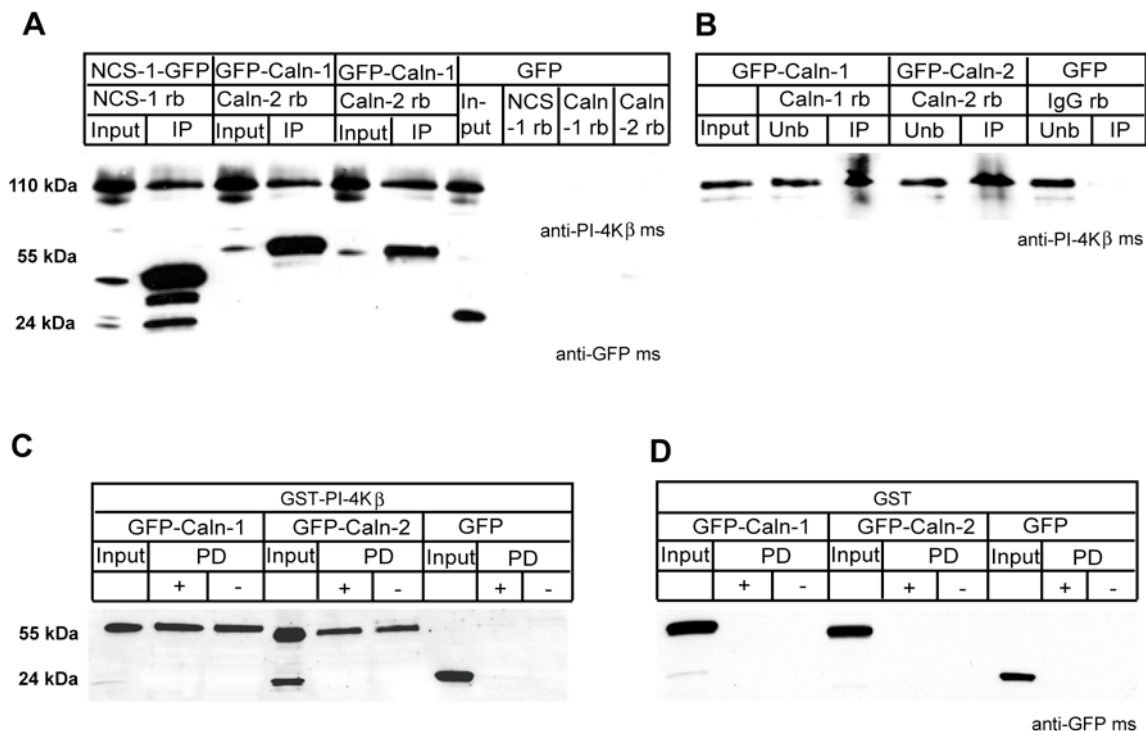


Figure 18. Calneurons interact with PI-4Kβ *in vivo* and *in vitro* in Ca<sup>2+</sup> independent manner. (A) Co-immunoprecipitation of GFP-tagged NCS-1, Calneuron-1 and -2 with PI-4Kβ after heterologous expression in COS-7 cells. PI-4Kβ (upper panel) co-precipitates in one complex with all three fusion proteins of interest but not with GFP alone. Staining with a GFP antibody demonstrates the amount of immunoprecipitated protein. (B) Co-immunoprecipitation of Calneuron-1 and -2 with PI-4Kβ from a rat brain extract. Rabbit polyclonal Calneuron antibodies were used for immunoprecipitation and the immunoblots were processed with a mouse PI-4Kβ antibody. Similar amounts of a rabbit IgG served as a control. A pull down assay with GST-PI-4Kβ coupled to the matrix and GFP tagged Calneuron-1 and -2 demonstrates a Ca<sup>2+</sup>-independent interaction of these proteins (C). “+” indicates the presence of Ca<sup>2+</sup> (2mM Ca<sup>2+</sup> and 1mM Mg<sup>2+</sup>) and “-“ Ca<sup>2+</sup>-free conditions (2mM EGTA and 1mM Mg<sup>2+</sup>). The blots were developed with a GFP-antibody. In the lane containing the Calneuron-2 GFP some breakdown product is visible. No specific pull down was visible in GFP and GST controls (D). Unb: unbound; IP: immunoprecipitate; Caln-1: Calneuron-1; Caln-2: Calneuron-2; ms, mouse; rb: rabbit.

We next analyzed the association of endogenous Calneurons and NCS-1 with PI-4Kβ using gel filtration of extracts from Golgi-enriched microsomal fractions. We first simulated low Ca<sup>2+</sup>-conditions by adding EDTA to the extracts. Under these conditions PI-4Kβ was detected in complexes with molecular weights of 700-300 kDa and co-elute with the Golgi marker Syntaxin 6 (Fig. 19A). Calneuron-1 and -2 are present in the higher molecular weight range of these PI-4Kβ positive fractions. In contrast, NCS-1 is associated with lower molecular weight complexes that show no overlap with Calneuron-containing fractions (Fig. 19A). These data indicate that PI-4Kβ might exist in a Calneuron- or NCS-1-bound form at the Golgi with no overlap of both complexes under low Ca<sup>2+</sup> conditions. Elevating Ca<sup>2+</sup> levels induced a shift of NCS-1 to higher molecular weight PI-4Kβ containing complexes (Fig. 19B), whereas Calneurons were excluded from these complexes



or shifted to lower molecular weight fractions containing PI-4K $\beta$  (Fig. 19B). This suggests a dynamic regulation of the PI-4K $\beta$  association for the two types of Ca<sup>2+</sup> sensors.

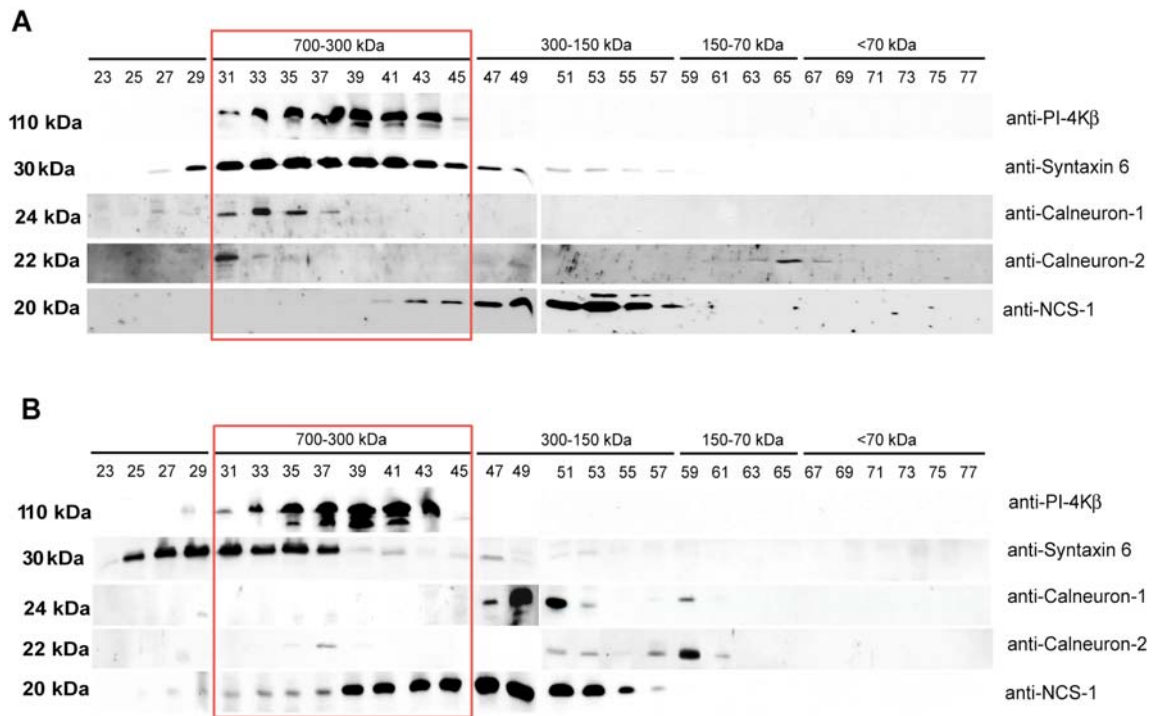


Figure 19. (A) Gel filtration of proteins from a microsomal preparation under low Ca<sup>2+</sup> conditions. Every second fraction is loaded on the gel. Fractions covering the range from ~900 to ~20 kDa were collected from EDTA treated extracted extracts, loaded on SDS-PAGE and analyzed by Western blotting. The red box highlights the PI-4K $\beta$  containing fractions. (B) Gel filtration of proteins from a microsomal preparation under high Ca<sup>2+</sup> conditions (2mM Ca<sup>2+</sup> and 1mM Mg<sup>2+</sup>). The red box highlights the PI-4K $\beta$  containing fractions. The same blots were incubated with a several different antibodies.

### 3.9 Calneurons physically interact with PI-4K $\beta$ and compete with NCS-1 binding in a Ca<sup>2+</sup>-dependent manner

The limited overlap of elution profiles from molecular sieves and the possibility that NCS-1 and Calneurons might be present in complexes with PI-4K $\beta$  not purified with a microsomal protein preparation lead us to ask under which Ca<sup>2+</sup> conditions Calneurons bind to PI-4K $\beta$  and whether binding competes with that of NCS-1. We could confirm binding of both GFP-Calneurons to GST-PI-4K $\beta$  in a GST pull-down assays (Fig. 18C and D). It has been shown previously that NCS-1 binds to PI-4K $\beta$  in a Ca<sup>2+</sup>-independent manner (Zhao et al., 2001). Similarly, binding of Calneurons to PI-4K $\beta$  was found in the presence of either Ca<sup>2+</sup> or the Ca<sup>2+</sup> chelator EGTA in the pull-down buffer (Fig. 18C and D). It is therefore plausible that Calneurons will associate with PI-4K $\beta$  at resting cellular Ca<sup>2+</sup> levels. To test

the hypothesis that this association will be competitive we performed competition pull-down assays with decalcified, bacterially expressed untagged Calneuron-1, GST-PI-4K $\beta$  and myr-NCS-1.

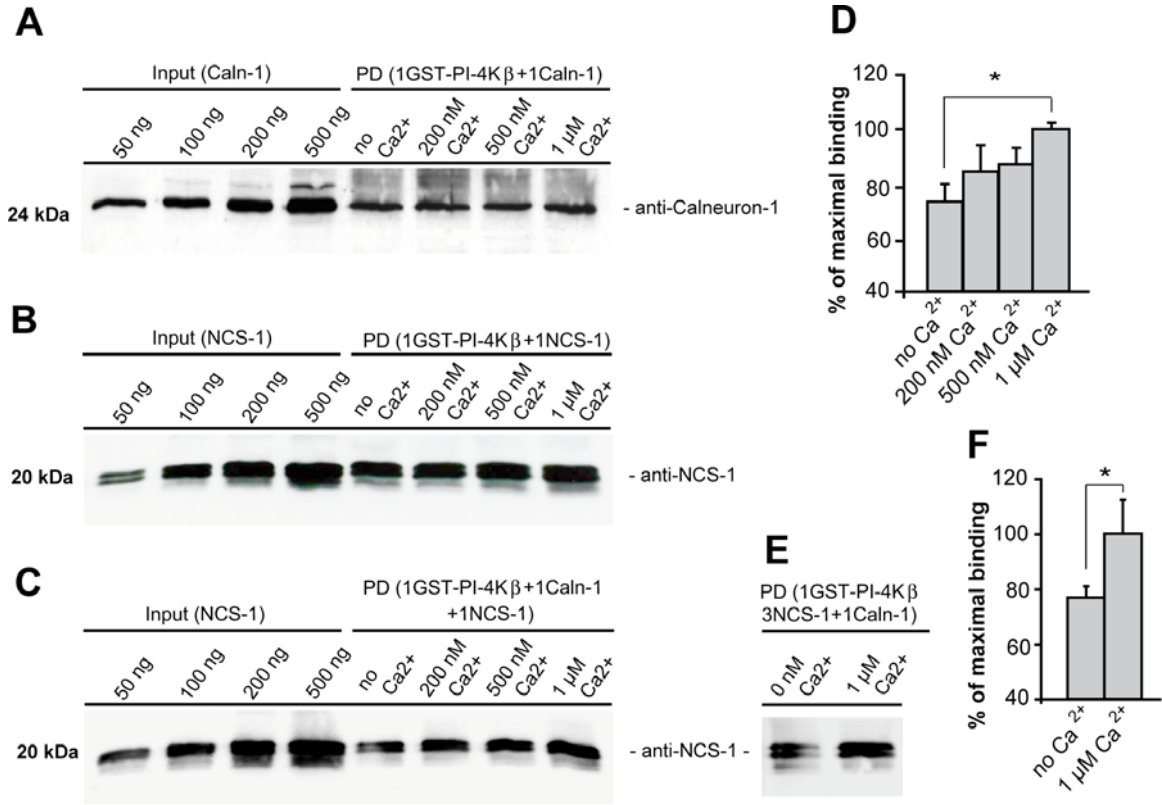


Figure 20. Both untagged myr-NCS-1 and untagged Calneuron-1 interact with GST-PI-4K $\beta$  in vitro and compete for the same binding site in a Ca<sup>2+</sup> dependent manner. (A) Calneuron-1 alone binds GST-PI-4K $\beta$  in a pull down assay independently from Ca<sup>2+</sup> concentrations. (B) myr-NCS-1 alone binds GST-PI-4K $\beta$  in a pull down assay independently from Ca<sup>2+</sup> concentrations. (C) Competition pull down with GST-PI-4K $\beta$  coupled to the matrix. Equimolar amounts of myristoylated NCS-1 and Calneuron-1 were used. Increased binding of NCS-1 with increasing Ca<sup>2+</sup>-concentrations is accompanied by decreased Calneuron binding. (D) Quantification of myr-NCS-1 binding in competition assay (n=4). Maximal binding at 1  $\mu$ M Ca<sup>2+</sup> was taken as 100%. (E) Competition pull down assay with triple amount of myr-NCS-1 and its quantification, n=3 (F). All experiments were done in the presence of 1mM Mg<sup>2+</sup>. 500 ng of Calneuron-1 and myr-NCS-1 were used for the pull downs and different amounts of these proteins are included as the inputs. All reaction were done overnight at 4°C. Error bars represent the SEM. p<0.05

We checked the Ca<sup>2+</sup> concentrations that can be achieved in the cells under physiological conditions. We observed direct binding of Calneuron-1 and NCS-1 to GST-PI-4K $\beta$  irrespective of the Ca<sup>2+</sup> concentrations used after overnight incubation at 4°C (Fig. 20A and B). When equimolar amounts of Calneuron-1 and myr-NCS-1 were added to the pull-down buffer a significant reduction of NCS-1 binding to GST-PI-4K $\beta$  was observed in the absence of Ca<sup>2+</sup> (Fig. 20C and D). Interestingly, binding of NCS-1 appears to be stronger at

higher  $\text{Ca}^{2+}$  levels. We repeated the same competition pull-down assay with a triple amount of myr-NCS-1 but even then there was less binding of NCS-1 to PI-4K $\beta$  under low  $\text{Ca}^{2+}$  conditions (Fig. 20E and F). The competition was  $\text{Ca}^{2+}$ -sensitive with most efficient NCS-1 binding to GST-PI-4K $\beta$  in the presence of equimolar amounts of Calneuron-1 at  $1\mu\text{M}$   $\text{Ca}^{2+}$  and most efficient competition by Calneuron-1 at  $200\text{ nM}$  or no  $\text{Ca}^{2+}$  in the buffer.

To get closer to the *in vivo* situation we replicated the same competition pull down assay at RT with 1 h incubation time (Fig. 21A). In the second set of experiments we used his-tagged Calneuron-1 because it has a higher expression yield in bacteria and the purification procedure does not requiring extraction of the proteins from inclusion bodies. GST control was also included for the each condition. Again we could observe the same tendency: with increasing  $\text{Ca}^{2+}$  concentrations the amount of NCS-1 bound to PI-4K $\beta$  was increasing and vice versa for Calneuron-1. There was also some non-specific binding of Calneuron-1 and NCS-1 to GST-sepharose observed that could be reduced by preincubation of beads with 5% BSA containing buffer for 15 min at RT (Fig. 21A). We next analyzed the amount of bound NCS-1 in the same way (maximal binding of NCS-1 at  $1\mu\text{M}$  of  $\text{Ca}^{2+}$  was taken as 100%) with subtraction of GST binding from each individual experiment (Fig. 21B) and found 45% reduction of binding at low  $\text{Ca}^{2+}$  levels. All competition pull downs were done in the presence of  $\text{Mg}^{2+}$ .

To confirm these data in a more quantitative manner we performed surface plasmon resonance measurements with His-tagged Calneuron-1 coupled to the sensor chip. Even with recombinant GST-PI-4K $\beta$  and NCS-1 in the running buffer, conditions which favour the initial formation of a GST-PI-4K $\beta$  / NCS-1 complex, we found a prominent competition between Calneuron-1 and NCS-1 for binding to PI-4K $\beta$  (Fig. 21C and D). Moreover, the competition was  $\text{Ca}^{2+}$ -sensitive with exclusive binding of PI-4K $\beta$  to Calneuron-1 under  $\text{Ca}^{2+}$ -free conditions (Fig. 21D) while competitive binding of Calneuron-1 was weaker in the presence of  $0.4\mu\text{M}$   $\text{Ca}^{2+}$  as compared to  $0.2\mu\text{M}$   $\text{Ca}^{2+}$  (Fig. 21D). Interestingly, the competition in binding to PI-4K $\beta$  was also influenced by adding  $\text{Mg}^{2+}$  to the buffer. Calneuron relative to NCS-1 binding was stronger in the presence of  $\text{Mg}^{2+}$  at  $0.2\mu\text{M}$  and  $0.4\mu\text{M}$   $\text{Ca}^{2+}$ .

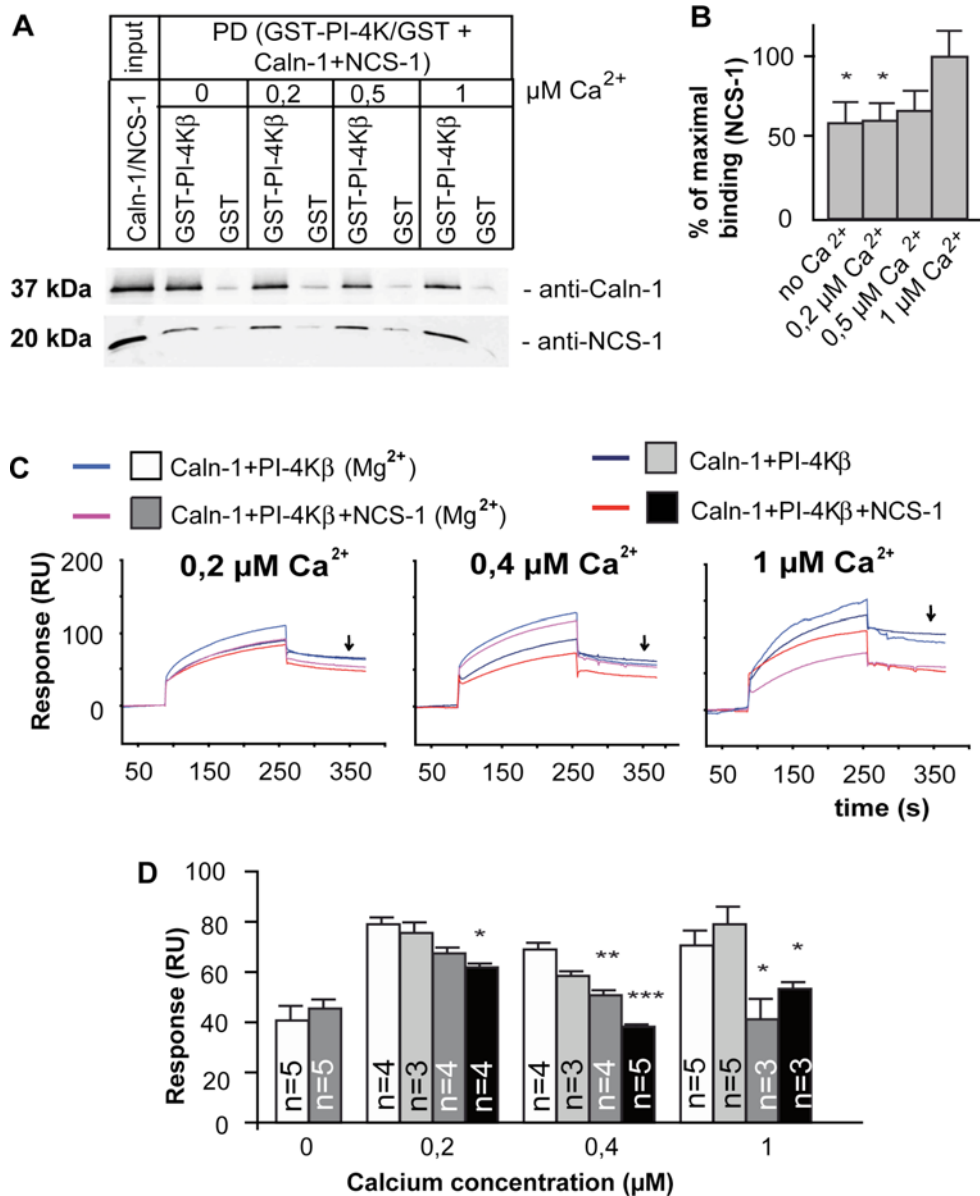


Figure 21. Calneuron-1 and untarged myr-NCS-1 compete for GST-PI-4K $\beta$  binding in a  $\text{Ca}^{2+}$ - and  $\text{Mg}^{2+}$ -dependent manner. (A) Competition pull-down with GST-PI-4K $\beta$  coupled to the matrix. Equimolar amounts of myristoylated NCS-1 and his-SUMO-Calneuron-1 were used. Increased binding of NCS-1 with increasing  $\text{Ca}^{2+}$  concentrations is accompanied by decreased Calneuron binding. All experiments were done in the presence of 1 mM  $\text{Mg}^{2+}$ . The same amount of NCS-1 and Calneuron-1 was used for the input and pull-downs. All reactions were performed for 1 hour at RT. (B) Significantly higher amounts of NCS-1 are bound to GST-PI-4K $\beta$  (binding to GST control was subtracted for the each individual case) in the presence of 1  $\mu\text{M Ca}^{2+}$  as compared with  $\text{Ca}^{2+}$ -free conditions. Five independent experiments were used for each condition. Error bars represent the SEM. (C) Surface plasmon resonance competition assay. His-SUMO-Calneuron-1 was directly immobilized on the sensor chip, and GST-PI-4K $\beta$  alone or equimolar amounts of GST-PI-4K $\beta$  and myr-NCS-1 were injected at different  $\text{Ca}^{2+}$  and  $\text{Mg}^{2+}$  concentrations. Representative examples of obtained binding curves at 0,2, 0,4 and 1  $\mu\text{M Ca}^{2+}$  are shown. (D) The response units (RU) at 350 s (dissociation phase) represent the amount of GST-PI-4K $\beta$  bound to Calneuron-1 on the sensor chip. Error bars represent the SEM. Note that under  $\text{Mg}^{2+}$ -free conditions less GST-PI-4K $\beta$  binds to calneuron-1 when coinjected with NCS-1 at low to moderate  $\text{Ca}^{2+}$  concentrations (0.2 and 0.4  $\mu\text{M}$ ). The minor unspecific binding of GST control alone or with NCS-1 to Calneuron-1 was subtracted from the GST-PI-4K $\beta$  values. \*\*\*,  $p < 0.001$ , \*\*,  $p < 0.01$ , \*,  $p < 0.05$ .

To evaluate the effect of  $Mg^{2+}$  on the interaction of PI-4K $\beta$  with Calneuron-1 and NCS-1 we coupled NCS-1 to the sensor chip and injected GST-PI-4K $\beta$  with different buffer conditions. For the relative evaluation of binding efficiency molar binding activity was calculated according to the formula suggested by Catimel et al. (1997).

Only the molar binding activity (MBA) of NCS-1 to PI-4K $\beta$  but not those of Calneuron-1 was reduced by adding  $Mg^{2+}$  into the reaction buffer (Table 5 and 6).

Table 5. MBA of myr-NCS-1 surfaces for GST-PI-4K $\beta$  in different  $Ca^{2+}/Mg^{2+}$  conditions

Myr-NCS-1 immobilized (ng/mm <sup>2</sup> )	GST-PI-4K $\beta$ ( $\mu$ M)	$Ca^{2+}$ concentration ( $\mu$ M)	$Mg^{2+}$ concentration ( $\mu$ M)	Signal (RU)	Molar binding activity
5,6	1	0,2	0	30	9,9E10 <sup>-4</sup>
5,6	1	0,2	200	23	7,9E10 <sup>-4</sup>
5,8	1	0,4	0	30	9,4E10 <sup>-4</sup>
5,6	1	0,4	200	22	7,2E10 <sup>-4</sup>

Table 6. MBA of His-SUMO-Calneuron-1 surfaces for GST-PI-4K $\beta$  in different  $Ca^{2+}/Mg^{2+}$  conditions

His-SUMO-Calneuron-1 immobilized (ng/mm <sup>2</sup> )	GST-PI-4K $\beta$ ( $\mu$ M)	$Ca^{2+}$ concentration ( $\mu$ M)	$Mg^{2+}$ concentration ( $\mu$ M)	Signal (RU)	Molar binding activity
7,6	5	0,2	0	74	3,9E10 <sup>-3</sup>
7,7	5	0,2	200	80	4,E10 <sup>-3</sup>
7,8	5	0,4	0	62	3,6E10 <sup>-3</sup>
7,7	5	0,4	200	75	3,9E10 <sup>-3</sup>

### 3.10 The $Ca^{2+}$ binding affinity of NCS-1 but not of Calneurons is regulated by $Mg^{2+}$

These results are puzzling because they suggest an association of Calneurons at low to intermediate  $Ca^{2+}$  levels, which is counteracted by NCS-1 at higher  $Ca^{2+}$  levels. However, the  $Ca^{2+}$ -binding affinities of Calneuron-1 and NCS-1 are reportedly very similar (Mikhaylova et al., 2006; Aravind et al., 2008). In search of a mechanistic explanation for this apparent contradiction we employed ITC to investigate the influence of structural  $Mg^{2+}$ -binding on  $Ca^{2+}$ -binding isotherms.

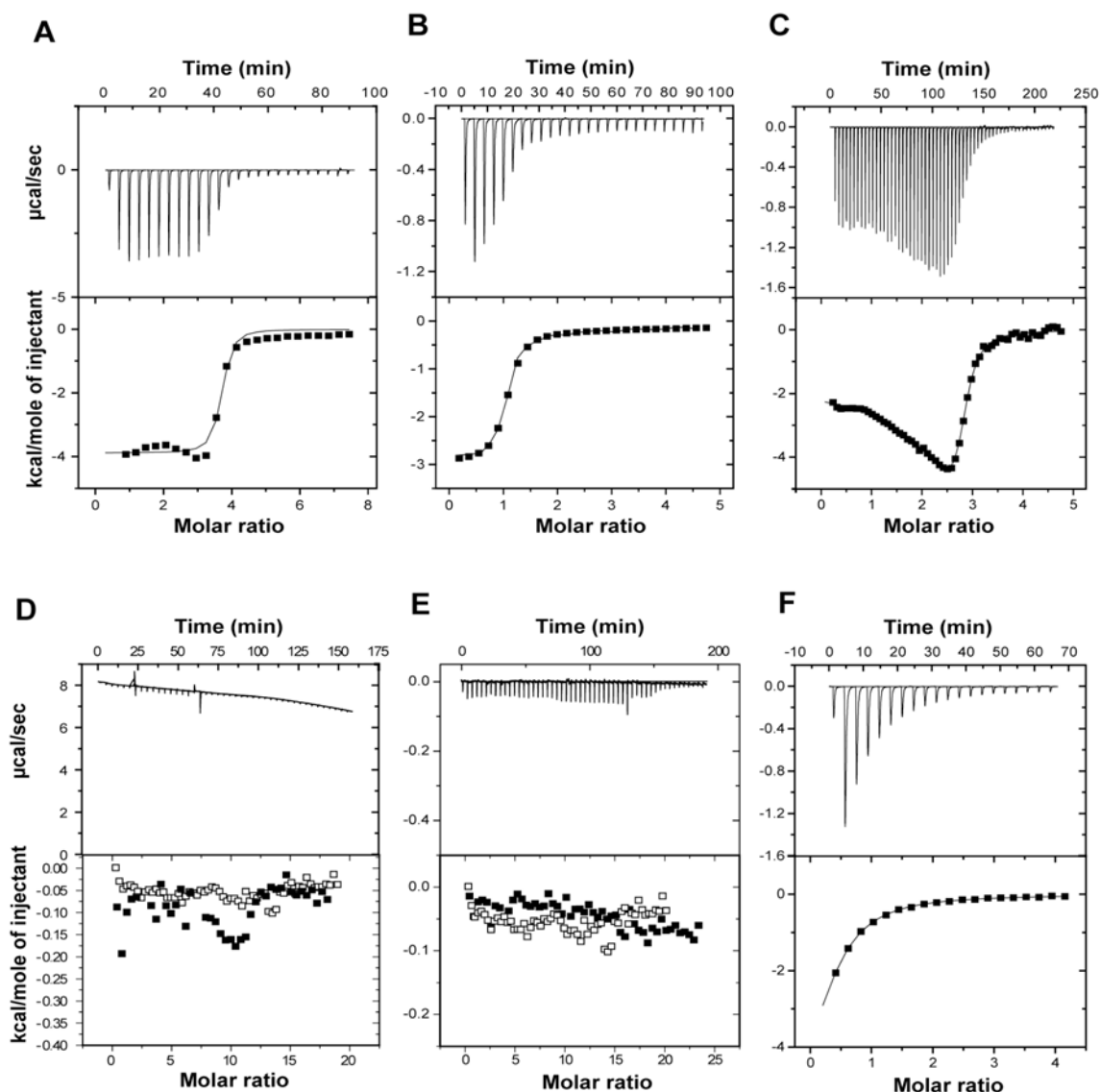


Figure 22. ITC measurements of  $\text{Ca}^{2+}$ - and  $\text{Mg}^{2+}$ -binding affinities of Calneuron-1, -2 and NCS-1. The ligand concentrations for the titration were 5 mM  $\text{Ca}^{2+}$  and 10 mM  $\text{Mg}^{2+}$ . Depicted are isotherms of  $\text{Ca}^{2+}$ -binding to untagged Calneuron-1 (A), MBP-tagged Calneuron-2 (B) and to untagged  $\text{Mg}^{2+}$ -bound myristoylated NCS-1 (C). D to F shows isotherms of  $\text{Mg}^{2+}$ -binding to untagged Calneuron-1, to MBP-tagged Calneuron-2 and to untagged myristoylated NCS-1

Previous work has shown that  $\text{Mg}^{2+}$ -binding to EF-hand-2 and -3 of NCS-1 reduces the  $\text{Ca}^{2+}$ -binding affinity of NCS-1 from 90nM to 440nM (Aravind et al., 2008). In sharp contrast to NCS-1, we found that  $\text{Mg}^{2+}$  does not bind at physiologically relevant concentrations to Calneuron-1 and -2 (Fig. 22A-F). Moreover, in contrast to  $\text{Ca}^{2+}$ ,  $\text{Mg}^{2+}$  did not affect the conformation of apo-Calneuron-1 as evidenced by fluorescence spectroscopy (Fig. 23A and B). ITC data demonstrate the presence of two high-affinity  $\text{Ca}^{2+}$ -binding sites (Table 7), with apparent global affinities of 180nM for Calneuron-1 and 230nM for

Calneuron-2 (Fig. 22B, Table 7). In conclusion, we propose that Calneurons, in contrast to NCS-1, have a very narrow dynamic range of  $\text{Ca}^{2+}$ -induced unfolding with much less reversibility to the  $\text{Ca}^{2+}$ -free state which explains their dominant role at low  $\text{Ca}^{2+}$ -concentrations.

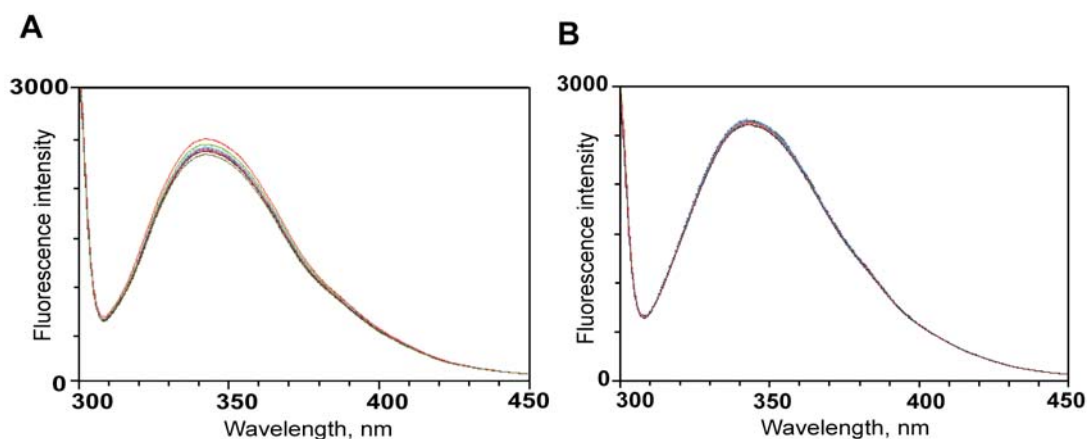


Figure 23. Tryptophan fluorescence spectroscopy of untagged Calneuron-1 in the presence of  $\text{Ca}^{2+}$  (A) or  $\text{Mg}^{2+}$  (B). Note that only  $\text{Ca}^{2+}$  but not  $\text{Mg}^{2+}$  changes the conformation of the protein.

Table 7: Thermodynamic and  $\text{Ca}^{2+}$  and  $\text{Mg}^{2+}$  binding parameter obtained for Calneuron-1 and Calneuron-2 calculated by ITC. Data on myr-NCS-1 data is also included in the table.

Proteins	Model	Association constant $K_A$ ( $\text{M}^{-1}$ )	Dissociation constant $K_D$ ( $\mu\text{M}$ )	$\Delta H$ (kcal/mol)	$T\Delta S$ (kcal/mol)	$\Delta G^\circ$ (kcal/mol)
Calneuron-1 $\text{Mg}^{2+}$ binding	Does not bind	-	-	-	-	-
Calneuron-1 $\text{Ca}^{2+}$ binding	1 set of sites	$5.38 \times 10^6$	0.18	$3.75 \pm 0.058$	5.57	-9.32
Calneuron-2* $\text{Mg}^{2+}$ binding	Does not bind	-	-	-	-	-
Calneuron 2* $\text{Ca}^{2+}$ binding	1 set of sites (Sequential binding sites)	$4.34 \times 10^6$	0.23	$3.43 \pm 0.368$	5.51	-8.94
myr-NCS-1 $\text{Mg}^{2+}$ binding	1 set of site	$3.97 \times 10^4$	25.18	$6.84 \pm 0.52$	-0.463	-6.37
$\text{Mg}^{2+}$ Bound myr-NCS-1 $\text{Ca}^{2+}$ binding	2 set of sites	$1.96 \times 10^6$ $6.43 \times 10^5$	0.89	$1.61 \pm 0.134$ $2.32 \pm 13.8$	7.12 -34.23	-8.73 -8.09

\* MBP-tagged protein was used; 1 set of sites:  $K_D = 1/K_A$ ; 2 set of sites:  $K_D = 1/\sqrt{K_{A1} * K_{A2}}$

### 3.11 Calneuron-1 regulates PI-4K $\beta$ activity in a Ca<sup>2+</sup>-dependent manner and opposing to NCS-1

To next address the question which functional consequences Calneuron-1 binding might have for PI-4K $\beta$ 's enzymatic activity we performed *in vitro* kinase assays using bacterially expressed proteins. Conflicting evidence exists whether myristoylated NCS-1 activates PI-4K $\beta$  *in vitro* in a Ca<sup>2+</sup>-dependent manner and whether the interaction by itself is Ca<sup>2+</sup>-independent (Zhao et al., 2001; Haynes et al., 2005). We found that the basal activity of the kinase was unaltered in the presence of myr-NCS-1 when Ca<sup>2+</sup> was omitted from the buffer. Addition of Ca<sup>2+</sup> led to an increase in PI-4K $\beta$  activity (Fig. 24).

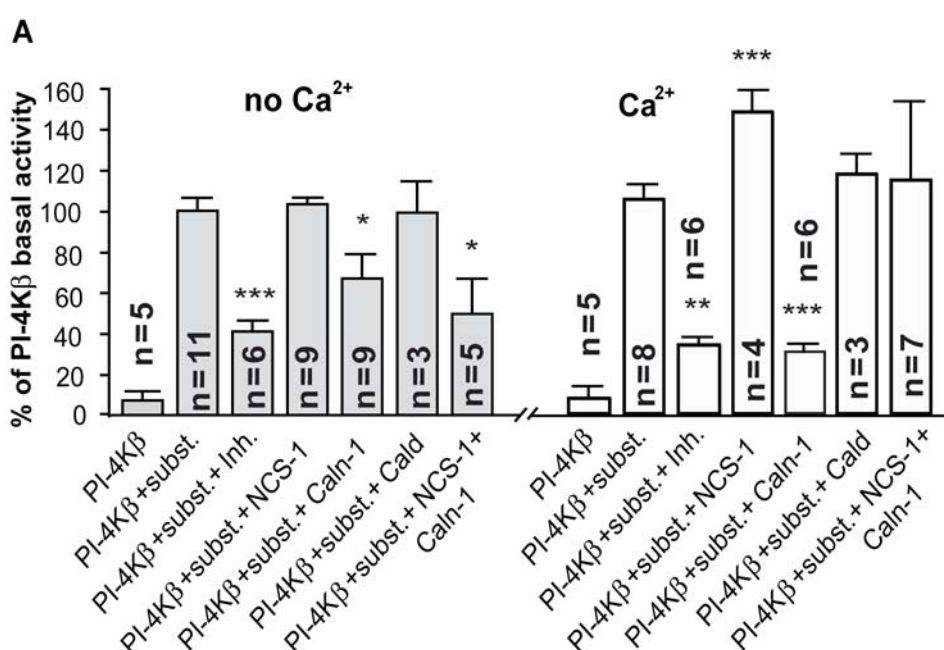


Figure 24. Calneuron-1 and NCS-1 have the opposite effect on PI-4K $\beta$  enzymatic activity. Under Ca<sup>2+</sup>-free conditions (grey boxes) Calneuron-1 suppresses the activity of PI4-K $\beta$  whereas NCS-1 increases enzyme activity. In the absence of Ca<sup>2+</sup> the effect of Calneuron-1 on PI-4K $\beta$  activity was not changed by adding equimolar amounts of NCS-1. In the presence of 1mM free Ca<sup>2+</sup> (white boxes) NCS-1 increases PI-4K $\beta$  activity whereas Calneuron-1 significantly decreases PI-4K $\beta$  activity. Addition of equimolar amounts of NCS-1 and Calneuron-1 led to a competition and NCS-1 reverses the suppressing effect of Calneuron-1. Caldendrin has no effect on PI-4K $\beta$  activity at any tested conditions. Error bars represent the SEM. PD: Pull-down; Inh.: The PI-4K $\beta$  inhibitor Wortmannine (8  $\mu$ M) was added to the assay buffer. \*\*\*p<0.001; \*\*p<0.01; \*p<0.05.

Strikingly, Calneuron-1 showed the opposite behavior with a strong inhibitory effect on kinase activity (~66% of basal activity) already in Ca<sup>2+</sup>-free conditions. Addition of Ca<sup>2+</sup> to the assay buffer further augmented the inhibitory effect of Calneuron-1 on PI-4K $\beta$  activity (~28% of basal activity). Caldendrin, the closest homologue of Calneurons in brain, had no effect on PI-4K $\beta$  kinase activity under any of the conditions tested (Fig. 23), suggesting in



conjunction with previous data (Hendricks et al., 2001; Strahl et al., 2003) that PI-4K $\beta$  is specifically regulated by only a subset of calcium sensor proteins. To simulate an *in vivo* situation where NCS-1 and Calneuron-1 might have competing influence on PI-4K $\beta$  activity we performed the assay with equimolar amounts of both proteins. In support of the previous observations we found that under low Ca<sup>2+</sup> conditions PI-4K $\beta$  activity was inhibited to 60% if both NCS1 and Calneuron-1 were present in equimolar amounts in the reaction mix. This effect was comparable to the effect of Calneuron-1 alone (Fig. 24). However, in the presence of high Ca<sup>2+</sup> concentrations NCS-1 was counteracting the inhibitory effect of Calneuron-1 (Fig. 24).

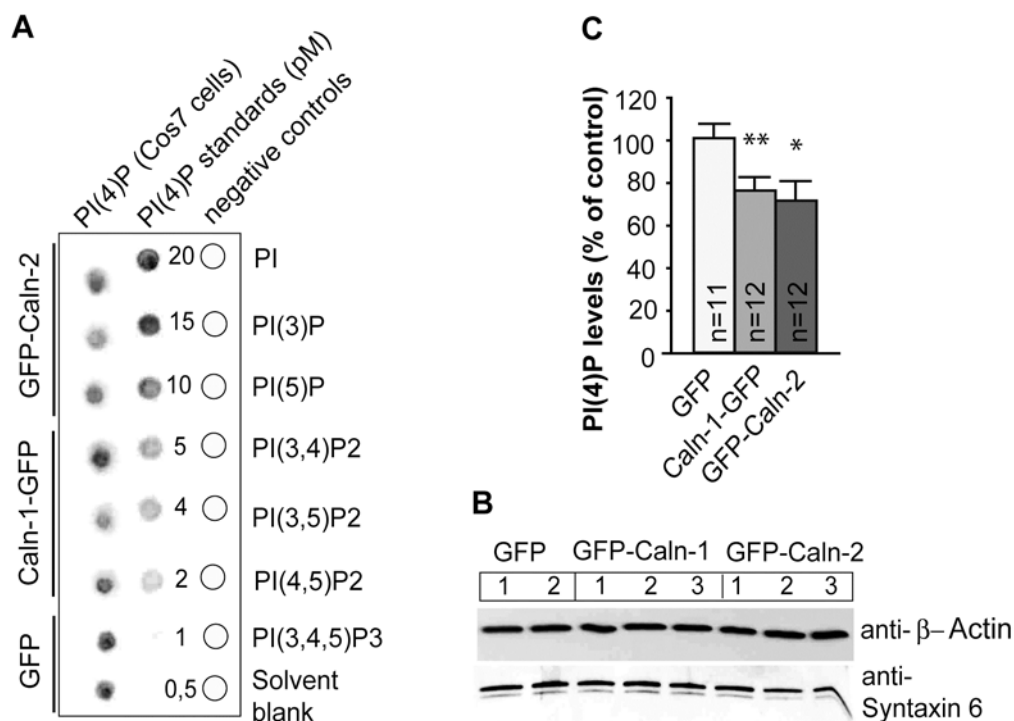


Figure 25. Over-expression of Calneuron-1-GFP and Calneuron-2-GFP reduces PI(4)P production in transfected COS-7 cells. (A) Representative dot blots showing a reduction of PI(4)P levels as evidenced by a protein-lipid overlay assay. (B) The presence of Golgi membranes was checked by immunoblotting of Syntaxin-6 and was in used in combination with  $\beta$ -actin immunoblots as loading controls to normalize the loading for the dot blot assay. (C) Quantification of PI(4)P levels. The amount of PI(4)P in GFP transfected cells was taken as 100% and the deviation for Calneuron-GFP transfected cells was calculated. Error bars represent the SEM. \*\*p<0.01; \*p<0.05.

To address the question whether Calneurons are also able to inhibit PI-4K $\beta$  activity *in vivo*, we transfected COS-7 cells, which do not endogenously express Calneurons (data not shown) with GFP-Calneuron-1 and -2 constructs. We enriched crude Golgi membranes by homogenizing COS-7 cells and centrifuging them for 10 min at 1000 xg. The pellet

fraction, containing nuclei and intracellular membranes were checked by immunoblotting for the presence of the Golgi marker Syntaxin 6 and the total protein concentration was equilibrated (Fig. 25B). The phospholipids were extracted and spotted on membranes containing standard amounts of PI(4)P and other phospholipids as negative controls (Fig. 25A). Quantification of PI(4)P-levels revealed that over-expression of both Calneuron-1 and -2 significantly reduced PI(4)P-production (Fig. 25C), indicating that Calneurons also inhibit PI-4K $\beta$  activity *in vivo*.

### **3.12 Calneurons regulate vesicular trafficking of the VSV-G protein**

VSV-G has been widely used to study membrane transport because of its reversible misfolding and retention in the ER at 40°C and its ability to move out of the ER and into the Golgi complex upon temperature reduction to 32°C (Presley et al., 1997). To further assess the *in vivo* role of Calneurons in Golgi-to-plasma membrane trafficking we performed VSV-G-GFP translocation assays in COS-7 cells. The cells were transfected with VSV-G-GFP alone or together with pcDNA3.1-Calneuron-1 or -2 constructs expressing untagged Calneuron proteins. Double transfection did not change the level of VSVG-GFP as confirmed by immunoblotting (Fig. 26A). To monitor the concentrations of intracellular free Ca<sup>2+</sup> under the employed experimental conditions we first filled the cells with the ratiometric Ca<sup>2+</sup> dye Fura2. Heating the cells to 40°C and subsequently cooling them down to 32°C caused an immediate and long-lasting increase of intracellular Ca<sup>2+</sup>-levels (Fig. 26B). In line, it was previously reported that over-expression of NCS-1 enhances VSV-G trafficking in this assay (Haynes et al., 2005). After co-transfection of Calneurons and VSV-G-GFP we could see strong Golgi accumulation of VSV-G-GFP already at basal conditions therefore we modified the original protocol and kept transfected cells at 40°C for VSV-G misfolding only for 30 min. Then cells were shifted to 32°C and fixed at 0, 30, 60, 90 and 120 minutes. COS-7 cells were stained for Calneuron-1 and -2 to visualize a double transfected cells and proceeded for confocal microscopy.

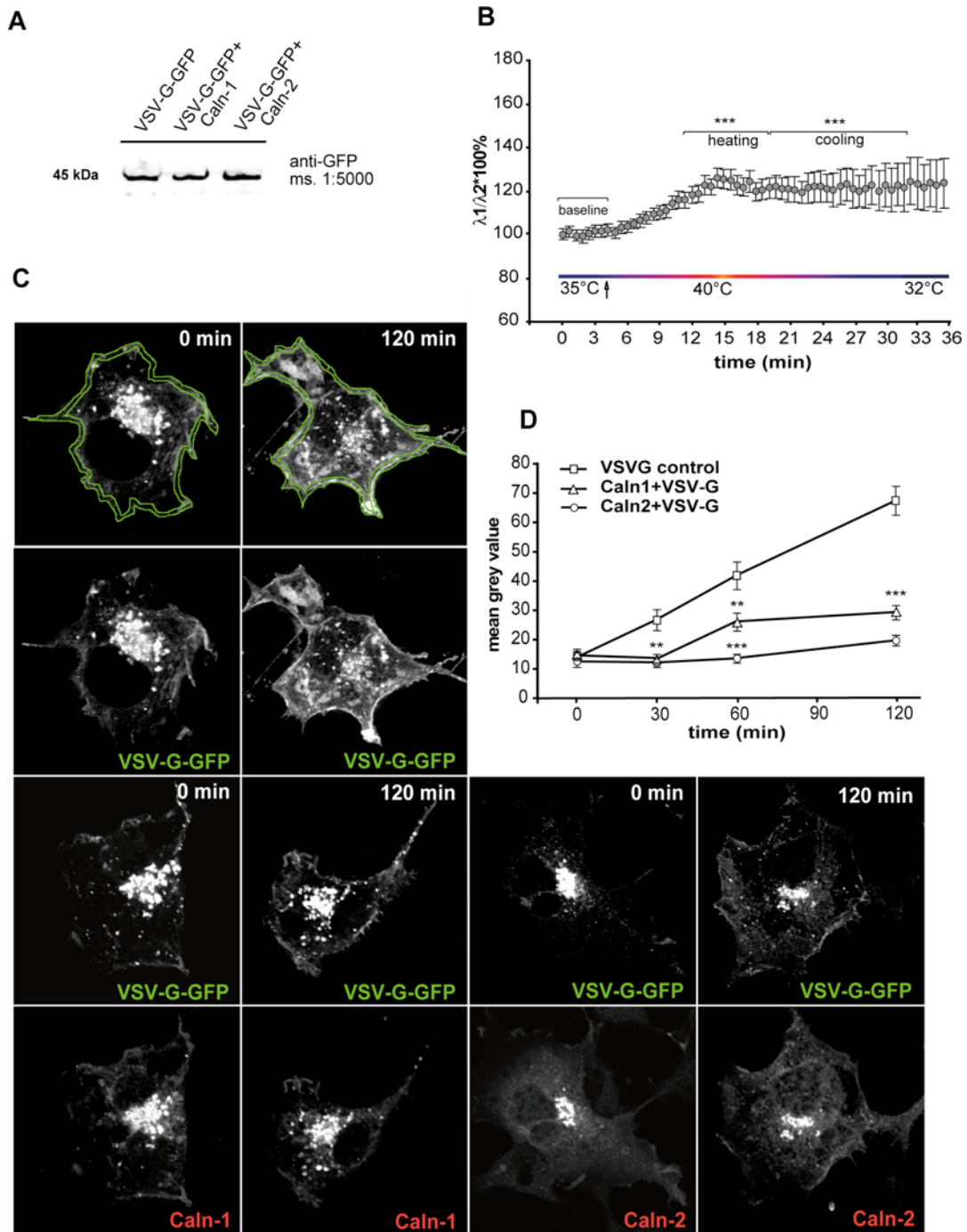


Figure 26. Calneuron-1 and -2 inhibit VSV-G Golgi trafficking in COS-7 cells. COS-7 cells co-transfected with different constructs were incubated at 40°C to induce reversible misfolding and ER retention of VSV-G-GFP and then shifted to 32°C – conditions allowing the vesicular trafficking from ER to Golgi complex and then to the plasma membrane. After temperature was shifted to 32°C COS-7 cells were fixed at different time points (0, 30, 60, 90 and 120 min). Calneuron-1 and -2 transfected cells were stained with the specific antibody to prove the double transfection and then analyzed by confocal microscope. (A) Level of VSV-G-GFP is not affected by co-expression with Calneurons. Immunoblot. (B) Monitoring of free intracellular  $Ca^{2+}$  levels during the experimental procedure for VSV-G trafficking assay shows high  $Ca^{2+}$  levels after increasing the temperature. (C) VSV-G assay: GFP-Fluorescence pictures showing the association VSV-G-GFP with the plasma membrane at different time points. (D) Quantification of the assay. The maximum projection images were created from z-stacks and mean grey value of GFP fluorescence was measured 2  $\mu$ m away from the plasma membrane. Error bars represent the SEM. \*\*\* $p < 0.001$ ; \*\* $p < 0.01$ ; \* $p < 0.05$ .

Mean grey values of the GFP-fluorescence at the plasma membrane were used to estimate the amount of VSV-G-GFP translocated under the different assay conditions (Fig. 26C). At 0 minutes (directly after shifting the temperature to 32°C) there were no differences in the membranous GFP-signal between cells transfected with VSV-G-GFP alone or cells co-transfected with Calneuron-1 and -2 (Fig. 26D). But already 30 minutes after the temperature shift the GFP fluorescence at the plasma membrane was significantly higher in controls than in Calneuron co-transfected cells (Fig. 26D). In Calneuron-1 expressing cells translocation of VSV-G-GFP to the plasma membrane was first visible only after 60 min (Fig. 26D), whereas in Calneuron-2 expressing cells the inhibition of VSV-G-GFP trafficking to the membrane lasted even longer (Fig. 26D).

Thus, the increase in intracellular  $\text{Ca}^{2+}$  in this assay is in the case of Calneuron-1 and -2 over-expression followed by an inhibition of VSV-G-trafficking. This is in stark contrast to the published effects of NCS-1 (Haynes et al., 2005) and further supports the idea that Calneurons have opposing roles to NCS-1 in Golgi-to-membrane trafficking.

### **3.13 Calneuron over-expression inhibits hGH release in PC12 cells**

To further assess the functional consequences of the Calneuron - PI-4K $\beta$  interaction *in vivo* we examined the effects of Calneuron over-expression in secretory cells where secretion can be driven by increased intracellular  $\text{Ca}^{2+}$  concentrations. PC12 cells are widely used as a model system to study secretory processes. These cells can be transfected with hGH and its release into the medium can be easily monitored by commercially available ELISA kits. Previous work has shown that PI-4K $\beta$  is crucially involved in the genesis of secretory vesicles in this assay and that Golgi-trafficking is enhanced by NCS-1 over-expression (Haynes et al., 2005; de Barry et al., 2006). Measurement of the total hGH concentration revealed no significant difference between hGH expression levels in the various Calneuron / hGH co-transfected cells and expression levels of the employed EGFP-Calneuron constructs were also comparable to those of control EGFP constructs (Fig. 27A and B). 30  $\mu\text{M}$  ATP added with a  $\text{Ca}^{2+}$ -containing stimulation buffer for 10 minutes induces an increase in intracellular  $\text{Ca}^{2+}$  (De Barry et al., 2006) and activates hGH exocytosis in transfected PC12 cells, which resulted in EGFP transfected cells in doubling the amount of released hGH (Figure 27C). In the case of Calneuron transfected PC12 cells, the amount of hGH release after stimulation was significantly lower and it was clearly reduced below the basal release (growth medium was exchanged by EGTA-containing stimulation buffer and kept for the same

time) observed with the same constructs (Figure 27C). Thus again, in line with the biochemical data, over-expression of Calneurons inhibits  $\text{Ca}^{2+}$ -evoked exocytosis *in vivo* in secretory cells.

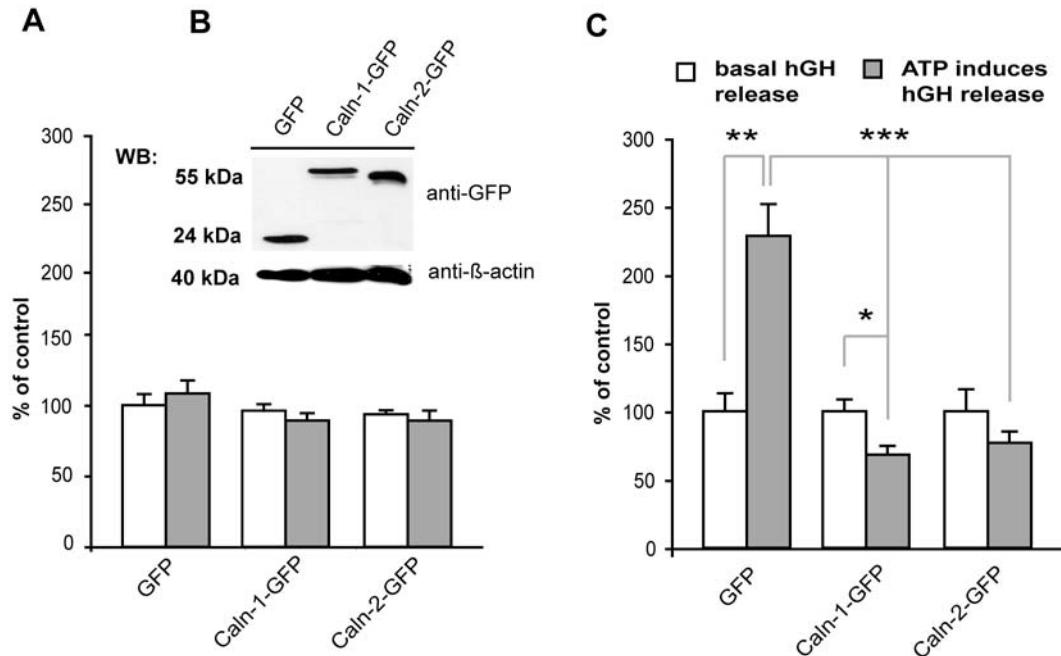


Figure 27. Calneurons in contrast to NCS-1 inhibits the ATP induced hGH release in PC12 cells (ELISA assay). (A) Total hGH levels (release and non-released) are not different between the groups. (B) Immunoblot showing that Calneuron-1 and -2-GFP plasmids exhibit equal expression levels. (C) To estimate the basal activity of PI-4K $\beta$  at resting  $\text{Ca}^{2+}$  concentrations the medium of transfected cells was replaced by EGTA-containing stimulation buffer and collected after 10 minutes. hGH release was induced by application of 30  $\mu\text{M}$  ATP in stimulation buffer, collected also after 10 min and used for the measurements. The basal release of hGH expressed as 100%. Error bars represent the SEM. \*\*\* $p < 0.001$ ; \*\* $p < 0.01$ ; \* $p < 0.05$ .

### 3.14 Overexpression of Calneurons in cortical neurons induces a prominent enlargement of TGN

In the final set of experiments we more directly addressed the question whether Calneurons have a role in neuronal TGN to plasma membrane trafficking. Double-immunofluorescence staining of endogenous and overexpressed proteins revealed indeed no overlap of Calneuron-1 with the endoplasmatic reticulum marker Calreticulin, and the cis-Golgi marker GM130 (Fig. 28A), and only limited overlap with the endosomal marker  $\beta$ -COP (Fig. 28E). Similarly PI-4K $\beta$  is highly abundant at the TGN and much less at the cis-Golgi (Fig. 28A). Moreover Calneuron-1 when over-expressed in neurons accumulates only at Syntaxin 6 and TGN38 positive TGN but not at the GM130 positive cis-Golgi (Fig. 28B, C and D).

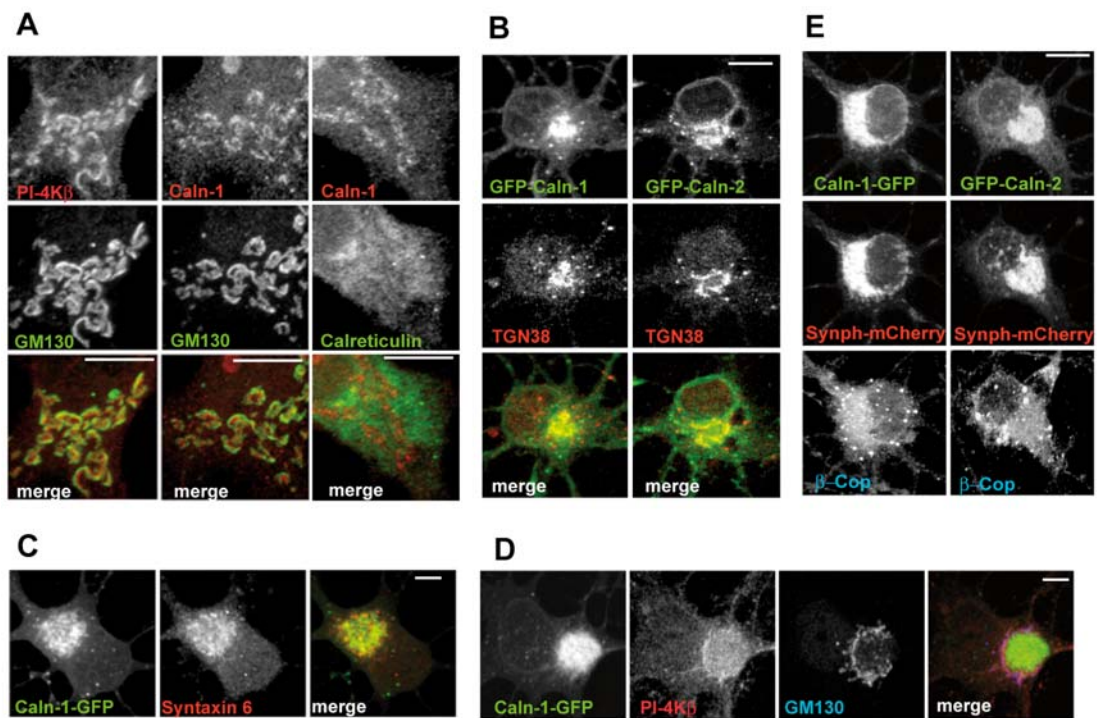


Figure 28. (A) Endogenous and over-expressed Calneurons co-localize with TGN-markers. (A) Cortical neurons (DIV21) co-stained with anti-PI-4K $\beta$  or Calneuron-1 antibody and GM130 – cis-Golgi marker. Note that all 3 proteins are restricted to the same structure but show relatively little overlap indicating that their localization is restricted to the different sub-compartments of the Golgi complex. Clareticulin – the endoplasmic reticulum marker showed very little overlap with Calneuron-1 staining. GFP-Calneuron-1 and -2 co-localize with the trans-Golgi network markers – TGN38 (B) and Syntaxin 6 (C). (D) Overexpressed Calneuron-1–GFP shows almost complete colocalization with PI-4K $\beta$  and the trans-Golgi marker Syntaxin 6 but only to a minor extent with the cis-Golgi marker GM130. (E) mcherry-Synaptophysin and Calneuron-1-GFP or GFP-Calneuron-2 co-transfected primary cortical neurons (DIV5) stained with another endosomal/TGN marker –  $\beta$ -Cop - show only some co-localization of all three proteins at the Golgi. Note the strong co-localization of GFP tagged Calneurons and mcherry–Synaptophysin at TGN. Scale bar is 10  $\mu$ m.

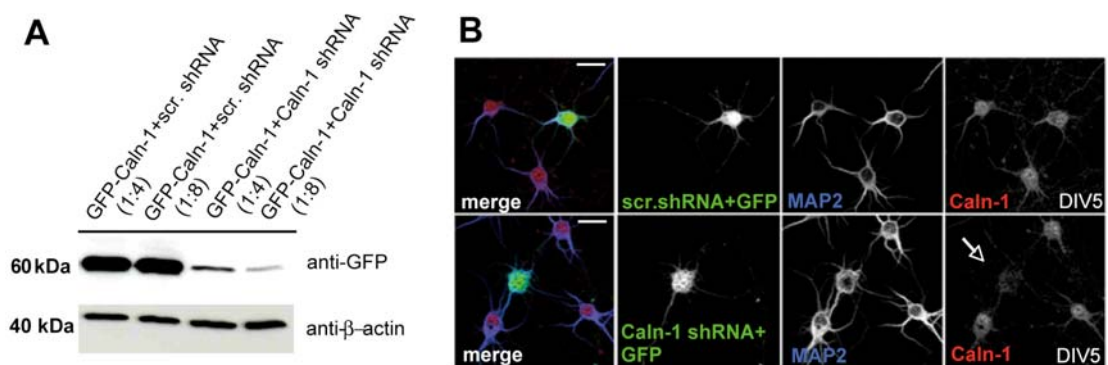


Figure 29. Validation of the Calneuron-1 shRNA protein knockdown. (A) COS-7 cells double transfected with shRNA for Calneuron-1 or the scrambled construct and GFP-Calneuron-1 in a ratio of 4:1 or 8:1. 72 hours later cells were harvested and protein levels were checked by IB with GFP and  $\beta$ -actin antibodies (the GFP antibody does not recognize tGFP from the pRS-GFP plasmid carrying the shRNA sequence). Strong inhibition of Calneuron-1 expression can be observed with 8:1 ratio of constructs. (B) Cortical neurons transfected on DIV2 and fixed 72 hours later were stained with a Calneuron-1 rabbit antibody. Arrow indicates the transfected neuron with significant reduction of Calneuron-1 immunoreactivity. Scale bar is 20  $\mu$ m.



Cortical neurons express high levels of Calneuron-1 whereas Calneuron-2 transcripts are barely detectable (Mikhaylova et al., 2006). Utilizing a Calneuron-1 RNAi knockdown we could therefore investigate how the suppression of Calneuron protein levels affects Golgi morphology and function. We obtained 29-mer shRNA knock down constructs from Origene. After validation in COS-7 cells (Fig. 29A) and then in the cortical neurons (Fig. 29B) one of the four sequences turned to be most efficient.

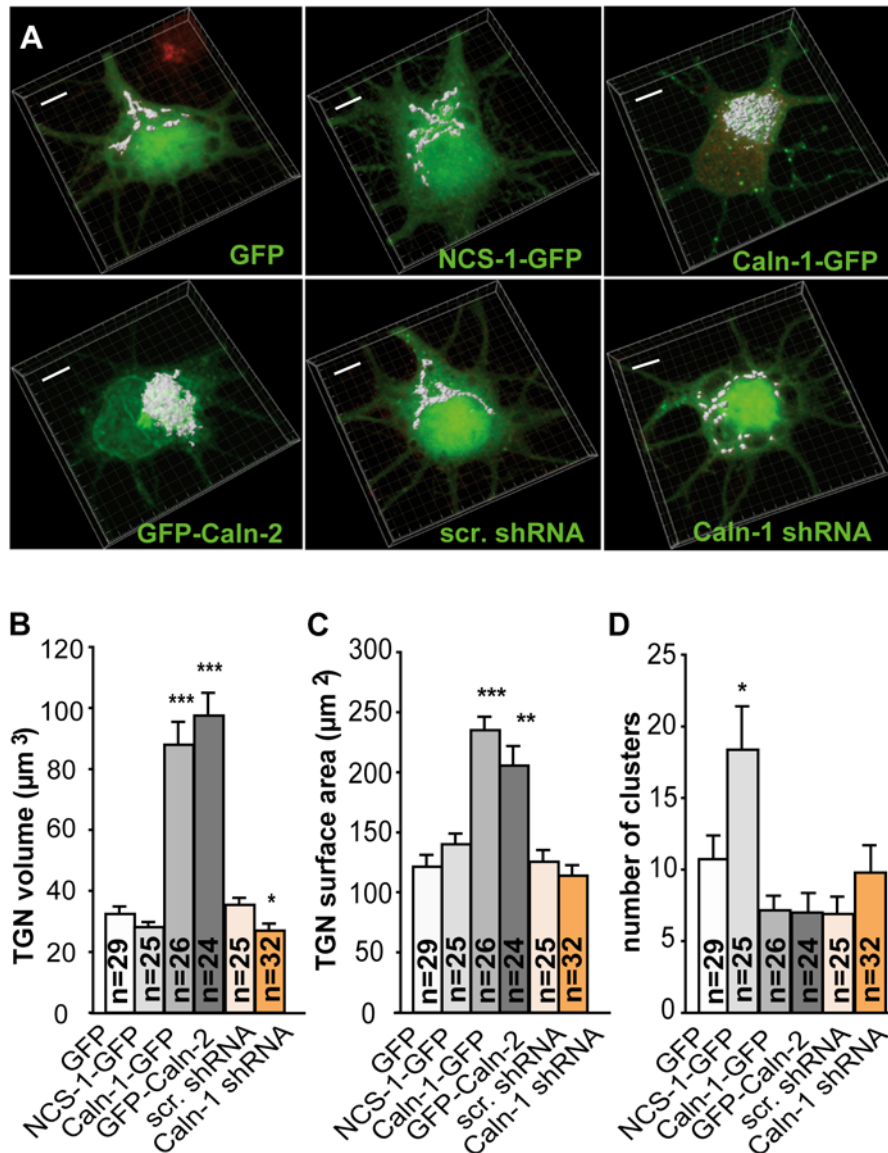


Figure 30. Overexpression of Calneuron-1 and Calneuron-2 in cortical neurons induces a prominent enlargement of the Golgi whereas RNAi knockdown of Calneuron-1 has the opposite effect. (A) 3D reconstruction of the TGN using Syntaxin 6 stainings and Imaris. Neurons were stained 24 h after transfection with GFP- Calneuron-1, GFP- Calneuron-2, NCS- 1-GFP, and GFP or 72 h after transfection with Calneuron-1 shRNA or scramble shRNA. The Syntaxin 6-positive area (depicted in gray) was reconstructed with Imaris and overlaid with the nonmodified GFP channel. Scale bar: 5  $\mu\text{m}$  (B-D) Quantification of different parameters of TGN size (volume, surface area and number of TGN clusters) using Imaris 3D reconstruction of the Syntaxin 6 staining. Error bars represent the SEM. \*\*\*,  $p < 0.001$ ; \*\*,  $p < 0.01$ , \*,  $p < 0.05$ .

Interestingly, we found that over-expression of both Calneurons at day in vitro (DIV) 5 cortical primary cultures led within 24 hrs to a significant enlargement of the TGN as evidenced by a three-dimensional reconstruction of Syntaxin 6 confocal lasercans with Imaris (Fig. 30B and C). In addition, the Golgi surface area was increased (Fig. 30C). Overexpression of NCS-1-GFP didn't have significant effect on the volume and surface area of TGN but number of TGN clusters was increased (Fig. 30B and D). A knockdown of Calneuron-1 was followed by a significant reduction in the size of the TGN, thus inducing the opposite effect than protein over-expression (Fig. 30A and B). Moreover, similar to the NCS-1 overexpression phenotype a higher number of dispersed and small TGN fragments were found (Fig. 30D).

### 3.15 Calneurons regulate vesicle trafficking at neuronal Golgi

On the next step we wanted to visualize the effect of Calneuron-1 transfection on Golgi – to plasma membrane trafficking in neurons *in vivo*. In DIV5 primary cortical neurons transfected with Calneuron-1 or -2 the enlarged TGN overlapped with the immunofluorescence for endogenous PI-4K $\beta$  and also the synaptic vesicle marker Synaptophysin (Fig. 31A and B).

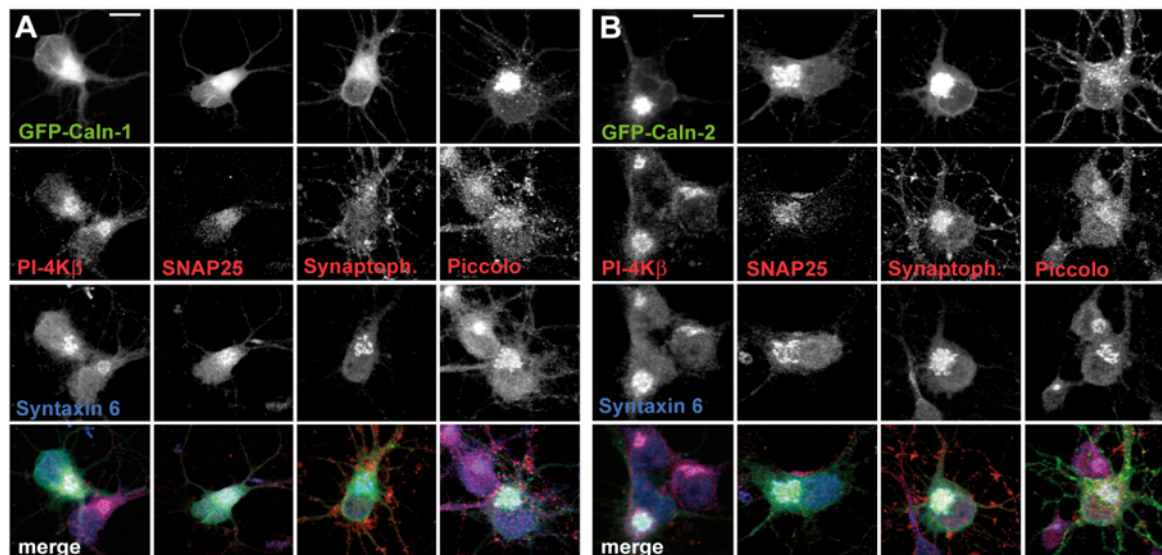


Figure 31. Over-expressed Calneurons induce enlargement of TGN by blocking the Golgi exit of secretory vesicles and an accumulation of vesicular proteins and membranes at TGN. Scale bar is 10  $\mu$ m. Synaptoph. – Synaptophysin.



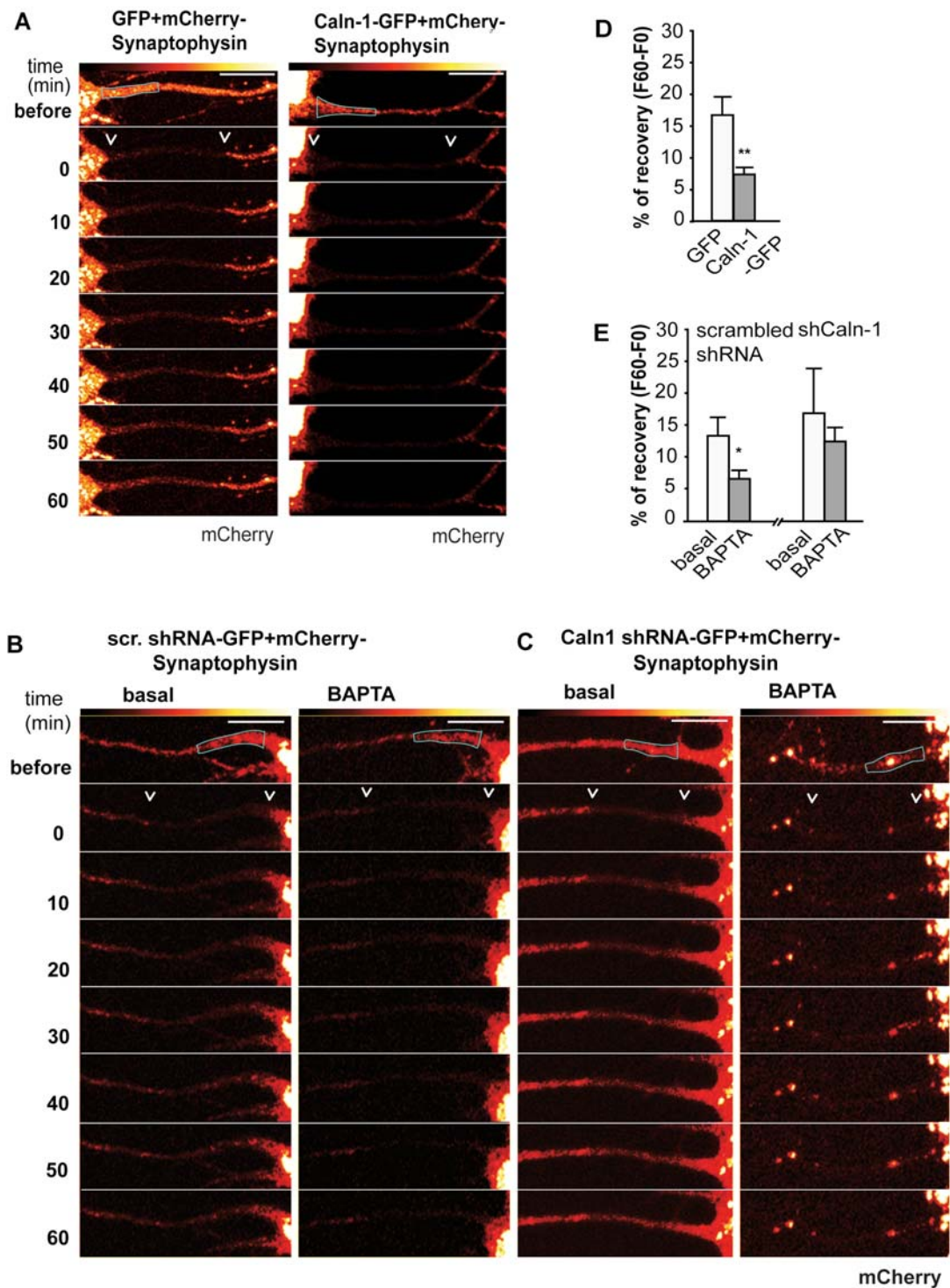


Figure 32. Calneuron-1 regulates the exit of Synaptophysin from the TGN. (A-C) Examples of time-lapse imaging of FRAP for mcherry-Synaptophysin. Arrows indicate the area that was photo-bleached. DIV 5–7 cortical neurons cotransfected with mcherry-Synaptophysin and Calneuron-1-GFP show much less recovery of axonal mCherry fluorescence after FRAP than neurons cotransfected with GFP. Scale bar: 10  $\mu$ m. (D) Quantification of FRAP 60 min after photo-bleaching. Initial fluorescence is taken as 100% and percentage of recovery is calculated as fluorescence at time point 60 (F60) minus fluorescence at time point 0 (F0) directly after photo-bleaching. (B, C, E) Incubation for 1 h with 10  $\mu$ M BAPTA-AM significantly reduced the basal recovery of mcherry-Synaptophysin in scrambled shRNA but not mcherry-Synaptophysin– Calneuron-1 shRNA-cotransfected neurons. Error bars represent the SEM. \*\*,  $P < 0.01$ ; \*,  $P < 0.05$ .

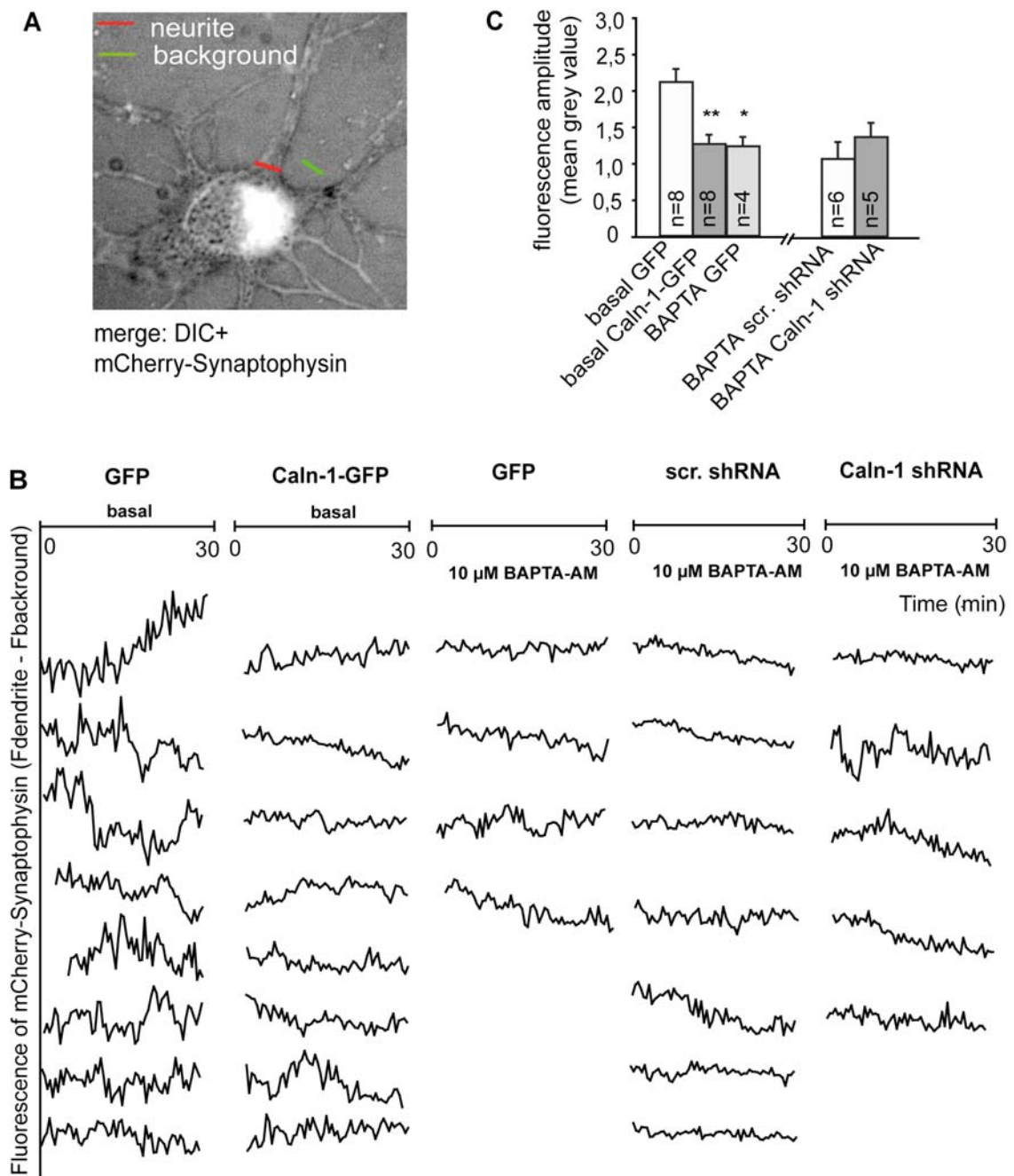


Figure 33. Line analysis of mcherry-Synaptophysin trafficking in cortical neurons overexpressing Calneuron-1-GFP or after it's shRNA knockdown. (A) Example of a GFP plus mcherry-synaptophysin-transfected neuron. The red line indicates the part of the neurite monitored during the experiment; the green line indicates the background used for normalization. (B) The fluorescence change traces of each recorded cell. (C) Line analysis of trafficking at the proximal part of the longest neurite of neurons cotransfected with mcherry-Synaptophysin and Calneuron-1-GFP shows decreased amplitude of mcherry fluorescence changes compared with GFP controls. This effect is similar to BAPTA-AM-preincubated GFP/mcherry-synaptophysin-cotransfected cells. Images were taken every 30 s for 30 min. Error bars represent the SEM. \*\*, P < 0.01; \*, P < 0.05.

Synaptophysin is a vesicular transmembrane protein that has to pass via the Golgi to enter the axon. We transfected cortical neurons with a mcherry-Synaptophysin fusion

protein and found a prominent Golgi and axonal localization of this construct (Fig. 28E / Dresbach et al., 2006). Using time-lapse imaging of FRAP we could follow the exit of the mCherry-fluorescence from the Golgi to the longest neurite as a read-out for trafficking of Synaptophysin-containing vesicles (Fig. 32A). In these experiments cells transfected with Calneuron-1-GFP showed a significantly reduced FRAP as compared to GFP-controls (Fig. 32A and B). In a complementary set of experiments we quantified the intensity of mcherry fluorescence in proximal parts of axons using line analysis without FRAP (Fig. 33A). Similar to the FRAP-experiments we found reduced fluorescence in Calneuron-1 transfected neurons in comparison to controls (Fig. 33B and C), indicating a reduced frequency of entry of Synaptophysin-containing vesicles into axons.

Accordingly, reducing Calneuron-1 protein levels increased FRAP of mcherry-Synaptophysin in proximal axons if  $\text{Ca}^{2+}$  levels were lowered with BAPTA (Fig. 32B, C, and E), suggesting that lower Calneuron-1 protein levels reduce the dependence on  $\text{Ca}^{2+}$  for mcherry-Synaptophysin to exit from the Golgi. Finally mcherry-Synaptophysin trafficking into proximal axons as quantified with line analysis was also decreased after application of BAPTA (Fig. 33B and C) while the Calneuron-1 knock down led only to a non-significant increase of the mcherry-Synaptophysin fluorescence as compared to scrambled controls (Fig. 33B and C), probably because the method is less sensitive than FRAP.

### **3.16 Calneurons regulate number of PTVs in axon at early developmental stages**

The data from COS-7 cells, PC12 cells and cortical neurons led us conclude that Calneurons might constitutively inhibit various types of vesicle transport at the Golgi. To prove this hypothesis more directly we wanted to look at vesicle transport without interference by over-expression of vesicle proteins such as VSV-G or Synaptophysin. At early stages of neuronal development components of the presynaptic cytomatrix are transported via the axon to nascent synaptic sites via so-called PTVs (Dresbach et al., 2006). PTVs are large dense core vesicles about 80 nm in diameter and can be easily identified because of their size, composition and discrete localization in axons (Zhai et al., 2001; Dresbach et al., 2006).

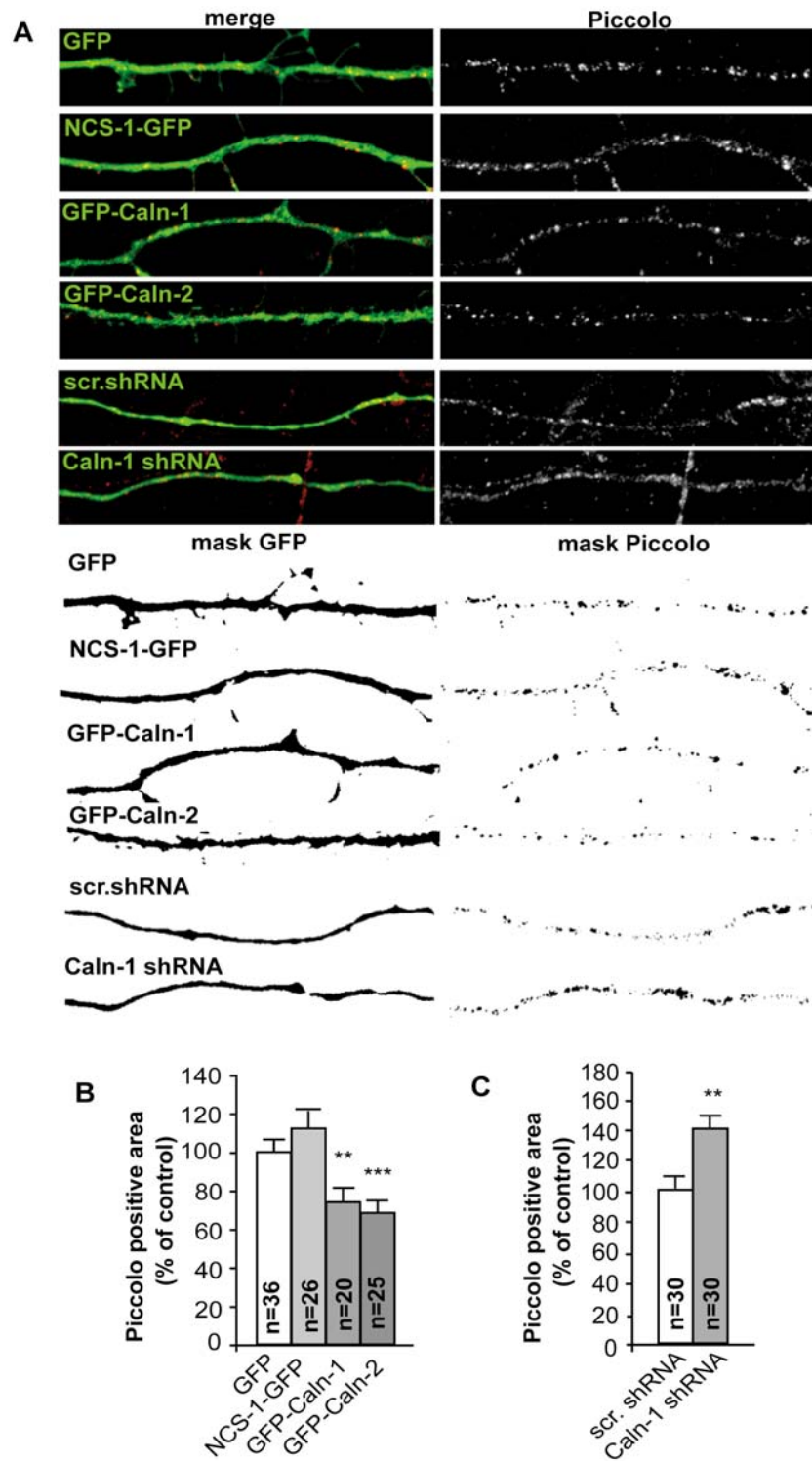


Figure 34. The number of PTVs in axons of DIV5 cortical neurons is significantly reduced 24 h after transfection of GFP– Calneuron-1 and Calneuron-2 but not NCS-1–GFP. shRNA knockdown of calneuron-1 has the opposite effect. (A) (Upper) A 50- $\mu$ m axonal segment from neurons transfected with different GFP-tagged constructs is shown. (Lower) Masks from images of the same segments from the GFP channel and the piccolo fluorescence channel are depicted. (B and C) The number of PTVs is represented as the ratio between the area covered by Piccolo immunoreactivity within a selected axonal segments and the total axonal area as defined by GFP fluorescence. The ratio in the case of GFP transfection was taken as 100% for the overexpression (B) and scrambled shRNA control for the knockdown experiments (C). Error bars represent the SEM. \*\*\*,  $P < 0.001$ ; \*\*,  $P < 0.01$ .

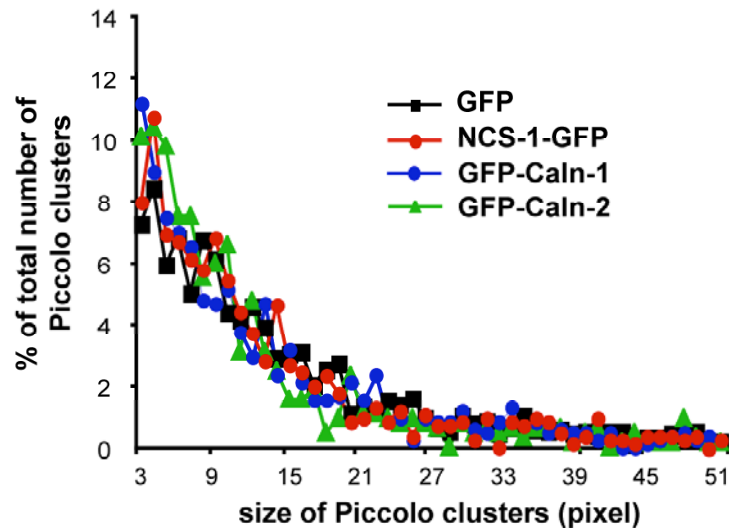


Figure 35. Distribution of Piccolo clusters in 50  $\mu$ m segment of axons after 24 hours of transfection with NCS-1-GFP, GFP-Calneuron-1, GFP-Calneuron-2 or GFP alone (DIV5).

We found that two protein components of these vesicles, Piccolo and SNAP-25 also accumulated at the trans-Golgi-network after Calneuron-1 over-expression (Fig. 30A and B). This was accompanied by a significantly reduced number of PTVs (identified by Piccolo fluorescence) in the axon (Figure 34A and B) while the size distribution of Piccolo-positive clusters was not affected (Fig. 35).

Over-expression of NCS-1 had no effect on the size of the trans-Golgi-network although the number of PTVs in the axon was slightly but not significantly elevated (Fig. 34A and B). Importantly, after Calneuron-1 protein knockdown the number of axonal PTVs was clearly elevated as compared to scrambled control transfected neurons (Fig. 34A and C), demonstrating that Calneurons are involved in the control of vesicle trafficking endogenously and will play this role already during neuronal development.

## 4 Discussion

NCS proteins play multiple and divergent roles in neuronal signaling. Members of this family closely resemble the structure of their common ancestor Calmodulin with four EF-hand  $\text{Ca}^{2+}$ -binding motifs. Despite their relatively high degree of similarity, NCS proteins are thought to serve highly specialized functions in neurons. It is generally believed that the specificity with respect to their target interactions is brought about by either a restricted subcellular localization, differences in calcium-binding affinities or modifications of their EF-hand structure that might provide a unique interface for protein interactions (Kinoshita-Kawada et al., 2005; Kreutz et al., 2007). In this thesis major insights were gained into the cellular function of three NCS proteins, namely Caldendrin and Calneuron-1 and -2. Previously it was shown that Caldendrin is a binding partner of Jacob (doctoral thesis of Dieterich DC, 2003). Strictly depending upon activation of NMDA-type glutamate receptors Jacob is recruited to neuronal nuclei, resulting in a rapid stripping of synaptic contacts and in a drastically altered morphology of the dendritic tree. Jacob's nuclear trafficking from distal dendrites crucially requires the classical Importin pathway. In this thesis it was shown that Caldendrin controls Jacob's extra-nuclear localization by  $\text{Ca}^{2+}$ -dependently competing with the binding of Importin- $\alpha$  to Jacob's nuclear localization signal. This competition requires sustained synapto-dendritic  $\text{Ca}^{2+}$ -levels, which presumably cannot be achieved by activation of extrasynaptic NMDARs, but are confined to  $\text{Ca}^{2+}$ -microdomains such as postsynaptic spines. Extrasynaptic NMDARs as opposed to their synaptic counterparts trigger the CREB shut-off pathway and cell death. We found that nuclear knock down of Jacob prevents CREB shut-off after extrasynaptic NMDARs activation while its nuclear overexpression induces CREB shut-off without NMDAR stimulation. This defines a novel mechanism of synapse-to-nucleus communication via a synaptic  $\text{Ca}^{2+}$ -sensor protein, which links the activity of NMDARs to nuclear signaling events involved in modelling synapto-dendritic input and NMDAR-induced cellular degeneration.

In the second part of the thesis the characterization of a new subfamily of NCS proteins – the Calneurons was provided. By virtue of their biophysical properties Calneurons are high affinity  $\text{Ca}^{2+}$  sensors that exhibit a relatively narrow dynamic range of  $\text{Ca}^{2+}$ -binding with respect to the resting  $\text{Ca}^{2+}$ -levels in neurons. In this study we show that Calneuron-1 and -2 physically associate with PI-4K $\beta$ , an enzyme involved in the regulated local synthesis of phospholipids that are crucial for trans-Golgi network to plasma membrane trafficking. Taken together the data assign a cellular function to Calneurons,



which add an important regulatory mechanism for stimulus-dependent dynamics in trans-Golgi-network to plasma membrane trafficking. These results should be discussed in more detail.

#### **4.1 Caldendrin and Calneurons are close but still rather different ‘relatives’ in the brain**

The primary characterization of Calneurons raises several important issues concerning their diverse structure as compared to other  $\text{Ca}^{2+}$  sensor proteins, their  $\text{Ca}^{2+}$  binding properties, their neuronal binding partners and their putative function for neuronal  $\text{Ca}^{2+}$  signaling. From the available data some interesting notions can be already deduced. In situ hybridization studies suggest that in many cases Caldendrin and Calneurons will not be expressed in the same neurons. Notable exceptions are the hippocampus where all three transcripts are abundantly present. Moreover, the expression of Calneuron-2 is strikingly restricted which suggests rather specific functions in a subset of neurons. Calneuron-1 exhibits a more widespread distribution and it is therefore plausible that it will be co-expressed with Caldendrin in the same cells.

A decisive question to be addressed is whether Caldendrin and Calneurons share a similar set of binding partners and whether they can substitute for each other. Since both Calneurons are distributed to different subcellular fractions (mainly Golgi membranes and cytoplasm/vesicles) as compared to Caldendrin that is enriched in the PSD it can also be predicted that both of them might have different binding partners already due to their different localization. Accordingly, the four to five times higher  $\text{Ca}^{2+}$  binding affinity of Calneuron-1 as compared to Caldendrin (Mikhaylova et al., 2006) might reflect that a number of  $\text{Ca}^{2+}$  dependent interactions will occur already at much lower free  $\text{Ca}^{2+}$  concentrations than the  $\text{Ca}^{2+}$  dependent interactions of Caldendrin that might happen in cell compartments like synapses which have very high  $\text{Ca}^{2+}$ - transients. A closer examination of known Caldendrin / CaBP1 target structures reveals that they have no clear preference for one specific type of CaM binding sites. Comparative studies with Calneurons might therefore help to learn more about the structural requirements for binding of both families, which will lead to a deeper appreciation of the molecular mechanisms.

Another important step in the search of Calneurons cellular function will be to understand the role of the long C-terminal extension in both proteins. Moreover, albeit EF-hands 3 and 4 are cryptic they seem to have a helix-loop-helix like structure and their amino

acid sequence is highly conserved between different species. In conjunction with the 38 amino acid extension as compared to Caldendrin / CaBPs and NCS proteins the C-terminal part of Calneuron might contribute to either  $\text{Ca}^{2+}$ -independent interactions or provide together with the first two EF-hands target specificity for certain binding partners. Alternatively the C-terminus might provide specific localization signals to target the protein to subcellular compartments. First published evidence already exists for this notion (McCue et al., 2009, Mikhaylova et al., 2009).

## **4.2 Caldendrin and Jacob are key molecules on a novel pathway from the synapse to the nucleus**

### ***4.2.1 Jacob is a synaptic binding partner of Caldendrin***

As the general conclusion from previous and current work we found that Caldendrin is a key player in a novel neuronal signaling pathway that is coupling NMDARs activity to the cell nucleus and triggers long-lasting changes in the cytoarchitecture of dendrites and the number of spine synapses. This novel pathway particularly couples activation of NR2B-containing NMDARs to morphogenetic signaling via the nuclear trafficking of Jacob. At resting conditions, Jacob is attached to extranuclear compartments in an either Importin- $\alpha$  bound or unbound state (see also Fig. 7).  $\text{Ca}^{2+}$ -influx through synaptic and extrasynaptic NMDA receptors is followed by a translocation of Importin- $\alpha$  from synapses and dendrites to the nucleus and we propose that Importin- $\alpha$ -bound Jacob will be recruited to the nucleus. Moreover, the presence of the NLS is essential for Jacob's translocation indicating that already trafficking from dendrites to the nucleus and not only nuclear import requires the classical Importin pathway. This is reminiscent of previous data showing NMDAR-dependent Importin trafficking from dendrites to the nucleus (Thompson et al., 2004), and establishes Jacob the first identified cargo of this trafficking event. Accordingly, we always found a tight correlation between Jacob's and Importin- $\alpha$ 1 nuclear translocation. Caldendrin binding can mask the bipartite NLS of Jacob in competition with Importin- $\alpha$  and thereby prevent its nuclear trafficking (Fig. 36). However, in contrast to Importin- $\alpha$  binding this requires high  $\text{Ca}^{2+}$ -levels and not only NMDAR activation (Fig. 36). The required free  $\text{Ca}^{2+}$ -levels of about 1  $\mu\text{M}$  (Dieterich et al., 2008) can only be reached in spine synapses (Köhr, 2006) and we therefore suggest that Caldendrin targets Jacob to synapses after enhanced synaptic activation (Fig. 36).



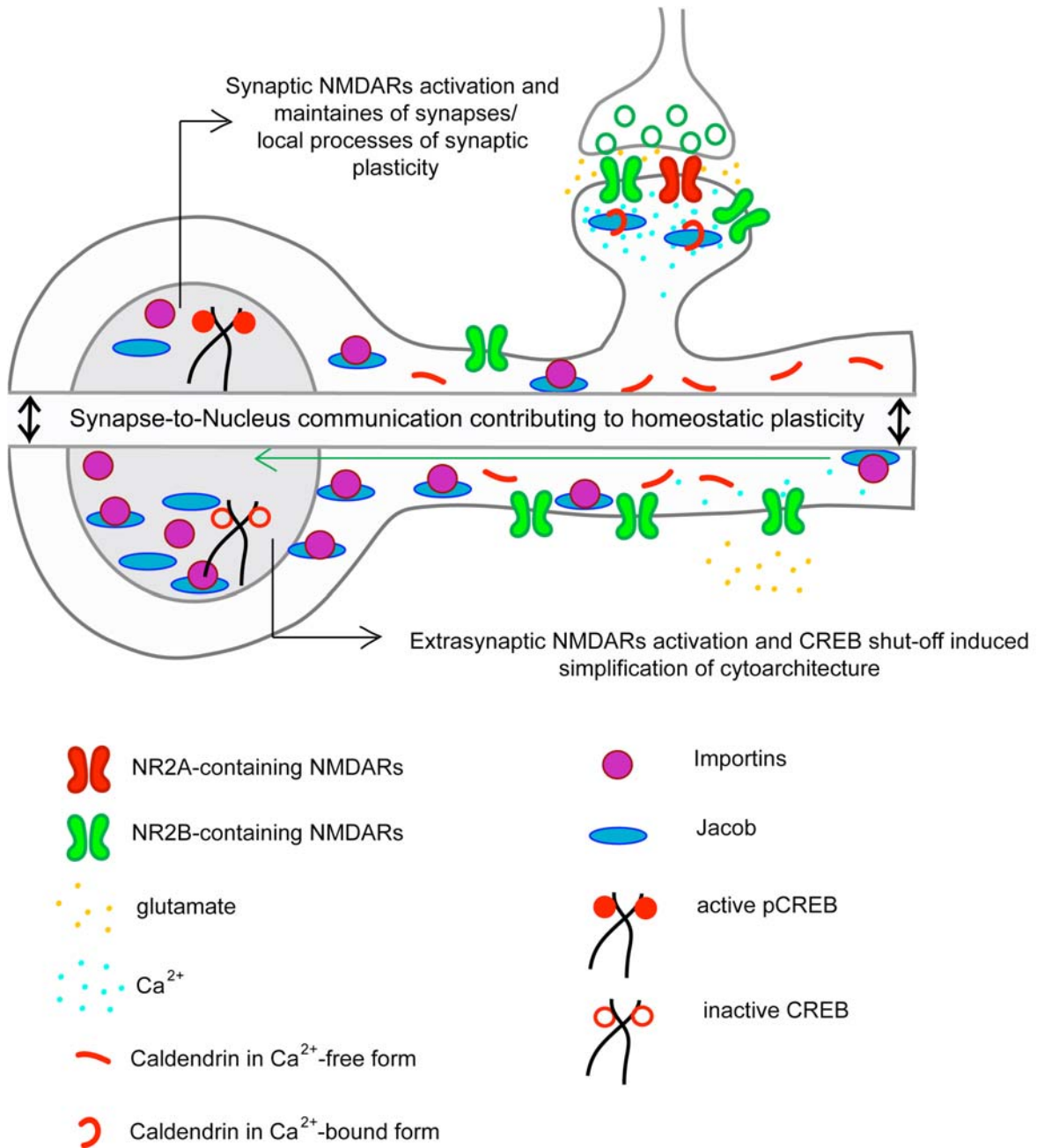


Figure 36. Model of cellular consequences of the Caldendrin-Jacob pathway after activation of synaptic or extrasynaptic NMDARs.

These data are in line with ITC measurements of the global Ca<sup>2+</sup> binding affinity of Caldendrin that turned to be in the range of 1-2 μM (Wingard et al., 2005; Mikhaylova et al., 2006). Accordingly, the nuclear import of Jacob was most efficient under conditions that result only in relatively low and transiently elevated intracellular Ca<sup>2+</sup>-levels like after stimulation of extrasynaptic NMDARs. Hence, extrasynaptic NMDARs have been shown to have particularly fast run-down times and to block voltage-dependent potassium channels in

neurons and thereby decreasing intracellular  $\text{Ca}^{2+}$ -levels (Petrozzino et al., 1995; Isaacson et al., 2001). In further support of this hypothesis, we could provide evidence that activation of NR2B- containing NMDARs, which are mainly located at extrasynaptic sites, is crucial for the nuclear import of Jacob and Importin- $\alpha$ 1. Interestingly, we found that blocking this receptor subtype did attenuate the nuclear accumulation of both proteins after stimulation of synaptic NMDARs that contain predominantly but not exclusively the NR2A subunit (Li et al., 2002; Thomas et al., 2006). This suggests the intriguing possibility that the nuclear Jacob-Importin pathway is physically coupled to one NMDAR subunit and that the presence or absence of  $\text{Ca}^{2+}$ -bound Caldendrin in the respective synapto-dendritic compartment will decide if local Jacob shuttles to the nucleus or not. Therefore we propose that an important function Caldendrin is in the integration NMDAR signals and to target Jacob to spine synapses after enhanced synaptic activation.

#### ***4.2.2 Caldendrin is a first example when the interaction of a $\text{Ca}^{2+}$ -sensor with a NLS can mask the site and prevent nuclear translocation by competing with Importin- $\alpha$ – binding***

A further intriguing aspect of this work is that it provides the first demonstration that an EF-hand CaM-like  $\text{Ca}^{2+}$ -sensor protein regulates the nuclear localization of a protein by competitive binding to its NLS in a  $\text{Ca}^{2+}$ -dependent manner. The significance of this novel mechanism of neuronal  $\text{Ca}^{2+}$ -signaling is further underscored by the fact that binding of Caldendrin is specific in that its ancestor and closest relative in brain, CaM, did not bind to Jacob at any  $\text{Ca}^{2+}$  concentration tested (Dieterich et al., 2008). This is of importance since CaM levels are probably more than a magnitude higher in neurons than those of Caldendrin (Seidenbecher et al., 2002). Computer modelling based on templates from crystallized structures shows that the outer surface of solvent exposed amino acids of particularly EF-hand 2, which seems to be crucial for binding to Jacob and another recently identified binding partner LC3 (Seidenbecher et al., 2004) are covered by residues that clearly differ between CaM and Caldendrin. Accordingly, LC3, a component of the microtubular cytoskeleton, apparently does not bind to CaM (Seidenbecher et al., 2004). The principal specificity of Caldendrin protein interactions is further supported by the observation that very few mutations occurred in this region during vertebrate development and that none of these mutations affected the solvent exposed amino acids of EF-hand 2 (Zhou et al., 2004). Thus, the singularity of the Caldendrin surface is intrinsic and independent from insertions

or deletions, and we therefore suggest that this is probably due to adaptations of its surface to a specific localization and function in neurons of higher vertebrates.

#### ***4.2.3 Caldendrin - Jacob interaction in the frame of neuronal function***

How could this singularity with respect to other  $\text{Ca}^{2+}$ -binding proteins relate to Caldendrin's neuronal function? In contrast to the interaction with Jacob, Caldendrin binding to most of its interaction partners is  $\text{Ca}^{2+}$ -independent, as already described above for the LC3 interaction (Seidenbecher et al., 2004). For instance,  $\text{Ca}^{2+}$ -, CaM and ATP-independent interaction of the C-terminal half of Caldendrin/CaBP1 was demonstrated for the IP3Rs (Haynes et al., 2004; Kasri et al., 2004). The functional consequence of Caldendrin binding is a reduction of IP3-triggered intracellular  $\text{Ca}^{2+}$  release (Haynes et al., 2004; Kasri et al., 2004). At the synapse, a  $\text{Ca}^{2+}$ -independent binding was reported for  $\text{Ca}_v1.2$  -channels (Zhou et al., 2002). This interaction will probably lead to increased  $\text{Ca}^{2+}$  currents following synaptic activation and thereby indirectly via increased synaptic activity promote Caldendrin's and possibly Jacob's synaptic localization. Low synaptic activity and, hence, low synapto-dendritic  $\text{Ca}^{2+}$ -levels will instead favour Caldendrin's binding to the IP3Rs. It is therefore conceivable that Caldendrin can thereby directly lower  $\text{Ca}^{2+}$  levels in dendritic microdomains and in consequence negatively regulate its own association with Jacob. Therefore, a switch of binding partners could directly relate to Caldendrin's role in regulating Jacob's nuclear transition. Along these lines it can be predicted that keeping the delicate balance between Jacob's nuclear and extranuclear localization via Caldendrin binding will provide a powerful regulatory mechanism in the transformation of dendritic  $\text{Ca}^{2+}$  signals into morphogenetic signals for the dendritic cytoarchitecture of principal neurons under pathophysiological and probably also under physiological conditions.

#### ***4.2.4 Nuclear Jacob induces pleiotropic negative effects on synapto-dendritic cytoarchitecture and induces CREB shut-off***

Based on the characteristics and consequences of its nuclear import we found conclusive evidence that Jacob is part of the CREB shut-off pathway. The most prominent nuclear target of neuronal NMDAR signaling is the transcription factor CREB (West et al., 2002; Deisseroth et al., 2003). Subsequent to its phosphorylation at serine 133 pCREB triggers gene expression crucially involved in processes of synaptic plasticity and neuronal survival (Lonze et al., 2002; Bito et al., 2003). Analysis of this pathway has demonstrated

that synaptic NMDARs strongly activate

CREB-dependent gene expression whereas extrasynaptic NMDARs trigger a CREB shut-off (Hardingham et al., 2002). A most intriguing finding in recent years has been that the antagonistic signaling of extrasynaptic versus synaptic NMDARs resembles their opposing actions on the activation of ERK1/2 kinases (Hardingham et al., 2001; Chandler et al., 2001; Kim et al., 2005; Ivanov et al., 2006). Activation of synaptic NMDARs is coupled to the Ras-ERK pathway and subsequent CREB-phosphorylation whereas extrasynaptic NR2B-containing receptors promote dephosphorylation and inactivation of the Ras-ERK-pathway (Hardingham et al., 2001; Chandler et al., 2001; Kim et al., 2005; Ivanov et al., 2006). One caveat of this scenario, however, is that shutting down Ras-ERK alone cannot explain the shut-off of CREB since other mechanisms, and here prominently nuclear CaMKIV, should be in principal sufficient to phosphorylate CREB in the absence of ERK-activity (Lonze et al., 2002; Bito et al., 2003). Thus, the opposing influence of both types of NMDA receptors after bath application of NMDA requires another mechanism that will actively trigger CREB shut off. Our data suggest that the same conditions that trigger shut-off of CREB and the Ras-ERK pathway drive Jacob into the nucleus (Fig. 35). Overexpression of Jacob in the nucleus - without activating these pathways - is sufficient to attenuate CREB phosphorylation and a nuclear knock down of Jacob prevents CREB shut off after triggering the pathway. Moreover, the nuclear knock down of Jacob significantly reduced neuronal cell death after triggering CREB shut-off. Finally, the rapid loss of synaptic contacts, one of the hallmarks of bath application of NMDA in hippocampal primary cultures, was prevented by reducing the amount of nuclear Jacob. We therefore propose that nuclear Jacob is an essential component of CREB shut-off that might be actively involved in rendering CREB in a dephosphorylated state.

#### ***4.2.5 What is Jacob's physiological role in the nucleus?***

In initial experiments, we could not establish a direct binding of Jacob to CREB although both proteins are found in the overlapping fractions after gel filtration of nuclear protein complexes (unpublished observations). Therefore, it is conceivable that Jacob is indirectly coupled via CREB-binding proteins to the CREB signalosome. To further support a role in gene expression we have provided compelling evidence that Jacob is highly enriched in two nuclear compartments associated with gene transcription and pre-mRNA processing. Jacob is abundant in euchromatin fractions and therefore present at active sites

of gene transcription (Dieterich et al., 2008). Moreover, its tight association with the nuclear matrix even after removal of chromatin (Dieterich & Kreutz, unpublished observations) suggests that it could also have a role in pre-mRNA processing and / or mRNA export. It should be also mentioned that the protein harbors long stretches of basic amino acid residues, which are well suited for DNA binding, although no known DNA-binding motif was identified in its primary structure. Thus, particularly with regard to the phenotype of its nuclear overexpression that involves a rapid destabilization of synaptic contacts and a retraction of dendrites, and which cannot be explained entirely by CREB shut-off it is reasonable to assume that Jacob will be part of additional nuclear signaling events.

The nature of such signaling events will be obviously related to the circumstances of Jacob's nuclear trafficking. CREB shut-off has been largely assigned so far to pathophysiological insults including spillover of glutamate after excessive stimulation or reversal of glutamate transporters in the context of epileptic seizures or brain ischemia (Hardingham & Bading, 2003). This view, however, is probably too narrow since in recent years a number of observations raise the possibility that the activation of extrasynaptic NR2B-containing NMDARs can occur in a physiological context. It was shown that in several brain regions sustained synaptic activation causes spillover of synaptically released glutamate to non-synaptic sites (Diamond et al., 2001; Hardingham & Bading, 2002). In addition, sustained synaptic activation favours non-synaptic release of glutamate from astrocytes (Fellin et al., 2004) and it has been suggested that this glia-neuron transmission via extrasynaptic NMDA receptors has profound effects on non-Hebbian types of neuronal plasticity (Wang et al., 2006). Moreover it was also claimed that activation of extrasynaptic NMDARs might directly induce heterosynaptic long-term depression at certain synapses in close proximity (Haydon et al., 2006). The evolving concept behind these studies is the idea of homeostatic scaling of synaptic input. Homeostatic plasticity refers to a process by which especially principal neurons constantly adjust the integration of synaptic input to optimize the contribution of a single synapse with reference to its location in the dendrite and the synchronized activity in a given neuronal network (Davis et al., 2001; Massey et al., 2004). A major aspect of homeostatic plasticity is the fact that uncontrolled potentiation of synapses will induce a ceiling effect characterized by epileptic activity and a decoupling of a given neuron from the dynamics of presynaptic input. Homeostatic plasticity reflects the necessity to either remove certain synapses that contribute less efficiently to the optimal activity within a neuronal network or to reduce the level of potentiation of synapses in this

network. Jacob's nuclear accumulation and its rapid morphogenetic effects are in favour for a role in the regulation of plasticity-related gene expression related to homeostatic synaptic plasticity (Fig. 36). Interestingly, this role includes a stripping of synaptic contacts that precedes the simplification and regression of dendritic processes. It is therefore conceivable that the loss of synapses is the initial trigger for the retraction of dendritic arbors. Moreover, this process is surprisingly rapid indicating that synapses are actively destabilized. This in turn suggests that Jacob either blocks an essential nuclear signaling event required to prevent the removal of synaptic input or regulates the expression of genes that will actively destabilize synapses. It is likely that the CREB shut-off pathway will be part of this mechanism but it is unclear whether it is sufficient to trigger solely the course of events following Jacob's nuclear import.

### **4.3 Calneurons provide a $Ca^{2+}$ threshold for trans-Golgi network to plasma membrane trafficking**

#### **4.3.1 *PI-4K $\beta$ is an interaction partner of Calneurons in the Golgi***

In search for the cellular function of Calneurons we performed a number of experiments that have shown that Calneurons localization is strongly associated to the Golgi. From that we concluded that their cellular function also most likely will be restricted to this compartment. One of the most prominent targets for the neuronal calcium sensor protein in the Golgi is PI-4K $\beta$ . In addition the regulated local synthesis of PI(4)P and PI(4,5)P<sub>2</sub> is crucial for trans-Golgi network to plasma membrane trafficking and the activity of PI-4K $\beta$  at the Golgi membrane is a first mandatory step in this process (Balla&Balla, 2006; De Matteus&Luini, 2008). A number of studies have shown that the enzymatic activity of PI-4K $\beta$  is regulated by  $Ca^{2+}$  via an interaction with Frq1/NCS-1 (Haynes et al., 2005; de Barry et al., 2006). This pathway exists in yeast where interaction of both proteins is very prominent,  $Ca^{2+}$  independent and vital for the cell function. Later in mammals there are more steps of regulation gets involved. According to these studies NCS-1 associates with PI-4K $\beta$  already at resting conditions while increasing  $Ca^{2+}$  levels leads to increased enzyme activity due to a  $Ca^{2+}$ -induced conformational change in NCS-1 (De Barry et al., 2006, Mikhaylova et al., 2009). So far NCS-1 is reported to be the only neuronal calcium sensor that can bind PI-4K $\beta$  (Hendricks et al., 1999; Haynes et al., 2005). We have found that both Calneuron-1 and -2 can associate with PI-4K $\beta$  *in vitro* and *in vivo*. Moreover it can directly bind PI-4K $\beta$  in calcium independent manner and has an opposite effect to NCS-1.

Calneurons can profoundly inhibit the enzyme activity already without  $\text{Ca}^{2+}$  and this effect can be even stronger if  $\text{Ca}^{2+}$  is around.

#### ***4.3.2 Calneurons are setting the ‘ $\text{Ca}^{2+}$ threshold’ for PI-4K $\beta$ activation***

The presented work demonstrates a molecular switch in the  $\text{Ca}^{2+}$  regulation of PI-4K $\beta$  activity and an amazing example about the versatility of the same structural motif, the EF-hand, in the transduction of different  $\text{Ca}^{2+}$  conditions to a target interaction. Our data suggest that Calneurons operate as a filter that suppresses PI-4K $\beta$  activity at resting or sub-maximal amplitudes of Golgi  $\text{Ca}^{2+}$ -transients and thereby provide a tonic inhibition that is only released under conditions of sustained  $\text{Ca}^{2+}$ -release. The mechanism predicts that a  $\text{Ca}^{2+}$ -dependent switch between inhibition and activation of PI-4K $\beta$  might exist at Golgi membranes (Fig. 37). The opposing roles of Calneurons and NCS-1 lead to a scenario with only two discrete states and little fine-tuning of enzyme activity between both states. Importantly, the switch from Calneuron to NCS-1 binding can induce a locally restricted 3- to 4-fold increase in PI(4)P production, which represents a major effect for the availability of this rare phospholipids and it is tempting to speculate that these interactions will be limited to discrete Golgi subdomains. It is known that  $\text{Ca}^{2+}$ -chelation prevents the exit of vesicles from the Golgi (Chen et al., 2002) and the inhibition of PI-4K $\beta$  provided by Calneurons might contribute to the necessity to reach a certain  $\text{Ca}^{2+}$ -level for overriding Calneurons by NCS-1. NCS-1 was till now the only  $\text{Ca}^{2+}$ -binding protein known to interact with PI-4K $\beta$  whereas Recoverin and KChIP apparently do not regulate the enzyme. That this mechanism appears to be highly specific for NCS-1 and Calneurons is further underscored by the finding that Caldendrin, the founding member of the neuronal CABP1-5 family (Seidenbecher et al., 1998; Burgoyne et al., 2004) and predominant isoform in brain (Laube et al., 2002) does not regulate PI-4K $\beta$  activity. Calneurons are highly conserved between different species with 100% identity at the amino acid level between mouse, rat, monkey and human orthologues, suggesting a tight structure-function relationship that is under considerable evolutionary pressure. The question that obviously arises is why there is a necessity at the neuronal Golgi for Calneurons as antagonists for NCS-1.

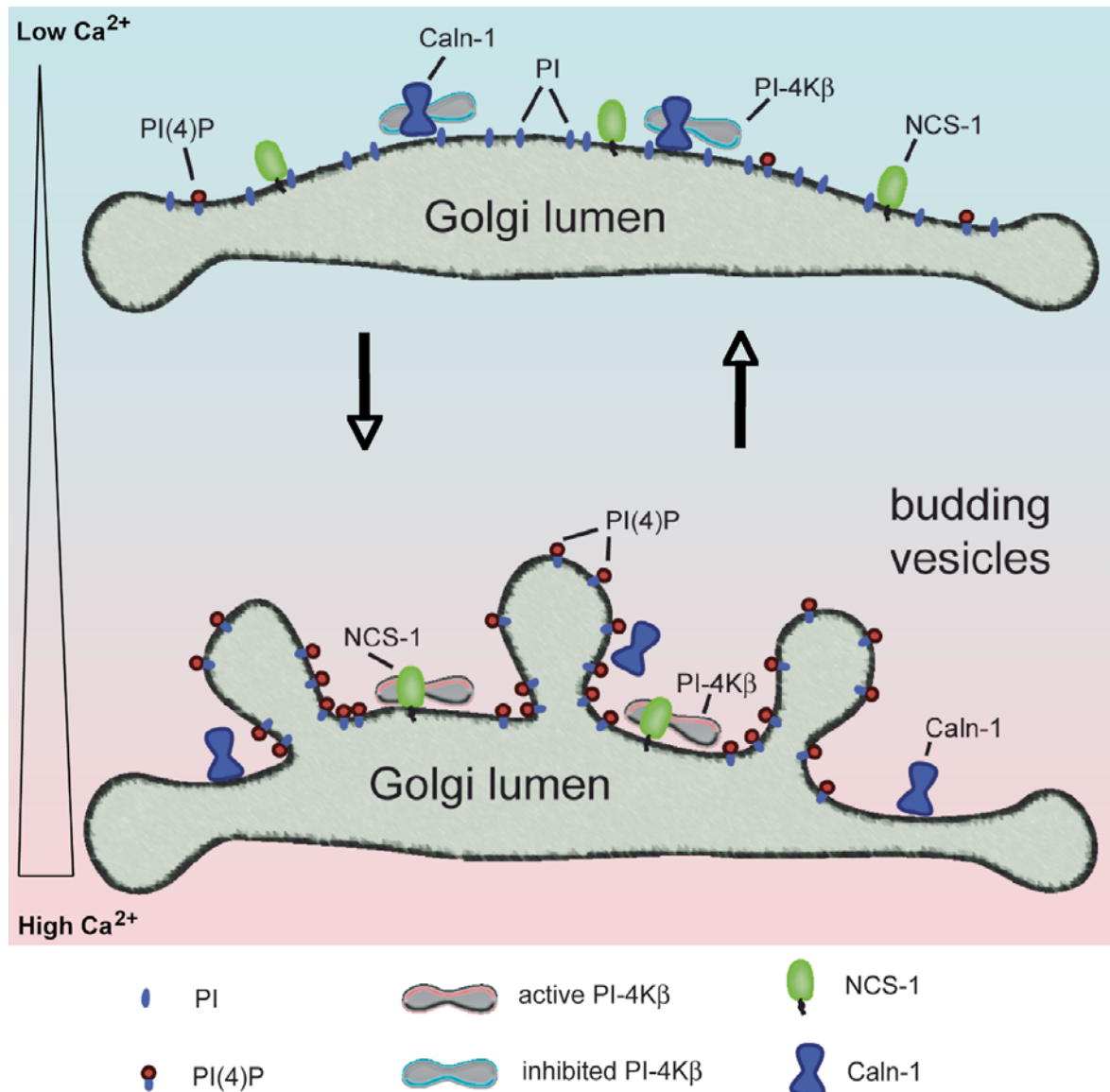


Figure 37. Calneurons and NCS-1 provide a  $\text{Ca}^{2+}$ -dependent molecular switch between inhibition and activation of PI-4K $\beta$  at Golgi membranes. At resting  $\text{Ca}^{2+}$  concentrations Calneurons are tightly bound to PI-4K $\beta$  and will inhibit PI-4K $\beta$  activity (upper part). This results in an inhibition of Golgi trafficking and the budding of vesicles (upper part). An increase of  $\text{Ca}^{2+}$  concentrations at the Golgi will favor binding of NCS-1 and Calneurons are released from the PI-4K $\beta$  complex (lower part). NCS-1 will stimulate the enzymatic activity of PI-4K $\beta$  and Golgi trafficking via a 3 to 4 fold increase in PI(4)P and PI(4,5)P<sub>2</sub> production (lower part).

The answer may come down to the not well understood  $\text{Ca}^{2+}$  regulation of PI-4K $\beta$  at the Golgi membrane. Although the existence of Golgi  $\text{Ca}^{2+}$  microdomains has been proposed (Dolman & Tepikin, 2006) it is unclear how  $\text{Ca}^{2+}$  feeds back locally to PI-4K $\beta$ . Thus, it is equally well conceivable that Calneurons and NCS-1 either associate with PI-4K $\beta$  at different Golgi subdomains or that they transduce  $\text{Ca}^{2+}$  signals to PI-4K $\beta$  in a competitive manner. At low  $\text{Ca}^{2+}$  levels both  $\text{Ca}^{2+}$ -binding proteins seem to be segregated in different



complexes and Calneurons dominate in the regulation of PI-4K $\beta$ . Increasing Ca<sup>2+</sup> seems to favor a complex consisting of NCS-1 and PI-4K $\beta$  with the possibility of a complex consisting of all three proteins and a predicted competing and counteracting role of NCS-1 and Calneurons at an intermediate state. This competition will be dynamically controlled by intracellular free Ca<sup>2+</sup> levels in a manner that NCS-1 will be able to override the inhibition of PI-4K $\beta$  activity via Calneurons only at Ca<sup>2+</sup> concentrations above ~400nM (Fig. 37).

#### ***4.3.3 The competitive binding of Calneurons and NCS-1 to PI-4K $\beta$ is regulated by Mg<sup>2+</sup>***

These results suggest the existence of a molecular switch in the association of the three proteins with a dominant regulatory role of Calneurons at low to middle Ca<sup>2+</sup>-levels, which is counteracted by NCS-1 at higher Ca<sup>2+</sup>-levels. However, the Ca<sup>2+</sup>-binding affinities of Calneuron-1 and NCS-1 are reportedly very similar. We could solve this puzzle by showing that Mg<sup>2+</sup> binding of NCS-1 drastically reduces its Ca<sup>2+</sup>-binding affinity from 90 nM up to 440 nM (Aravind et al., 2008). In sharp contrast to NCS-1, magnesium does not bind at physiologically relevant concentrations to Calneurons. Independently from Mg<sup>2+</sup> levels Ca<sup>2+</sup> associates at Ca<sup>2+</sup>-specific regulatory sites with apparent global affinities of approximately 180 nM for Calneuron-1 and 230 nM for Calneuron-2. It is important to note that free Mg<sup>2+</sup> levels in a cell will render NCS-1 always in a Mg<sup>2+</sup>-bound state. This in turn will promote the reversibility to a Ca<sup>2+</sup>-free state since the resting calcium-levels of about 100 nM would otherwise keep NCS-1 always in a Ca<sup>2+</sup>-bound state. Calneurons, however, have in contrast to NCS-1 a very narrow dynamic range of Ca<sup>2+</sup>-induced unfolding with much less reversibility to the Ca<sup>2+</sup>-free state and this explains why they dominate in the regulation PI-4K $\beta$  activity at low to middle Ca<sup>2+</sup>-concentrations.

Sustained intracellular Ca<sup>2+</sup> release in neurons usually requires high-frequency stimulation, a condition that is associated with an increased demand of membrane proteins, secretory vesicles and TGN to plasma membrane trafficking (Shapira et al., 2003; Gogolla et al., 2007). PI(4)P and PI(4,5)P2 are essential for this latter process and one can therefore speculate that Calneurons add a further level of regulation particularly in secretory cells like neurons that exhibit stimulus-dependent dynamics in TGN to plasma membrane trafficking. In the best available model for this, neuronal primary cultures, we could document a major role of Calneuron-1 in this process (Fig. 38). The data suggest that Calneurons can interfere with the exit of PTVs from the Golgi in early postnatal development and potentially also other synaptic vesicles at later stages.

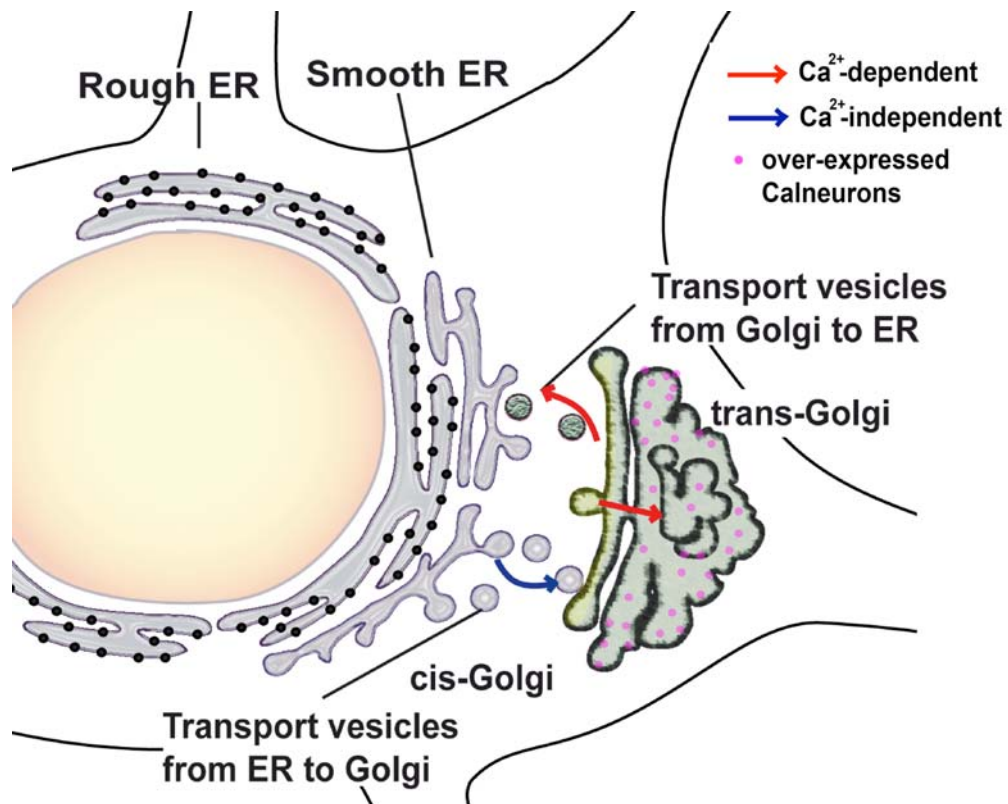


Figure 38. Model: Over-expressed Calneurons induce enlargement of TGB by blocking the Golgi exit of secretory vesicles and an accumulation of vesicular proteins and membranes at TGN.

We have chosen PTVs as a read-out of Calneurons' function at the neuronal Golgi complex because they are, due to their size, small number and segregation in axons, the most accessible vesicle type for quantification (Shapira et al., 2003). Hence we found that not only Piccolo and SNAP25, which are specific PTV markers (Shapira et al., 2003), but that also Synaptophysin that is present on all synaptic vesicles accumulates at the Golgi membranes after Calneuron over-expression and is released from there after a corresponding Calneuron protein knockdown. Taken together the data provide evidence for a role of both calcium sensor proteins in the control of Golgi trafficking of exocytotic vesicles as well as PTVs. It will be an interesting question to understand why overriding the Calneuron-induced inhibition of PI-4K $\beta$  via local  $\text{Ca}^{2+}$  release is an advantageous regulatory mechanism for neurons.

The structural bases of the opposing actions of Calneurons and NCS-1 with regard to PI-4K $\beta$  activity are most plausibly related to their different EF-hand organization and structure. In addition it was shown that the stimulatory effect of NCS-1 on PI-4K $\beta$  activity

requires its N-terminal myristoylation (Zhao et al., 2001), which might provide a Golgi membrane anchor. Calneurons do not harbor an N-myristoylation motif and therefore the question arises how they can be tethered to the Golgi. While this thesis work was underway it was reported that Calneurons contain in their C-terminus a transmembrane domain that might be responsible for Golgi targeting of the over-expressed protein (McCue et al., 2009). This point should be definitely proven by electron microscopy after immunogold labeling or other techniques. It remains, however, elusive how this can provide a Golgi membrane anchor. Interestingly, Golgi recruitment of PI-4K $\beta$  in mammals is predominantly not regulated by NCS-1 but most likely involves NCS-1 binding to ARF1 (Haynes et al., 2005; Haynes et al., 2007). The interaction is Ca<sup>2+</sup>-dependent and ARF1 is instrumental for the recruitment of PI-4K $\beta$  to the TGN and subsequent modification of membrane trafficking (Haynes et al., 2005; Haynes et al., 2007). It is therefore plausible that an interaction with another partner like ARF1 provides a structural link for Calneurons to Golgi membranes.

Calneurons are highly conserved between different species with 100% identity at the amino acid level between mouse, rat, monkey and human orthologues, suggesting a tight structure-function relationship that is under considerable evolutionary pressure. Taken together the work assigns a cellular function to Calneurons, which add an important regulatory mechanism for stimulus-dependent dynamics in trans-Golgi-network to plasma membrane trafficking.

## 5 References

- Aihara Y, Inoue T, Tashiro T, Okamoto K, Komiya Y, Mikoshiba K. Movement of endoplasmic reticulum in the living axon is distinct from other membranous vesicles in its rate, form, and sensitivity to microtubule inhibitors. *J Neurosci Res.* 2001 65(3):236-46.
- Ames JB, Ishima R, Tanaka T, Gordon JI, Stryer L, Ikura M. Molecular Mechanics of Calcium-Myristoyl Switches. *Nature.* 1997 389(6647):198–202.
- Aravind P, Chandra K, Reddy PP, Jeromin A, Chary KV, Sharma Y. Regulatory and Structural EF-Hand Motifs of Neuronal Calcium Sensor-1:  $Mg^{2+}$  Modulates  $Ca^{2+}$  Binding,  $Ca^{2+}$ -Induced Conformational Changes, and Equilibrium Unfolding Transitions. *J Mol Biol.* 2008 376(4):1100-15.
- Ashby MC, Tepikin AV. ER calcium and the functions of intracellular organelles. *Semin Cell Dev Biol.* 2001 12(1):11-7.
- Augustine GJ, Santamaria F, Tanaka K. Local calcium signaling in neurons. *Neuron.* 2003 40(2):331-46.
- Babini E, Bertini I, Capozzi F, Chirivino E, Luchinat C. A structural and dynamic characterization of the EF-hand protein CLSP. *Structure.* 2006 14(6):1029-38.
- Baimbridge KG, Celio MR, Rogers JH. Calcium-binding proteins in the nervous system. *Trends Neurosci.* 1992 15(8):303-8.
- Balla A, Balla T. Phosphatidylinositol 4-kinases: old enzymes with emerging functions. *Trends Cell Biol.* 2006 16(7):351-61.
- Baudry M. Synaptic plasticity and learning and memory: 15 years of progress. *Neurobiol Learn Mem.* 1998 70(1-2):113-8.
- Bengtson CP, Dick O, Bading H. A quantitative method to assess extrasynaptic NMDA receptor function in the protective effect of synaptic activity against neurotoxicity. *BMC Neurosci.* 2008 9:11.
- Bernstein HG, Seidenbecher CI, Smalla KH, Gundelfinger ED, Bogerts B, Kreutz MR. Distribution and cellular localization of caldendrin immunoreactivity in adult human forebrain. *J Histochem Cytochem.* 2003 51(8):1109-12.
- Berridge MJ. Neuronal calcium signalling. *Neuron.* 1998 21(1):13-26.
- Jones HC, Keep RF. The control of potassium concentration in the cerebrospinal fluid and brain interstitial fluid of developing rats. *J Physiol.* 1987 383:441-53.
- Bhatt DH, Zhang S, Gan WB. Dendritic spine dynamics. *Annu Rev Physiol.* 2009 71:261-82.

- Bitto H, Takemoto-Kimura S. Ca(2+)/CREB/CBP-dependent gene regulation: a shared mechanism critical in long-term synaptic plasticity and neuronal survival. *Cell Calcium*. 2003 34(4-5):425-30.
- Blasiolo B, Kabbani N, Boehmler W, Thisse B, Thisse C, Canfield V, Levenson R. Neuronal calcium sensor-1 gene *ncs-1* is essential for semicircular canal formation in zebrafish inner ear. *J Neurobiol*. 2005 64(3):285-97.
- Bourne Y, Dannenberg J, Pollmann V, Marchot P, Pongs O. Immunocytochemical localization and crystal structure of human frequenin (neuronal calcium sensor 1). *J Biol Chem*. 2001 276(15):11949-55.
- Burgoyne RD, Clague MJ. Calcium and calmodulin in membrane fusion. *Biochim Biophys Acta*. 2003 1641(2-3):137-43.
- Burgoyne RD, O'Callaghan DW, Hasdemir B, Haynes LP, Tepikin AV. Neuronal Ca<sup>2+</sup> - sensor proteins: multitasking regulators of neuronal function. *Trends Neurosci*. 2004 27(4):203-9.
- Burgoyne RD. Neuronal calcium sensor proteins: generating diversity in neuronal Ca<sup>2+</sup> signalling. *Nat Rev Neurosci*. 2007 8(3):182-93.
- Camp AJ, Wijesinghe R. Calretinin: Modulator of neuronal excitability. *Int J Biochem Cell Biol*. 2009 May 18. [Epub ahead of print]
- Catimel B, Nerrie M, Lee FT, Scott AM, Ritter G, Welt S, Old LJ, Burgess AW, Nice EC. Kinetic analysis of the interaction between the monoclonal antibody A33 and its colonic epithelial antigen by the use of an optical biosensor. A comparison of immobilisation strategies. *J Chromatogr A*. 1997 776(1):15-30.
- Chandler LJ, Sutton G, Dorairaj NR, Norwood D. N-methyl D-aspartate receptor-mediated bidirectional control of extracellular signal-regulated kinase activity in cortical neuronal cultures. *J Biol Chem*. 2001 276(4):2627-36.
- Chattopadhyaya R, Meador WE, Means AR, Quijcho FA. Calmodulin structure refined at 1.7 Å resolution. *J Mol Biol*. 1992 228(4):1177-92.
- Chen JL, Ahluwalia JP, Stamnes M. Selective effects of calcium chelators on anterograde and retrograde protein transport in the cell. *J Biol Chem*. 2002 277(38):35682-7.
- Chen S, Diamond JS. Synaptically released glutamate activates extrasynaptic NMDA receptors on cells in the ganglion cell layer of rat retina. *J Neurosci*. 2002 22(6):2165-73.
- Cheney RE, Mooseker MS. Unconventional myosins. *Curr Opin Cell Biol*. 1992 4(1):27-35.
- Cohen AS, Moore KA, Bangalore R, Jafri MS, Weinreich D, Kao JP. Ca(2+)-induced Ca<sup>2+</sup> release mediates Ca<sup>2+</sup> transients evoked by single action potentials in rabbit vagal afferent neurones. *J Physiol*. 1997 499(Pt 2): 315–328.

Conti R, Lisman J. A large sustained Ca<sup>2+</sup> elevation occurs in unstimulated spines during the LTP pairing protocol but does not change synaptic strength. *Hippocampus*. 2002 12(5):667-79.

Davis GW, Bezprozvanny I. Maintaining the stability of neural function: a homeostatic hypothesis. *Annu Rev Physiol*. 2001 63:847-69.

De Barry J, Janoshazi A, Dupont JL, Procksch O, Chasserot-Golaz S, Jeromin A, Vitale N. Functional implication of neuronal calcium sensor-1 and phosphoinositol 4-kinase-beta interaction in regulated exocytosis of PC12 cells. *J Biol Chem*. 2006 281(26):18098-18111.

De Matteis MA, Luini A. Exiting the Golgi complex. *Nat Rev Mol Cell Biol*. 2008 9(4):273-84.

Deisseroth K, Heist EK, Tsien RW. Translocation of calmodulin to the nucleus supports CREB phosphorylation in hippocampal neurons. *Nature*. 1998 392(6672):198-202.

Diamond JS. Neuronal glutamate transporters limit activation of NMDA receptors by neurotransmitter spillover on CA1 pyramidal cells. *J Neurosci*. 2001 21(21):8328-38.

Dieterich DC, Karpova A, Mikhaylova M, Zdobnova I, König I, Landwehr M, Kreutz M, Smalla KH, Richter K, Landgraf P, Reissner C, Boeckers TM, Zuschratter W, Spilker C, Seidenbecher CI, Garner CC, Gundelfinger ED, Kreutz MR. Caldendrin-Jacob: A Protein Liaison That Couples NMDA Receptor Signalling to the Nucleus. *PLoS Biol*. 2008 6(2):e34.

Dolman NJ, Tepikin AV. Calcium gradients and the Golgi. *Cell Calcium*. 2006 40(5-6):505-12.

Dresbach T, Torres V, Wittenmayer N, Altmann WD, Zamorano P, Zuschratter W, Nawrotzki R, Ziv NE, Garner CC, Gundelfinger ED. Assembly of active zone precursor vesicles: obligatory trafficking of presynaptic cytomatrix proteins Bassoon and Piccolo via a trans-Golgi compartment. *J Biol Chem*. 2006 281(9):6038-47.

Fellin T, Pascual O, Gobbo S, Pozzan T, Haydon PG, Carmignoto G. Neuronal synchrony mediated by astrocytic glutamate through activation of extrasynaptic NMDA receptors. *Neuron*. 2004 43(5):729-43.

Ferris CD, Snyder SH. Inositol 1,4,5-trisphosphate-activated calcium channels. *Annu Rev Physiol*. 1992 54:469-88.

Flanagan CA, Schnieders EA, Emerick AW, Kunisawa R, Admon A, Thorner J. Phosphatidylinositol 4-kinase: gene structure and requirement for yeast cell viability. *Science*. 1993 262(5138):1444-8.

Franks KM, Sejnowski TJ. Complexity of calcium signaling in synaptic spines. *Bioessays*. 2002 24(12):1130-44.

- Gogolla N, Galimberti I, Caroni P. Structural plasticity of axon terminals in the adult. *Curr Opin Neurobiol.* 2007 17(5):516-24.
- Gomez M, De Castro E, Guarin E, Sasakura H, Kuhara A, Mori I, Bartfai T, Bargmann CI, Nef P. Ca<sup>2+</sup> signaling via the neuronal calcium sensor-1 regulates associative learning and memory in *C. elegans*. *Neuron.* 2001 30(1):241-8.
- Haeseleer F, Imanishi Y, Sokal I, Filipek S, Palczewski K. Calcium-binding proteins: intracellular sensors from the calmodulin superfamily. *Biochem Biophys Res Commun.* 2002 290(2):615-23.
- Haeseleer F, Imanishi Y, Maeda T, Possin DE, Maeda A, Lee A, Rieke F, Palczewski K. Essential role of Ca<sup>2+</sup>-binding protein 4, a Cav1.4 channel regulator, in photoreceptor synaptic function. *Nat Neurosci.* 2004 7(10):1079-87.
- Haeseleer F, Sokal I, Verlinde LMJ, Erdjumen-Bromage H, Tempst P, Pronin AN, Benovic JL, Fariss RN, Palczewski K. Five members of a novel Ca<sup>2+</sup>-binding protein (CaBP) subfamily with similarity to calmodulin. *J Biol Chem.* 2000 275(2):1247-60.
- Halpain S, Hipolito A, Saffer L. Regulation of F-actin stability in dendritic spines by glutamate receptors and calcineurin. *J Neurosci.* 1998 18(23):9835-44.
- Hardingham GE, Arnold FJ, Bading H. Nuclear calcium signaling controls CREB-mediated gene expression triggered by synaptic activity. *Nat Neurosci.* 2001 4(3):261-7.
- Hardingham GE, Arnold FJ, Bading H. A calcium microdomain near NMDA receptors: on switch for ERK-dependent synapse-to-nucleus communication. *Nat Neurosci.* 2001 4(6):565-566.
- Hardingham GE, Bading H. Coupling of extrasynaptic NMDA receptors to a CREB shut-off pathway is developmentally regulated. *Biochim Biophys Acta.* 2002 1600(1-2):148-53.
- Hay JC. Calcium: a fundamental regulator of intracellular membrane fusion? *EMBO Rep.* 2007 8(3):236-40.
- Haydon PG, Carmignoto G. Astrocyte control of synaptic transmission and neurovascular coupling. *Physiol Rev.* 2006 86(3):1009-31.
- Haynes LP, Sherwood MW, Dolman NJ, Burgoyne RD (2007) Specificity, promiscuity and localization of ARF protein interactions with NCS-1 and phosphatidylinositol-4 kinase-III beta. *Traffic.* 2007 8(8):1080-92.
- Haynes LP, Tepikin AV, Burgoyne RD. Calcium-binding protein 1 is an inhibitor of agonist-evoked, inositol 1,4,5-trisphosphate-mediated calcium signaling, *J Biol Chem.* 2004 279(1):547-55.
- Haynes LP, Thomas GM, Burgoyne RD. Interaction of neuronal calcium sensor-1 and ADP-ribosylation factor 1 allows bidirectional control of phosphatidylinositol 4-kinase beta and trans-Golgi network-plasma membrane traffic. *J Biol Chem.* 2005 280(7):6047-54.

Hendricks KB, Wang BQ, Schnieders EA, Thorner J. Yeast homologue of neuronal frequenin is a regulator of phosphatidylinositol-4-OH kinase. *Nat Cell Biol.* 1999 1(4):234-41.

Hilfiker S, Greengard P, Augustine GJ. Coupling calcium to SNARE-mediated synaptic vesicle fusion. *Nat Neurosci.* 1999 2(2):104-6.

Hirsch JC, Crepel F. Postsynaptic calcium is necessary for the induction of LTP and LTD of monosynaptic EPSPs in prefrontal neurons: an in vitro study in the rat. *Synapse.* 1992 10(2):173-5.

Hoesch RE, Yienger K, Weinreich D, Kao JP. Coexistence of functional IP(3) and ryanodine receptors in vagal sensory neurons and their activation by ATP. *J Neurophysiol.* 2002 88(3):1212-9.

Holthoff K, Tsay D. Calcium dynamics in spines: link to synaptic plasticity. *Exp Physiol.* 2002 87(6):725-31.

Horton AC, Ehlers MD. Dual modes of endoplasmic reticulum-to-Golgi transport in dendrites revealed by live-cell imaging. *J Neurosci.* 2003;23(15):6188-99.

Horton AC, Rácz B, Monson EE, Lin AL, Weinberg RJ, Ehlers MD. Polarized secretory trafficking directs cargo for asymmetric dendrite growth and morphogenesis. *Neuron.* 2005 48(5):757-71.

Huttner IG, Strahl T, Osawa M, King DS, Ames JB, Thorner J. Molecular interactions of yeast frequenin (Frq1) with the phosphatidylinositol 4-kinase isoform, Pik1. *J Biol Chem.* 2003 278(7):4862-74.

Impey S, Goodman RH. CREB signaling--timing is everything. *Sci STKE.* 2001 2001(82):PE1.

Impey S, McCorkle SR, Cha-Molstad H, Dwyer JM, Yochum GS, Boss JM, McWeeney S, Dunn JJ, Mandel G, Goodman RH. Defining the CREB regulon: a genome-wide analysis of transcription factor regulatory regions. *Cell.* 2004 119(7):1041-54.

Isaacson JS, Murphy GJ. Glutamate-mediated extrasynaptic inhibition: direct coupling of NMDA receptors to Ca(2+)-activated K<sup>+</sup> channels. *Neuron.* 2001 31(6):1027-34.

Ivanov A, Pellegrino C, Rama S, Dumalska I, Salyha Y, Ben-Ari Y, Medina I. Opposing role of synaptic and extrasynaptic NMDA receptors in regulation of the extracellular signal-regulated kinases (ERK) activity in cultured rat hippocampal neurons. *J Physiol.* 2006 572(Pt 3):789-98.

Kasri NN, Holmes AM, Bultynck G, Parys JB, Bootman MD, Rietdorf K, Missiaen L, McDonald F, De Smedt H, Conway SJ, Holmes AB, Berridge MJ, Roderick HL. Regulation of InsP3 receptor activity by neuronal Ca<sup>2+</sup>-binding proteins. *EMBO J.* 2004 23(2):312-21.



- Kennedy MJ, Ehlers MD (2006) Organelles and trafficking machinery for postsynaptic plasticity. *Annu Rev Neurosci* 29:325-362.
- Kim MJ, Dunah AW, Wang YT, Sheng M. Differential roles of NR2A- and NR2B-containing NMDA receptors in Ras-ERK signalling and AMPA receptor trafficking. *Neuron*. 2005 46(5):745-60.
- Kinoshita-Kawada M, Tang J, Xiao R, Kaneko S, Foskett JK, Zhu MX. Inhibition of TRPC5 channels by Ca<sup>2+</sup>-binding protein 1 in *Xenopus* oocytes. *Pflugers Arch*. 2005 450(5):345-54.
- Köhr G. NMDA receptor function: subunit composition versus spatial distribution. *Cell Tissue Res*. 2006 326(2):439-46.
- Krebs J (EDT) / Michalak M. Calcium : A Matter of Life or Death (New Comprehensive Biochemistry) -US-. ISBN:9780444528056; 2007; 53-55; 63-65.
- Kretsinger RH, Nockolds CE. Carp muscle calcium-binding protein. II. Structure determination and general description. *J Biol Chem*. 1973 248(9):3313-26.
- Kreutz MR, Seidenbecher CI, Gundelfinger ED. Caldendrin - a neuronal calcium binding protein involved in synapto-dendritic Ca<sup>2+</sup> signaling. In: *Neuronal Calcium Sensor Proteins* (Phillipov P & Koch K-W eds) Nova Science Publishers. 2007; 301-313.
- Laube G, Seidenbecher CI, Richter K, Dieterich DC, Hoffmann B, Landwehr M, Smalla KH, Winter C, Böckers TM, Wolf G, Gundelfinger ED, Kreutz MR. The neuron-specific Ca<sup>2+</sup>-binding protein caldendrin: gene structure, splice isoforms and expression in the rat central nervous system. *Mol Cell Neurosci*. 2002 19(3):459-75.
- Lewit-Bentley A, Réty S. EF-hand calcium-binding proteins. *Curr Opin Struct Biol*. 2000 10(6):637-43.
- Li B, Chen N, Luo T, Otsu Y, Murphy TH, Raymond LA. Differential regulation of synaptic and extra-synaptic NMDA receptors. *Nat Neurosci*. 2002 5(9):833-4.
- Llinás R, Sugimori M, Silver RB. Microdomains of high calcium concentration in a presynaptic terminal. *Science*. 1992 256(5057):677-9.
- Lonze BE, Ginty DD. Function and regulation of CREB family transcription factors in the nervous system. *Neuron*. 2002 35(4):605-23.
- M Aridor, J Weissman, S Bannykh, C Nuoffer, W E. Balch. Cargo Selection by the COPII Budding Machinery during Export from the ER. *J Cell Biol*. 1998 141(1): 61–70.
- Mark F. Yeckel, Amanda A. Sleeper, John S. Fitzpatrick, Daniel N. Hertle, Anna M. Hagenston and Robin T. Garner. Intracellular Calcium Waves Transmit Synaptic Information to the Nucleus in Hippocampal Pyramidal Neurons. In: *Transcriptional Regulation by Neuronal Activity. To the Nucleus and Back*. (Dudek SM, ed); SpringerLink, Nov 24, 2007: 73-89.

- Marrion NV, Adams PR. Release of intracellular calcium and modulation of membrane currents by caffeine in bull-frog sympathetic neurones. *J Physiol*. 1992 445: 515–535.
- Massey PV, Johnson BE, Moulton PR, Auberson YP, Brown MW, Molnar E, Collingridge GL, Bashir ZI. Differential roles of NR2A and NR2B-containing NMDA receptors in cortical long-term potentiation and long-term depression. *J Neurosci*. 2004 24(36):7821-8.
- McCue H, Burgoyne RD, Haynes LP. Membrane targeting of the EF-hand containing calcium-sensing proteins CaBP7 and CaBP8. *Biochem Biophys Res Commun*. 2009 380(4):825-31.
- McFerran BW, Weiss JL, Burgoyne RD. Neuronal Ca<sup>(2+)</sup> sensor 1. Characterization of the myristoylated protein, its cellular effects in permeabilized adrenal chromaffin cells, Ca<sup>(2+)</sup>-independent membrane association, and interaction with binding proteins, suggesting a role in rapid Ca<sup>(2+)</sup> signal transduction. *J Biol Chem*. 1999 274(42):30258-65.
- McNiven MA, Thompson HM. Vesicle formation at the plasma membrane and trans-Golgi network: the same but different. *Science*. 2006 313(5793):1591-4.
- Mikhaylova M, Sharma Y, Reissner C, Nagel F, Aravind P, Rajini B, Smalla KH, Gundelfinger ED, Kreutz MR. Neuronal Ca<sup>2+</sup>-signaling in the brain via Caldendrin and Calneurons. *Biochim Biophys Acta*. 2006 1763(11):1229-37.
- Mogami H, Tepikin AV, Petersen OH. Termination of cytosolic Ca<sup>2+</sup> signals: Ca<sup>2+</sup> reuptake into intracellular stores is regulated by the free Ca<sup>2+</sup> concentration in the store lumen. *EMBO J*. 1998 17(2):435-42.
- Noguchi J, Matsuzaki M, Ellis-Davies GC, Kasai H. Spine-neck geometry determines NMDA receptor-dependent Ca<sup>2+</sup> signalling in dendrites. *Neuron*. 2005 46(4):609-22.
- O'Callaghan DW, Ivings L, Weiss JL, Ashby MC, Tepikin AV, Burgoyne RD. Differential use of myristoyl groups on neuronal calcium sensor proteins as a determinant of spatio-temporal aspects of Ca<sup>2+</sup> signal transduction. *J Biol Chem*. 2002 277(16):14227-37.
- Oheim M, Kirchhoff F, Stühmer W. Calcium microdomains in regulated exocytosis. *Cell Calcium*. 2006 40(5-6):423-39.
- Petrozzino JJ, Pozzo Miller LD, Connor JA. Micromolar Ca<sup>2+</sup> transients in dendritic spines of hippocampal pyramidal neurons in brain slice. *Neuron*. 1995 14(6):1223-31.
- Pinton P, Pozzan T, Rizzuto R. The Golgi apparatus is an inositol 1,4,5-trisphosphate-sensitive Ca<sup>2+</sup> store, with functional properties distinct from those of the endoplasmic reticulum. *EMBO J*. 1998 17(18):5298-308.
- Pongs O, Lindemeier J, Zhu XR, Theil T, Engelkamp D, Krah-Jentgens I, Lambrecht HG, Koch KW, Schwemer J, Rivosecchi R, et al. Frequenin — A novel calcium-binding protein that modulates synaptic efficacy in the Drosophila nervous system. *Neuron*. 1993 11(1):15-28.

- Porat A, Elazar Z. Regulation of intra-Golgi membrane transport by calcium. *J Biol Chem.* 2000 275(38):29233-7.
- Presley JF, Cole NB, Schroer TA, Hirschberg K, Zaal KJ, Lippincott-Schwartz J. ER-to-Golgi transport visualized in living cells. *Nature.* 1997 389(6646):81-5.
- protein Caldendrin and CaMKII are localized in spinules of the carp retina. J. Rivosecchi R, Pongs O, Theil T, Mallart A. Implication of frequenin in the facilitation of transmitter release in *Drosophila*. *J Physiol.* 1994 474(2):223-32.
- Rumbaugh G, Vicini S. Distinct synaptic and extrasynaptic NMDA receptors in developing cerebellar granule neurons. *J Neurosci.* 1999 19(24):10603-10.
- Sabatini BL, Oertner TG, Svoboda K. The life cycle of Ca(2+) ions in dendritic spines. *Neuron.* 2002 33(3):439-52.
- Sala C, Rudolph-Correia S, Sheng M. Developmentally regulated NMDA receptor-dependent dephosphorylation of cAMP response element-binding protein (CREB) in hippocampal neurons. *J Neurosci.* 2000 20(10):3529-36.
- Sayer RJ. Intracellular Ca<sup>2+</sup> handling. *Adv Exp Med Biol.* 2002 513:183-96.
- Seidenbecher CI, Langnaese K, Sanmartí-Vila L, Boeckers TM, Smalla KH, Sabel BA, Garner CC, Gundelfinger ED, Kreutz MR. Caldendrin, a novel neuronal calcium-binding protein confined to the somato-dendritic compartment. *J Biol Chem.* 1998 273(33):21324-31.
- Schultz K, Janssen-Bienhold U, Gundelfinger ED, Kreutz MR, Weiler R. Calcium-binding protein Caldendrin and CaMKII are localized in spinules of the carp retina. *J Comp Neurol.* 2004 479(1):84-93.
- Seidenbecher CI, Reissner C, Kreutz MR. Caldendrins in the inner retina, *Adv Exp Med Biol.* 2002 514:451-63.
- Shapira M, Zhai RG, Dresbach T, Bresler T, Torres VI, Gundelfinger ED, Ziv NE, Garner CC. Unitary assembly of presynaptic active zones from Piccolo-Bassoon transport vesicles. *Neuron.* 2003 38(2):237-52.
- Shmigol A, Verkhatsky A, Isenberg G. Calcium-induced calcium release in rat sensory neurons. *J Physiol.* 1995 489(Pt 3): 627-636.
- Smalla KH, Seidenbecher CI, Tischmeyer W, Schicknick H, Wyneken U, Böckers TM, Gundelfinger ED, Kreutz MR. Kainate-induced epileptic seizures induce a recruitment of caldendrin to the postsynaptic density in rat brain. *Brain Res Mol Brain Res.* 2003 116(1-2):159-62.
- Stosiek C, Garaschuk O, Holthoff K, Konnerth A. In vivo two-photon calcium imaging of neuronal networks. *Proc Natl Acad Sci U S A.* 2003 100(12):7319-24.

- Strahl T, Grafelmann B, Dannenberg J, Thorner J, Pongs O. Conservation of regulatory function in calcium-binding proteins: human frequenin (neuronal calcium sensor-1) associates productively with yeast phosphatidylinositol 4-kinase isoform, Pik1. *J Biol Chem.* 2003 278(49):49589-99.
- Strahl T, Hama H, DeWald DB, Thorner J. Yeast phosphatidylinositol 4-kinase, Pik1, has essential roles at the Golgi and in the nucleus. *J Cell Biol.* 2005 171(6):967-79.
- Swede T, Kopp J, Guex N, Peitsch MC. SWISS-MODEL: an automated protein homology-modelling server. *Nucleic Acids Res.* 2004 Jan 1;32(Database issue):D230-4.
- Tanaka T, Ames JB, Harvey TS, Stryer L, Ikura M. Sequestration of the membrane-targeting myristoyl group of recoverin in the calcium-free state. *Nature.* 1995 376(6539):444-7.
- Taverna E, Francolini M, Jeromin A, Hilfiker S, Roder J, Rosa P. Neuronal calcium sensor 1 and phosphatidylinositol 4-OH kinase beta interact in neuronal cells and are translocated to membranes during nucleotide-evoked exocytosis. *J Cell Sci.* 2002 115(Pt 20):3909-22.
- Thomas CG, Miller AJ, Westbrook GL. Synaptic and extrasynaptic NMDA receptor NR2 subunits in cultured hippocampal neurons. *J Neurophysiol.* 2006 95(3):1727-34.
- Thompson KR, Otis KO, Chen DY, Zhao Y, O'Dell TJ, Martin KC. Synapse to nucleus signalling during long-term synaptic plasticity; a role for the classical active nuclear import pathway. *Neuron.* 2004 44(6):997-1009.
- Tovar KR, Westbrook GL. The incorporation of NMDA receptors with a distinct subunit composition at nascent hippocampal synapses in vitro. *J Neurosci.* 1999 19(10):4180-8.
- Vanoevelen J, Raeymaekers L, Parys JB, De Smedt H, Van Baelen K, Callewaert G, Wuytack F, Missiaen L. Inositol trisphosphate producing agonists do not mobilize the thapsigargin-insensitive part of the endoplasmic-reticulum and Golgi  $Ca^{2+}$  store. *Cell Calcium.* 2004 35(2):115-21.
- Voeltz GK, Rolls MM, Rapoport TA. Structural organization of the endoplasmic reticulum. *EMBO Rep.* 2002 3(10):944-50.
- Wang X, Lou N, Xu Q, Tian GF, Peng WG, Han X, Kang J, Takano T, Nedergaard M. Astrocytic  $Ca^{2+}$  signalling evoked by sensory stimulation in vivo. *Nat Neurosci.* 2006 9(6):816-23.
- West AE, Griffith EC, Greenberg ME. Regulation of transcription factors by neuronal activity. *Nat Rev Neurosci.* 2002 3(12):921-31.
- Wingard JN, Chan J, Bosanac I, Haeseleer F, Palczewski K, Ikura M, Ames JB. Structural analysis of  $Mg^{2+}$  and  $Ca^{2+}$  binding to CaBP1, a neuron-specific regulator of calcium channels. *J Biol Chem.* 2005 280(45):37461-70.

Wu GY, Deisseroth K, Tsien RW. Activity-dependent CREB phosphorylation: convergence of a fast, sensitive calmodulin kinase pathway and a slow, less sensitive mitogen-activated protein kinase pathway. *Proc Natl Acad Sci U S A*. 2001 98(5):2808-13.

Wu YQ, Lin X, Liu CM, Jamrich M, Shaffer LG. Identification of a human brain-specific gene, calneuron 1, a new member of the calmodulin superfamily. *Mol Genet Metab*. 2001 72(4):343-50.

Zhai RG, Vardinon-Friedman H, Cases-Langhoff C, Becker B, Gundelfinger ED, Ziv NE, Garner CC. Assembling the presynaptic active zone: a characterization of an active zone precursor vesicle. *Neuron*. 2001 29(1):131-43.

Zhao X, Várnai P, Tuymetova G, Balla A, Tóth ZE, Oker-Blom C, Roder J, Jeromin A, Balla T. Interaction of neuronal calcium sensor-1 (NCS-1) with phosphatidylinositol 4-kinase beta stimulates lipid kinase activity and affects membrane trafficking in COS-7 cells. *J Biol Chem*. 2001 276(43):40183-9.

Zhou H, Kim SA, Kirk EA, Tippens AL, Sun H, Haeseleer F, Lee A. Ca<sup>2+</sup>-binding protein-1 facilitates and forms a postsynaptic complex with Cav1.2 (L-type) Ca<sup>2+</sup> channels. *J Neurosci*. 2004 24(19):4698-708.

Zhou H, Yu K, McCoy KL, Lee A. Molecular mechanism for divergent regulation of Cav1.2 Ca<sup>2+</sup> channels by calmodulin and Ca<sup>2+</sup>-binding protein-1. *J Biol Chem*. 2005 280(33):29612-9.

## 6 Supplementary information

### 6.1 Supplementary Table 1. List of the constructs produced in the lab

cDNA	Plasmid	Resistance	Cloning sites	Application	Obtained from
Calneuron-1 short isoform (A)	pGEM-Teasy	Amp	Topo vector	Subcloning	Marina Mikhaylova
Calneuron-1 short isoform (A)	pEGFP-C1	Kana	ApaI/SalI	Heterologues expression, PD, IP, overexpression in neurons	Marina Mikhaylova
Calneuron-1 short isoform (A)	pEGFP-N1	Kana	BamHI	Heterologues expression, PD, IP, overexpression in neurons	Marina Mikhaylova
Calneuron-1 short isoform, STOP (A) (expression without tag)	pcDNA3.1	Amp	NotI	Heterologues expression, PD, IP, overexpression in neurons	Marina Mikhaylova
Calneuron-1 (A)	pMAL-C2X	Amp	BamHI/SalI	Bacterial expression, antibody production, PD, FS, ITC	Marina Mikhaylova
Calneuron-1 (A)	pGEX	Amp	BamHI/XhoI	Bacterial expression (goes to inclusion bodies)	Marina Mikhaylova
Calneuron-1 (A)	pTrcHis2B	Amp	NcoI (bland ligation, site was destroyed)	Bacterial expression, PD, ITC, kinase assay	Marina Mikhaylova
Calneuron-1 (A)	pET21a	Amp	NdeI (bland)/SalI	Bacterial expression (no induction)	Marina Mikhaylova
Calneuron-1 long isoform (B)	pGEM-Teasy	Amp	Topo vector	Subcloning	Marina Mikhaylova
Calneuron-1 long isoform (B), STOP (expression without tag)	pcDNA3.1	Amp	NotI	Heterologues expression, PD, IP, overexpression in neurons	Marina Mikhaylova
Calneuron-2 full length	pGEM-Teasy	Amp	Topo vector	Subcloning	Marina Mikhaylova
Calneuron-2 full length	pEGFP-C1	Kana	SacI/SacII	Heterologues expression, PD, IP, overexpression in neurons	Marina Mikhaylova
Calneuron-2	pMAL-C2X	Amp	EcoRI/PstI	Bacterial expression, antibody production, PD, FS, ITC	Marina Mikhaylova
Calneuron-2	pGEX	Amp	EcoRI/XhoI	Bacterial expression (goes to inclusion bodies)	Marina Mikhaylova
Calneuron-2	pTrcHis2B	Amp	NcoI (bland ligation, site was destroyed)	Bacterial expression (goes to inclusion bodies)	Marina Mikhaylova
Caldendrin full length (recloned, aa 1-298)	pEGFP-N1	Kana	EcoRI/BamHI	Heterologues expression, PD, IP, overexpression in neurons	Marina Mikhaylova
Caldendrin - C-terminus (aa 137-298)	pGHEB	Amp	EcoRI/BamHI	Bacterial expression, PD, ITC, FS	Dr. M. Landwehr

Caldendrin - C-terminus (aa 137-298)	pET21	Amp	NdeI/EcoRI	Bacterial expression, PD, ITC, FS	Dr. Y. Sharma
Caldendrin-N-terminus	pET-SUMO	Kana	Topo vector	Bacterial expression, PD, SH3 domain array	Marina Mikhaylova
Caldendrin full length	pET-SUMO	Kana	Topo vector	Bacterial expression, PD	Paramesh Reddy
NCS-1	pEGFP-N1	Kana	EcoRI/BamHI	Heterologue expression, IF	Almira Bikkinina
NCS-1	pET21a	Amp	Nde/BamHI	Bacterial expression, PD, ITC, FS	Dr. Y. Sharma
Jacob full length	pEGFP-N1	Kana	EcoRI/BamHI	Heterologues expression PD, IP	Dr. D.C. Dieterich
Jacob full length	pcDNA	Amp	EcoRI/BamHI	Heterologues expression PD, IP	Dr. D.C. Dieterich
Dmyr-Jacob full length (aa 1-532, mutation G2A)	pSFV1	Amp	SmaI (site destroyed)	Infection of primary neurons	Marina Mikhaylova
GFP	pSFV1	Amp	SmaI (site destroyed)	Infection of primary neurons	Marina Mikhaylova
Jacob-N-terminus (aa 1-230)	pMAL-C2X	Amp	EcoRI/BamHI	Bacterial expression, PD	Dr. D.C. Dieterich

## 6.2 Supplementary Table 2. List of the constructs obtained from the collaborators

cDNA	Plasmid	Resistance	Application	Obtained from
Caldendrin full length	pRC	Amp	Heterologues expression, PD, IP	Dr. C. Seidenbecher
N-myristoyl transferase	pBB131	Amp	Co-expression with NCS-1 in bacteria	Dr. A Jeromin
PI-4K $\beta$	pGEX	Amp	Bacterial expression, PD, Kinase assay	Dr. T. Balla
hGH	pXGH5	Amp	Exocytosis assay in PC12 cells	Dr. R. Burgoyne
VSV-G	pGFP-N1	Kana	VSV-G trafficking assay	Drs. M.M Kessels and B. Qualmann
Synaptophysin	pmCherry-C1	Kana	FRAP and vesicle trafficking experiments	Dr. A. Fejtova

## 6.3 Supplementary Table 3. Plasmids used for the cloning and protein expression

Name of the vector	Supplier	Expression system
pcDNA3.1	Invitrogen	mammalian
pGEM-Teasy	Promega	Prokaryotic (cloning vector)
pGEX-4T	AP Biotech, Freiburg, Germany	prokaryotic
pGHEB	pGEX4T modified by Dr. W. Altmann	prokaryotic
pEGFP-N1	Clontech	mammalian
pEGFP-C1	Clontech	mammalian
pET21a	Novagene	prokaryotic
pET21-SUMO	Invitrogen	prokaryotic
pMAL-C2X	NEB	prokaryotic
pmCherry-C1	Clontech	mammalian

pSFV1	Invitrogene	mammalian
pTrcHis 2B	Invitrogene	prokaryotic

#### 6.4 Supplementary Table 4. Common buffers

Name	Composition	pH	applications
Electrophoresis buffer	192 mM glycine, 0.1 % (w/v) SDS, 25 mM Tris-base,	8,3	SDS-PAAG gel electrophoresis
Blotting buffer	192 mM Glycine, 0.2 % (w/v) SDS, 20% (v/v) Methanol, 25 mM Tris-base	8,3	SDS-PAAG gel transfer
4x SDS-sample buffer	250 mM Tris-HCl, pH 6.8, 1% (w/v) SDS, 40% (v/v) Glycerol 20% (v/v) b-mercaptoethanol, 0,004 % Bromophenol Blue	6,8	Denaturing sample buffer for SDS-PAAG gels
TBS	25 mM Tris-HCl, 150 mM NaCl	7,4	Wash buffers, PD, IP, Lysis buffers, buffers for protein purification
TBS-T	TBS+ 0,1% (v/v) Twien-20	7,4	Wash buffers
TBS-A	TBS+0,02% NaN <sub>3</sub>	7,4	Antibody dilution, sepharoses and membranes storage
Ponceau solution	0.5 % (w/v) Ponceau S in 3% (v/v) acetic acid solution		Staining of the proteins on the nitrocellulose membrane
Blocking solution (for IB)	5% (w/v) non-fatty milk powder (or BSA) in TBS-T		Blocking of nitrocellulose membranes after the protein transfer
Coomassie Brilliant Blue staining solution	0.125 % (w/v) Coomassie Brilliant Blue R250, 50% (v/v) methanol, 10% (v/v) acetic acid		Staining of proteins on SDS-PAAG gel
Coomassie destaining solution	7% (v/v) acetic acid		Removal of unspecific staining of SDS-PAAG gels
Drying buffer	50% (v/v) methanol, 5% (v/v) glycerol		Drying of coomassie stained SDS-PAAG gels
10x PBS	1.4 M NaCl, 83 mM Na <sub>2</sub> HPO <sub>4</sub> , 17mM NaH <sub>2</sub> PO <sub>4</sub>	7,4	IF, wash buffers
50xTAE buffer	2 M Tris-acetate, 0.05 M EDTA		Agarose gel electrophoresis
6x DNA loading dye	30% glycerol, 0.25 % bromophenol blue, 0.25 % xylene cyanol, 50 mM EDTA, pH 8.0		Loading dye for agarose gel electrophoresis
Permeabilization buffer	PBS, 0,25% Triton-X-100	7,4	Permeabilization of cells for immunocytochemistry
Blocking buffer	PBS+ 2% BSA, 2% Glycin, 0,2% Gelatine, 50 mM NH <sub>3</sub> Cl	7,4	Blocking of cells for immunocytochemistry, dilution of antibody
Biacore buffer	10 mM Hepes, 150 mM NaCl, 0.005% Surfactant P20	7.4	Biacore experiments, PD

#### 6.5 Supplementary Table 5. Common media

Name	Composition	Application
SOC-medium	20 g/l Bacto- trypton, 5 g/l Yeast-extract, 10 mM NaCl, 2,5 mM KCl, 10 mM Mg <sub>2</sub> SO <sub>4</sub> , 10 mM MgCl <sub>2</sub> , 20 mM Glucose	Bacterial medium
LB-medium	5 g/l Yeast-extract, 10 g/l Bacto- trypton, 5 g/l NaCl	Bacterial medium
Neurobasal medium “-”	Neurobasal™, 1x B27 (Gibco), 100 U/ mL Penicillin, 0.5 mM L-Glutamine	Primary neuronal cell culture, thansfections
Neurobasal medium “+”	Neurobasal™, 1x B27 (Gibco), 100 U/ mL	Primary neuronal cell



	Penicillin, 100 µg/mL Streptomycin, 0.5 mM L-Glutamine	culture
DMEM for neuronal culture	DMEM (-), 10% FCS, 100 U/ mL Penicillin, 100 µg/mL Streptomycin, 2 mM L-Glutamine	Primary neuronal cell culture
DMEM “-”	DMEM (Gibco)	Cell culture of COS-7 cells, transfections
DMEM “+”	DMEM (-), 10% fetal calf serum (FCS), 2 mM L-Glutamine, 100 U/mL Penicillin, 100 µg/mL Streptomycin (Gibco)	Cell culture of COS-7 cells
F12 (HAM)	F12 media (Gibco), 10% fetal calf serum (FCS), 2 mM L-Glutamine, 100 U/mL Penicillin, 100 µg/mL Streptomycin (Gibco)	Cell culture of CHO-K1 cells
RPMI-1640 “+”	RPMI-1640 medium (Gibco), 5% fetal bovine serum, 10% horse serum, 100 U/mL Penicillin, 100 µg/mL Streptomycin (Gibco)	Cell culture of PC12 cells
Stimulation buffer	20 mM Na-HEPES pH 7.4, 15 mM MgCl <sub>2</sub> , 1.5 mM CaCl <sub>2</sub> , 150 mM NaCl, 5 mM KCl, 30 mM Glucose	Life imaging experiments, stimulation experiments

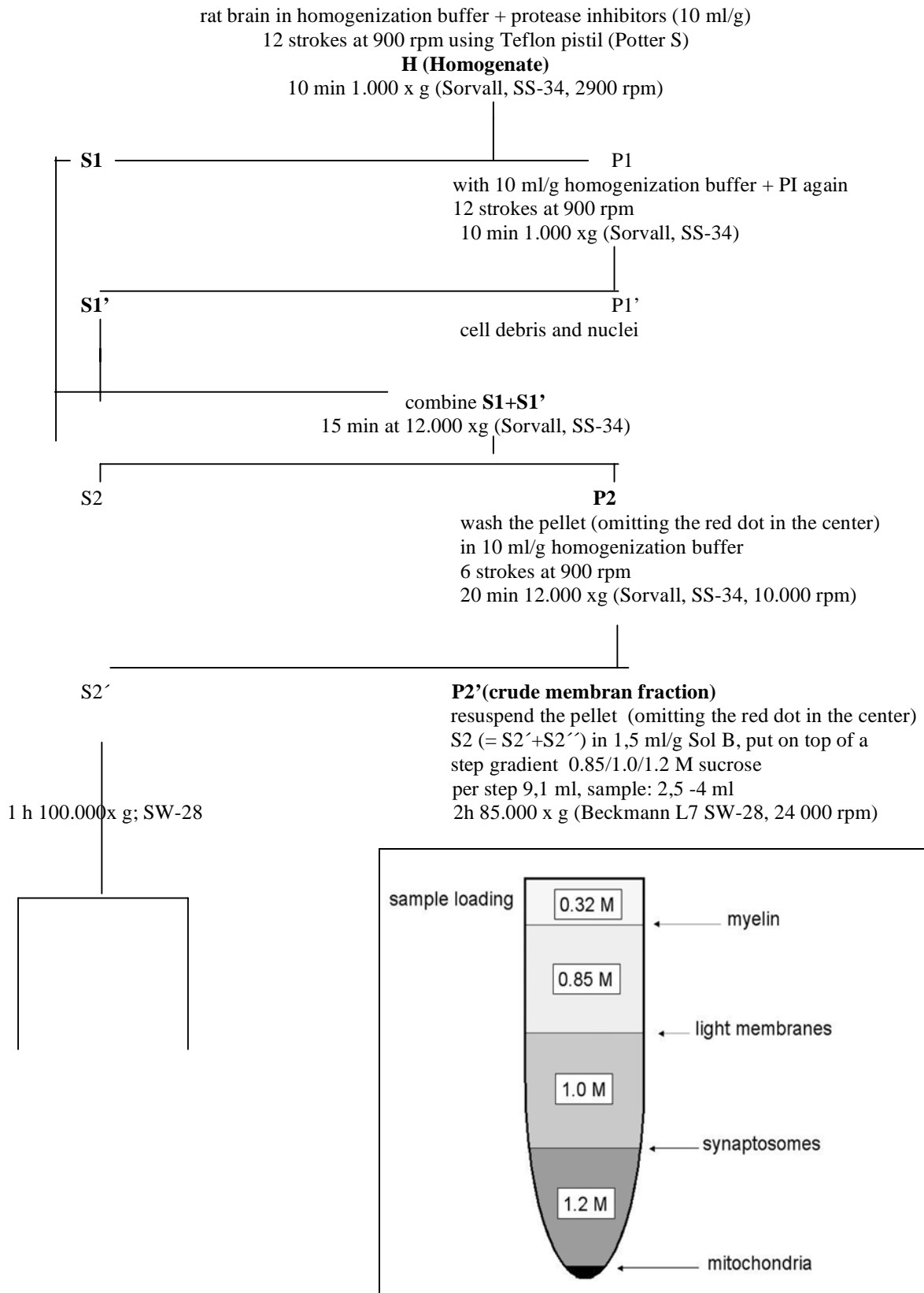
## 6.6 Supplementary Table 6. Solutions for PSD preparation

500 mM HEPES pH 7.4 (5,958 g plus ca. 40 ml bidest, add 50 ml)	50 ml
500 mM Tris/HCl pH 8.1 (6,057g plus ca. 90 ml bidest, add 100 ml)	100 ml
2 M Sucrose (410,76g add 600 ml)	600 ml
Protease-Inhibitor Cocktail tablets (PI)	(1 per 50 ml)

### buffers

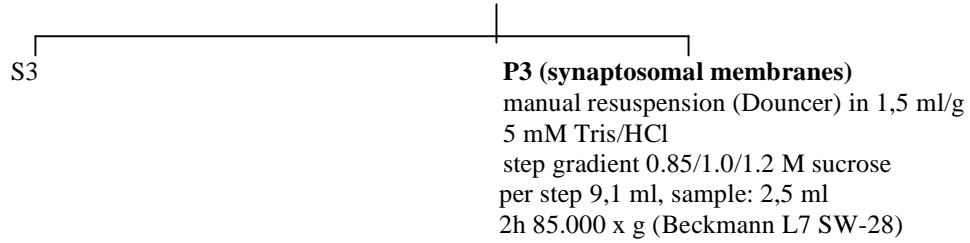
buffer A: 0.32 M sucrose, 5 mM HEPES, pH 7.4 80 ml (2M), 5 ml (0,5M)	500 ml
buffer A + PI <i>prepare freshly</i>	150 ml
buffer B: 0.32 M sucrose, 5 mM Tris, pH 8.1 32 ml (2M), 2 ml (0,5M)	200 ml
buffer C: 0.32 M sucrose, 12 mM Tris, pH 8.1, 1% Triton 32 ml (2M), 4,8 ml (0,5M), 20 ml (10%)	200 ml
1 mM Tris/HCl pH 8.1 <i>prepare freshly</i> (0,4 ml (0,5M))	200 ml
5 mM Tris/HCl pH 8.1 <i>prepare freshly</i> (2,0 ml (0,5M))	100 ml
0.85 M Sucrose/5 mM Tris/HCl pH 8.1 85 ml (2M), 2ml (0,5M)	200 ml
1.0 M Sucrose/5 mM Tris/HCl pH 8.1 100 ml (2M), 2ml (0,5M)	200 ml
1.2 M Sucrose/5 mM Tris/HCl pH 8.1 120 ml (2M), 2ml (0,5M)	200 ml
1.5 M Sucrose/5 mM Tris/HCl pH 8.1 37,5 ml (2M), 0,5 ml (0,5M)	50 ml
ca 2 M Sucrose/5 mM Tris/HCl pH 8.1 15 ml (2M), 150 µl (0,5M)	15 ml

## 6.7 Supplementary Scheme 1. PSD preparation



### Synaptosomes

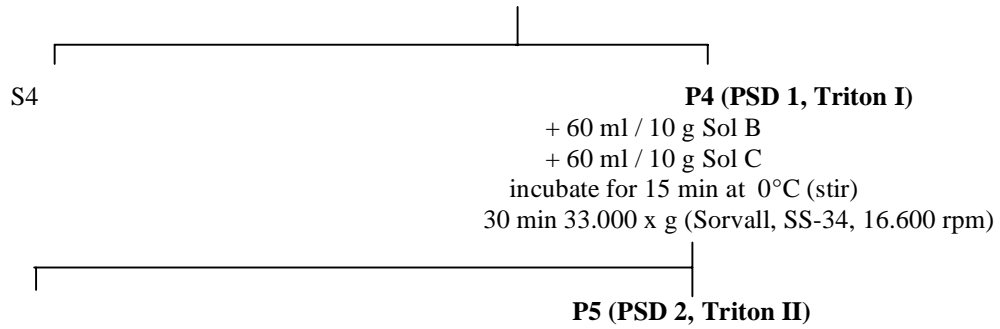
harvested at 1.0/1.2 interface  
+ 5 Vol. Tris/HCl 1 mM, pH 8,1(hypo-osmotic shock)  
stir for 30 min at 0°C  
30 min at 33.000 x g (Sorvall, SS-34)



**only when going further to postsynaptic densities:**

### Interphase (synaptic junctions)

harvested at 1.0/1.2 Interphase  
+ 60 ml / 10 g Sol B  
+ 60 ml / 10 g Sol C  
incubate for 15 min at 0°C (stir)  
30 min 33.000 x g (Sorvall, SS-34, 16.600 rpm)



## 7 Abbreviations

The single or triple letter code was used for amino acids

aa	amino acid(s)
4-AP	4-aminopyridine
ACSF	artificial cerebrospinal fluid
Amp	ampicillin
ANS	1-anilinonaphthalene-8-sulfonate
AOTF	acousto-optic-tunable filter
ARF1	GTPase ADP-ribosylation factor 1
ARF1	ADP-ribosylation factor 1
ATP	adenosine triphosphate
BAPTA	1,2-bis(o-aminophenoxy)ethane-N,N,N',N'-tetraacetic acid
BSA	bovine serum albumin
<i>C. elegans</i>	<i>Caenorhabditis elegans</i>
Ca <sup>2+</sup>	calcium ion
CaBPs	Ca <sup>2+</sup> -binding proteins
Cald	Caldendrin
Caln-1	Calneuron-1
Caln-2	Calneuron-2
CaM	Calmodulin
CaMKII	Calcium/calmodulin-dependent protein kinase II
cAMP PDE	Cyclic adenosine monophosphate phosphodiesterase
Ca <sub>v</sub> 1.2	voltage-gated Ca <sup>2+</sup> channels (L type)
Ca <sub>v</sub> 2.1	voltage-gated Ca <sup>2+</sup> channels (P/Q type)
cDNA	complementary DNA
CHO-K1	Chinese hamster ovary cell line
CICR	calcium induced calcium release
CLSP	CaM-like skin protein
COS-7	african green monkey kidney cell line
CREB	cyclic-AMP response element binding protein
C-terminus	carboxy terminus
Cyt	cytosol fraction
<i>D. melanogaster</i>	<i>Drosophila melanogaster</i>
DAPI	4'-6-Diamidino-2-phenylindole
DIV	day in vitro
DNA	deoxyribonucleic acid
dNTPs	deoxy-nucleotide-triphosphates
DTT	dithiothreitol
EC	entorhinal cortex
<i>E.coli</i>	<i>Escherichia coli</i>
EDTA	ethylenediamine-N,N,N',N'-tetraacetic acid
EGTA	ethylene glycol-bis(2-aminoethylether)-N,N,N',N'-tetraacetic acid
ER	endoplasmic reticulum
ERK1/2	extracellular signal-regulated protein kinases 1/2
EST	expressed sequence tag
Fig.	figure
FRAP	fluorescence recovery after photobleaching

FRAP	fluorescence recovery after photobleaching
Frq1	Frequenin
GABA <sub>A</sub>	A-type of gamma-amino butyric acid receptor
GC	Guanylyl Cyclase
GFP	green fluorescent protein
gp	guinea pig
GST	glutathione S-transferase
HEPES	4-(2-hydroxyethyl)-1-piperazineethanesulfonic acid
hGH	human growth hormone
hrs	hours
IB	immunoblots
ICa	Ca <sup>2+</sup> current
IF	immunofluorescence
IgG	immunoglobulin G
Inh	inhibitor
IP	immunoprecipitations
IP3	Inositol 1,4,5-triphosphate
IP3Rs	Inositol 1,4,5-triphosphate receptors
IR	immunoreactivity
ITC	Isothermal titration calorimetry
Kana	kanamycin
KChiP	Kv4/K channel- interacting protein
kDa	kilo Dalton
LC3	microtubule-associated protein light chain 3
LKU	lipid kinase unique domain
LM	light membranes
LTD	long-term depression
LTP	long-term potentiation
MBP	maltose binding protein
MeOH	methanol
min	minutes
mRNA	messenger RNA
ms	mouse
MS	microsomes
myr-NCS-1	myristoylated NCS-1
n	number of scored cells/samples
NCS	neuronal calcium sensor
NLS	nuclear localization signal
NMDA	N-methyl D-aspartate
NMDARs	N-methyl D-aspartate receptors
NOS	Nitric oxide syntase
N-terminus	amino terminus
ON	overnight
PBS	phosphate buffered saline
PC12	cell line derived from pheochromocytoma of the rat adrenal medulla
PCR	polymerase chain reaction
pCREB	cyclic-AMP response element binding protein phosphorylated at Ser133

PD	pull-down
PFA	paraformaldehyde
pH	potentium hydrogenii
PI	Phosphatidylinositol
PI(4)P	Phosphatidylinositol 4'-monophosphate
PI(4,5)P	phosphatidylinositol 4,5-bisphosphate
PI(4,5)P2	Phosphatidylinositol 4,5-bisphosphate
PI-4K $\beta$	Phosphatidylinositol 4-OH kinase III $\beta$
PKC	protein kinase C
POPOP	1,4-bis(5-phenyloxazol-2-yl) benzene
PPO	Poly(p-phenylene oxide)
PSD	the postsynaptic density
PTVs	piccolo bassoon transport vesicles
rb	rabbit
RNA	ribonucleic acid
RNAi	RNA interference
ROI	region of interest
RT	room temperature
RT-PCR	reverse transcription PCR
RYRs	ryanodine receptors
scr.	scrambled
SDS-PAGE	sodium dodecyl sulfate polyacrylamide gel
SEM	standard error mean
SFV	Semliki Forest Virus
shRNA	short hairpin RNA
SJ	synaptic junctions
Ss	synaptosomes
TBS	tris buffered saline
temp.	temperature
TGN	trans-Golgi network
TRPC	transient receptor potential channels
TTX	tetrodotoxin
Unb	unbound
VDCC	voltage-dependent calcium channel
VSV-G	vesicular stomatitis virus glycoprotein
VTCs	vesicular tubular clusters
wt	wild type
Y2H	yeast two hybrid
$\Delta$	deletion

## **Curriculum Vitae**

**Name:** Mikhaylova Marina Gennadievna  
**Birth date:** 01.03.1981  
**Birthplace:** Ufa, Russia  
**Nationality:** Russian Federation  
**Professional affiliation:** PG Neuroplasticity, Leibniz Institute for Neurobiology, Brenneckestr. 6, 39118 Magdeburg, Germany  
**Academic track record:** Sept 1999-June 2004 Diploma in Biology, specialization - Neurophysiology; Bashkir State University, Department of Biology, Ufa, Russian Federation  
Grade Achieved: 5 / summa cum laude, 1 – 5

### **Education and Experience:**

Nov 2005 - July 2009 Ph.D student in the Project Group 'Neuroplasticity' ((Leibniz-Institute for Neurobiology, Magdeburg, Germany; P.I.: Dr. Michael R. Kreutz).

July 2004 – Oct 2005 Fellowship in the Department of Neurophysiology (Leibniz-Institute for Neurobiology, Magdeburg, Germany; P.I.: Dr. T. Behnisch).

June 2004 Diploma thesis defense. Title “EEG characteristics after injection of Sacricin in WAG/Rij rats”.

Feb 2003 – June 2004 “student job” as a research assistant (P.I.: Dr. Julia V. Vachitova); Inst. of Biochemistry and Genetics, Russian Academy of Science, Ufa Science Center.

July 2002 Internship in the Laboratory of Prof. S.A.Chepurnov, Department of Biology, Lomonosov Moscow State University

2002-2004 Member of the graduate group ‘Animal /Human Physiology and Morphology’; Trainee in the Laboratory of Neurophysiology; P.I.– Dr. Arthur F.Bikbaev;

1999-2004 student at the Bashkir State University, Department of Biology, Ufa, Russia

1988-1998 High School, Ufa, Russia

### **Awards and Honours:**

Participated at the 59<sup>th</sup> Meeting of Nobel Laureates 2009 (nominated by the Leibniz Society), 19<sup>th</sup> Forum dedicated to Chemistry June 28-July 4 at Lake Constance, Lindau, Germany

Invited for a talk at the Edinburgh/UK, 7<sup>th</sup> Junior Academics Meeting “Molecular Mechanisms of Exocytosis and Endocytosis”, April 5-7, 2009, Talk: “Calcineurons provide a Calcium-threshold for trans-Golgi network to plasma membrane trafficking”

FENS / IBRO travel stipend for attending the FENS Forum in Geneva, July 12-16, 2008

Travel grant for the 7<sup>th</sup> meeting of the German Neuroscience society, March 28 to April 1 2007

## **Scientific publications:**

Karpova A, Mikhaylova M, Thomas U, Knöpfel T, Behnisch T. Involvement of protein synthesis and degradation in long term potentiation of Schaffer collateral CA1 synapses. *J Neurosci.* 2006 26(18):4949-55.

Mikhaylova M, Sharma Y, Reissner C, Nagel F, Aravind P, Rajini B, Smalla, K-H, Gundelfinger, ED, Kreutz MR. Neuronal Ca<sup>2+</sup>-signaling via Caldendrin and Calneurons. *Biochim Biophys Acta, Mol Cell Res.*, 2006 1763(11):1229-37.

Mikhaylova M, Vakhitova JV, Yamidanov RS, Salimgareeva MKh, Seredenin SB, Behnisch T. The effects of ladasten on dopaminergic neurotransmission and hippocampal synaptic plasticity in rats. *Neuropharmacology.* 2007 53(5):601-8.

Kreutz MR, König I, Mikhaylova M, Spilker C, Zuschratter W. Molecular mechanisms of dendritic spine plasticity in development and aging. *Handbook of Neurochemistry and Molecular Neurobiology*, 3rd Edition, A Lajtha (Editor-in-chief), Volume 17: „Developmental and aging changes“, Perez-Polo JR & Roßner S (volume eds), Springer, New York, USA. pp. 245-259, 2008.

Dieterich DC\*, Karpova A\*, Mikhaylova M\*, Zdobnova I, König I, Landwehr M, Kreutz M, Smalla KH, Richter K, Landgraf P, Reissner C, Böckers TM, Zuschratter W, Spilker C, Seidenbecher CI, Garner CC, Gundelfinger ED, Kreutz MR. Caldendrin – Jacob: A Protein Liaison that Couples NMDA Receptor Signalling to the Nucleus. *PLoS Biology* 2008 6(2):e34.

\*shared first authorship

Smalla K-H, Mikhaylova M, Sahin J, Bernstein H-G, Bogerts B, Roel van der Schors, August B, Smit AB, Li KW, Gundelfinger ED, Kreutz MR. A comparison of the synaptic proteome in human chronic schizophrenia and rat ketamine psychosis suggest that Prohibitin is involved in the synaptic pathology of schizophrenia. *Mol Psychiatry.* 2008 13(9):878-96.

Mikhaylova M, Pasham P, Munsch T, Suman S, Smalla K-H, Gundelfinger ED, Sharma Y, Kreutz MR. Calneurons provide a Calcium-threshold for trans-Golgi network to plasma membrane trafficking. *Proc. Natl. Acad. Sci. U.S.A.*, 2009 106(22):9093-8.

Kindler S, Dieterich DC, Schütt J, Sahin J, Karpova A, Mikhaylova M, Gundelfinger ED, Kreienkamp H-J, Kreutz MR. Dendritic mRNA targeting of Jacob and NMDA-induced nuclear translocation after Calpain-mediated proteolysis. *J Biol Chem.* 2009 Jul 16. (Epub ahead of print)

Vandanapu RR, Singh AK, Mikhaylova M, Reddy PP, Sharma Y, Kreutz MR. Structural differences between the SH3-HOOK-GuK domains of SAP90/PSD-95 and SAP97. *Protein Expression and Purification* (in press).

Mikhaylova M, Pasham P and Kreutz MR. The role of neuronal calcium-sensor proteins in Golgi-to-cell-surface membrane traffic. Minireview. *Biochemical Society Transactions* (under revision).



Ronicke R, Mikhaylova M, Ronicke S, Meinhardt J, Schroder U, Fändrich M, Reiser G, Kreuz MR, Reymann KG. Early neuronal dysfunction by amyloid  $\beta$  oligomers depends on activation of NR2B-containing NMDA receptors. *Neurobiology of Aging* (submitted).